UNIVERSIDADE FEDERAL DO RIO GRANDE DO NORTE
CENTRO DE CIÊNCIAS EXATAS E DA TERRA
PROGRAMA DE PÓS-GRADUAÇÃO EM GEODINÂMICA E GEOFÍSICA

TESE DE DOUTORADO

CARTOGRAFIA DOS ENXAMES DE DIQUES MÁFICOS DA PROVÍNCIA BORBOREMA COM BASE EM DADOS AEROGEOFÍSICOS E MAPAS AUTO-ORGANIZÁVEIS

Autora:

Alanny Christiny Costa de Melo

Orientador:

Prof. Dr. David Lopes de Castro

Tese n.º 64/PPGG

Abril de 2021

Natal/RN, Brasil

ALANNY CHRISTINY COSTA DE MELO

CARTOGRAFIA DOS ENXAMES DE DIQUES MÁFICOS DA PROVÍNCIA BORBOREMA COM BASE EM DADOS AEROGEOFÍSICOS E MAPAS AUTO-ORGANIZÁVEIS

Tese apresentada em 30 de abril de 2021 ao Programa de Pós-Graduação em Geodinâmica e Geofísica (PPGG) da Universidade Federal do Rio Grande do Norte (UFRN) como requisito à obtenção do Título de Doutora em Geodinâmica e Geofísica, Área de Concentração Geofísica.

BANCA EXAMINADORA:

PROF. DR. DAVID LOPES DE CASTRO
Presidente e orientador (PPGG-UFRN)

PROF. DR. WALTER EUGÊNIO DE MEDEIROS
Membro interno (PPGG-UFRN)

PROF. DR. ZORANO SÉRGIO DE SOUZA
Membro interno (PPGG-UFRN)

PROF. DR. CARLOS JOSÉ ARCHANJO
Membro externo (IAG-USP)

PROF. DR. CLEYTON DE CARVALHO CARNEIRO
Membro externo (Poli-USP)

Universidade Federal do Rio Grande do Norte - UFRN
Sistema de Bibliotecas - SISBI
Catalogação de Publicação na Fonte. UFRN - Biblioteca Setorial Prof. Ronaldo Xavier de Arruda - CCET

Melo, Alanny Christiny Costa de.
Cartografia dos enxames de diques máficos da Província Borborema com base em dados aerogeofísicos e mapas auto-organizáveis / Alanny Christiny Costa de Melo. - 2021.
vx, 122f.: il.

Tese (doutorado) - Universidade Federal do Rio Grande do Norte, Centro de Ciências Exatas e da Terra, Programa de Pós-Graduação em Geodinâmica e Geofísica. Natal, 2021.
Orientador: David Lopes de Castro.

1. Geofísica - Tese. 2. Dados aerogeofísicos - Tese. 3. Mapas auto-organizáveis (SOM) - Tese. 4. Enxames de diques máficos - Tese. 5. Análise estrutural - Tese. 6. Província Borborema - Tese. I. Castro, David Lopes de. II. Título.

RN/UF/CCET CDU 550.3

Elaborado por Joseneide Ferreira Dantas - CRB-15/324

AGRADECIMENTOS

Agradeço ao Programa de Pós-Graduação em Geodinâmica e Geofísica (PPGG) pela oportunidade de realizar o curso de doutorado, e à dedicação de todos seus professores e servidores.

Ao Serviço Geológico do Brasil (CPRM) e à Agência Nacional do Petróleo, Gás Natural e Biocombustíveis (ANP) pela cessão dos dados aerogeofísicos.

Ao Programa de Formação de Recursos Humanos PRH-PB 229 (FUNPEC/UFRN/PETROBRAS) pela bolsa de doutorado (projeto 672013), à Coordenação de Aperfeiçoamento de Pessoal de Nível Superior (Capes) pela bolsa de doutorado (N. 88882.461729/2019-01) e pela bolsa de doutorado sanduíche (N. 88881.188664/2018-01) durante o período de pesquisa na *Australian Commonwealth Scientific and Industrial Research Organization* (CSIRO) e na *University of Queensland* (UQ).

Agradeço também ao meu orientador, Prof. Dr. David Lopes de Castro por te me aceitado mais uma vez como aluna. E por todo aprendizado adquirido ao logo da minha jornada na pós-graduação, fornecendo-me ótimas oportunidades para a conclusão dessa tese. Além de ter me motivado nos momentos mais difíceis.

À Professora Dra. Maria Helena Hollanda idealizadora do projeto EQUAMP LIP (2017/08423-9), ao qual esta tese está associada, e ao Prof. Dr. Carlos José Archanjo por todo o apoio durante os trabalhos de campo e discussões sobre o tema. Ao meu colega de projeto Antomat Macêdo Filho que esteve presente me apoiando em todas as fases do doutorado, desde a elaboração do plano de trabalho até a conclusão desta tese, além de ter me acompanhado durante parte do período sanduíche no exterior, sendo responsável por grande parte das coletas de campo e de muitas discussões inseridas neste trabalho.

Ao meu coorientador australiano Stephen Fraser, que me recebeu gentilmente em seu país, tendo a paciência e a dedicação de me ensinar desde os conceitos mais básicos do SOM aos procedimentos mais elaborados. Também sou grata ao CSIRO *Mineral Resources Flagship*, localizado no *Queensland Centre for Advanced Technologies* (QCAT) em Brisbane, por fornecer o *software* SiroSOM e as instalações para a realização do processamento e análises do SOM.

Aos Professores Dr. Rick Valenta e Dr. Paul Gow da UQ por suas contribuições, a todos que fazem parte do *W.H. Bryan Mining & Geology Research Centre* e à UQ por ter me fornecido estrutura para continuar minha pesquisa durante parte do doutorado sanduíche.

Aos pesquisadores do Grupo Barreirinhas, que me acolheram na sala do projeto no último ano, principalmente ao colaborador MSc. Diógenes Custódio de Oliveira que, com toda sua experiência no estudo dos diques tornou possível o segundo artigo desta tese, e ao Dr. Duvan Herrera pelo auxílio na confecção do mapa de densidade dos diques.

Deixo aqui meus agradecimentos ao Prof. Dr. Zorano Sérgio de Souza por ter cedido algumas de suas amostras para a medição de susceptibilidade magnética.

Aos colegas do PPGG, que vivenciaram comigo dúvidas, angústias e alegrias. Em especial: à agora Dra. Rafaela Alves, minha companheira desde a graduação, que me confortou e me incentivou durante todo esse período; e ao Alexandre Paixão pelo auxílio na coleta das amostras complementares e medição de suas susceptibilidades magnéticas. Agradeço também a minha amiga Ms. Lívian Rafaely Pinheiro por todo o apoio que me deu ao longo dessa jornada. Não poderia deixar de incluir meus colegas brasileiros do Programa Doutorado Sanduíche (PDSE-CAPES) que conheci em Brisbane, e que foram minha família durante o tempo que fiquei na Austrália, principalmente minhas amigas Dra. Juliana Afonso, Dra. Bárbara Mazetti, Nathália Rossigali e Beatriz Morise.

Quero agradecer aos meus pais, Auridéa e Cláudio, meus maiores incentivadores. Por fim, também agradeço ao meu namorado Danilo, por todo carinho e companheirismo, além de sempre se dispor a revisar meus manuscritos.

RESUMO

O mapeamento de enxames de diques vem sendo utilizado no estudo de processos tectônicos que culminam em rifteamento continental, especialmente em suas fases iniciais e intrusão de magma. Sendo assim, enxames de diques se tornaram elementos chave para estudar a atividade de plumas do manto, grandes províncias ígneas (LIP's) e fragmentação continental. Dados magnéticos aerotransportados são eficaz para determinar a extensão de enxames de diques em escala continental devido ao expressivo contraste magnético entre corpos magmáticos e rochas hospedeiras. No entanto, muitas características geológicas exibem padrões magnéticos semelhantes, tornando a interpretação qualitativa dos mapas de anomalias magnéticas bastante subjetiva e ambígua. Para melhorar e otimizar o mapeamento preditivo de enxames de diques, esta pesquisa apresenta uma análise multivariada de levantamentos geofísicos aerotransportados, aplicando a técnica Mapas Auto-Organizáveis (SOM), com a adoção de duas variáveis magnéticas e três variáveis gama-espectrométricas. O método SOM foi aplicado para investigar um conjunto de enxames de diques máficos cretáceos, que intrudiram a Província Borborema (PB), a Bacia do Parnaíba (BP) e o Cráton do São Francisco (SFC) no NE do Brasil. Esses diques fazem parte de um vasto evento magmático associado à ruptura do supercontinente Pangeia, que formou o Oceano Atlântico Equatorial no Cretáceo (145-100 Ma), denominado EQUAMP. Inicialmente, os parâmetros SOM foram definidos, executando o algoritmo em uma área representativa na parte central da PB. Esta área de treinamento funcionou como uma configuração padrão dos parâmetros do SOM, a partir do qual todos os dados da área foram processados. A análise semiautomática do SOM identificou sete populações diferentes, de acordo com as características encontradas nas cinco variáveis geofísicas de entrada. Duas dessas populações estão associadas aos diques máficos, reduzindo a subjetividade da interpretação dos diques a partir da simples observação das anomalias magnéticas. Essas populações representam alto erro de quantização do SOM, o que significa que esses grupos representam os dados mais anômalos, evidenciados no conjunto de dados aerogeofísicos. Esses resultados foram validados durante o trabalho de campo, revelando que os enxames de diques ocorrem de forma mais ampla do que se conhecia anteriormente, em todo a PB, intrudindo também o SFC, e revelando algumas ocorrências de diques intrudindo o preenchimento sedimentar paleozoico da borda leste da BP. Em um segundo momento, técnicas de realce de anomalias foram também aplicadas aos dados magnéticos para obter a distribuição espacial dos diques e estimar a profundidade das fontes causativas das anomalias. Uma análise estrutural foi realizada integrando padrões magnéticos, dados de campo e uma compilação de mapas geológicos anteriores para descrever a distribuição detalhada dos enxames de diques na PB. Nossas análises demonstram que os enxames de diques se estendem por 6,8 x 10^6 km^2. Os 1388 diques máficos mapeados estão agrupados em três enxames distintos: 1135 - Rio Ceará-Mirim (RCM); 168 - Canindé (CD); e 86 - Riacho do Cordeiro - (RC). Os enxames de diques mostram três tendências preferenciais para E-W, NW-SE e NE-SW. Os enxames invadem as unidades do embasamento pré-cambriano e bordejam as bacias sedimentares do Cretáceo. A distribuição espacial e a análise estrutural dos diques permitiram estabelecer o campo de paleotensão ativo no momento da intrusão. Para o RCM, as trajetórias de paleotensão representam uma extensão N-S, rotacionando para NW-SE na porção oeste do enxame. Já para CD, a orientação de paleotensão demonstra uma extensão NW-SE rotacionando para NE-SW. Enquanto para o RC, as trajetórias se mostram semelhantes às traçadas para o RCM, apresentando uma extensão NW-SE predominante.

Palavras-chave: Dados Aerogeofísicos; Mapas Auto-Organizáveis (SOM); Enxames de Diques Máficos; Análise Estrutural; Província Borborema.

ABSTRACT

Mapping widespread dyke swarms shed light on the tectonic processes that culminate in continental fragmentation, especially in the early phases of the crustal extension and magma emplacement. Airborne magnetic data are an effective geophysical tool to clarify the extent of dyke swarms in continental-scale areas due to the expressive magnetic contrast between magmatic bodies and host rocks. However, many geological features display similar magnetic patterns, making the qualitative interpretation of magnetic anomalies quite subjective and ambiguous. To improve and optimize the predictive mapping of dyke swarms, this research presents a multivariate analysis of airborne geophysical surveys, applying a Self-Organizing Maps (SOM) approach using two magnetic and three gamma-spectrometric variables. The SOM method was applied to investigate a set of mafic dyke swarms that intruded in the Neoproterozoic Borborema Province (BP), Parnaíba Basin (PB) and the São Francisco Craton (SFC) in NE Brazil. These dykes are part of a large magmatic event associated with the supercontinent Pangea breakup, which formed the Equatorial Atlantic Ocean in the Early Cretaceous, denominated EQUAMP. First, the SOM hyperparameters were defined by running the algorithm in a representative area in the central part of the BP. This training area worked as a SOM template, through which all data from the study area were processed. The SOM analysis identified seven different populations, according to responses found in the five geophysical input variables. Two of these populations were associated with the mafic dykes, reducing the subjectivity of the magnetic anomaly interpretation. These populations represent high SOM quantization error, which means that these groups are the most anomalous values, evidenced in airborne magnetic data. These results was checked during fieldwork, revealing that dyke swarms occur more widely than was previously known, throughout the BP, intruding the SFC, and showing some occurrences intro in the Paleozoic sedimentary infill of the eastern border of the PB. We also apply anomaly enhancement techniques to magnetic data to obtain the spatial distribution and depth estimate of the causative sources. A structural analysis was carried out, integrating magnetic patterns, field data and a compilation of previous geological maps to describe the detailed distribution of the dyke swarms in BP. Our analyses demonstrated that the dyke swarms extend over 6.8 x10^6 km^2. The 1388 mapped mafic dykes are grouped in three distinct swarms: 1135 – Rio Ceará-Mirim (RCM); 168 – Canindé (CD); and 86 – Riacho do Cordeiro – RC. The dyke swarms show three preferential trends to E-W, NW-

SE and NE-SW. The swarms intrude both the Precambrian basement units and the Cretaceous sedimentary basins. The geometry and structural analysis of the dykes allowed interpreting the paleostress field active at the intrusion time. To the RCM, the paleostress trajectories represent a N-S extension, rotating to NW-SE in the western portion of the swarm. While for CD, the paleostress orientation shows a NW-SE extension rotating to NE-SW. As for the RC, the trajectories were similar to those traced for the RCM, showing a predominant NW-SE extent.

Keywords: Airborne Geophysical Data, Self-Organizing Maps (SOM), Mafic Dyke Swarms, Structural Analysis, Borborema Province.

SUMÁRIO

Agradecimentos i

Resumo iii

Abstract v

Sumário vii

Lista de Figuras x

Lista de Tabelas xv

1. INTRODUÇÃO 1

1.1. Apresentação 2

1.2. Estrutura da Tese 3

1.3. Justificativa 4

1.4. Localização da área de estudo 5

1.5. Objetivos 7

2. ASPECTOS GERAIS DOS DIQUES 8

2.1. Diques Máficos 9

2.2. Morfologia de Diques 10

2.3. Geometria dos Enxames de diques 11

2.4. Grandes Províncias Ígneas (LIP's) 13

3. FUNDAMENTAÇÃO TEÓRICA 15

3.1. Anomalias Magnéticas de Rochas Ígneas 16

3.2. Técnicas de Filtragem Geofísica 17

3.2.1. Redução ao Polo 18

3.2.2. Matched Filter 19

3.2.3. Amplitude do Sinal Analítico 20

3.3. Fundamentos da Gamaespectrometria 20

3.3.1. Radioelementos 21

3.3.2. Imagens Ternárias (RGB e CMY) 22

3.4. Mapas Auto-Organizáveis (*Self-Organizing Maps* — SOM) 23

4. ARTIGO 1: USING SELF-ORGANIZING MAPS IN AIRBORNE GEOPHYSICAL DATA FOR MAPPING MAFIC DYKE SWARMS IN NE BRAZIL 26
Abstract 27
4.1. Introduction 28
4.2. Geological Setting 31
4.3. Data and Methods 32
4.3.1. Airborne Geophysical Database 32
4.3.2. Self-Organizing Map (SOM) 36
4.4. SOM Analysis 37
4.4.1. SOM Training Test Area 41
4.4.2. Semi-automatic Mapping of the Test Area 43
4.4.3. Correlation of the SOM Solutions with the Surface Geology in the Test Area 47
4.4.4. SOM Solution Validation 50
4.5. SOM Analysis of Dyke swarms in NE Brazil 51
4.6. Conclusions 56
Acknowledgments 57
References 58

5. ARTIGO 2: MESOZOIC DYKE SWARMS IN BORBOREMA PROVINCE (NE BRAZIL): A STRUCTURAL ANALYSIS BASED ON AIRBORNE GEOPHYSICAL DATA AND FIELDWORK 65
Abstract 67
5.1. Introduction 68
5.2. Regional Scale Lithostructural Host Domains 71
5.2.1. Proterozoic Borborema Province 71
5.2.2. São Francisco Craton 72
5.2.3. Paleozoic Parnaíba Basin 73
5.3. Mafic Dykes in NE Brazil 74
5.4. Airborne Geophysical Database 76
5.4.1. *Gamma-spectrometric Data Processing and Analyzing* 78
5.4.2. Magnetic Data Processing and Analyzing 80
5.4.3. Airborne geophysical interpretation 85
5.5. Field Relationships 86

5.6. Structural Characterization of Dyke 88
5.6.1. Rio Ceará-Mirim dyke swarm (RCM) 92
5.6.2. Canindé Dyke Sub-swarm (CD) 94
5.6.3. Riacho do Cordeiro Dyke Sub-swarm (RC) 95
5.6.4. Spatial Distribution of Dykes 95
5.7. Discusions 97
5.7.1. Chronological relationship analysis of dyke sets 97
5.7.2. *Geodynamic Analysis* 98
5.8. Conclusions 101
Acknowledgments 102
References 102

6. CONSIDERAÇÕES FINAIS 113

REFERÊNCIAS 116

LISTA DE FIGURAS

Figura 1.1: Mapa geológico simplificado da Província Borborema. As principais estruturas e eventos magmáticos foram compilados e/ou modificados de Oliveira (1992), Cavalcante et al. (2003), Delgado et al. (2003), Angelim et al. (2006), Van Schmus et al. (2008), Oliveira e Medeiros (2012). …….…………………………………..........…… 6

Figura 2.1: Morfologia de deslocamento de diques. As ilustrações mostram casos em que há o desmembramento e a movimentação dextral ou sinistral dos segmentos de diques para a formação de Ponte (A, B, C e D); Salto (E); Degrau (F) e Chifre (G). Adaptado de Rickwood (1990). 11

Figura 2.2: Geometria dos grandes enxames de diques. Padrão linear de leque contínuo (A); Padrão em leque subdividido em subenxame (B); Subenxames em diques paralelos, que irradiam de um ponto comum (C); Diques subparalelos espalhados por uma área (D); Diques subparalelos em uma zona restrita (E); Padrão radial (F). As estrelas indicam a localização da pluma. Adaptado de Ernst e Buchan (1997, 2001). 13

Figura 2.3: As estrelas representam a distribuição global das LIP's. Em vermelho: LIP's geradas por uma cabeça de pluma transitória. Em azul: LIP's geradas por uma cauda de pluma persistente. Modificado de Coffin e Eldholm (1994) e Cinzia e Hofmann (2011). 14

Figura 3.1: Valores médios de susceptibilidade magnéticos para os principais tipos de rocha. Modificado de Kearey et al. (2009). 17

Figura 3.2:Ilustração da aplicação do filtro de redução ao polo. Adaptado de Blakely (1996). 18

Figura 3.3: Espectro de potência dos dados magnéticos (em verde) e o espectro de quatro camadas equivalentes (em vermelho) (A). Os filtros passa-banda correspondem às quatro camadas equivalentes (B). Fonte: Phillips (2001). ...……………….............................. 19

Figura 3.4: Espectro típico da radiação gama indicando as janelas energéticas convencionais do potássio (K), urânio (U) e tório (Th). Modificado de Minty et al. (1997). ...……………….. 21

Figure 3.5: Síntese das etapas de uma análise em ambiente de Self-Oganizing Maps. Adaptado de Carneiro (2010). ………………………………………………………… 25

Figure 4.1: Simplified geological map of the Borborema Province (BP), NE Brazil. Main structures and magmatic events were compiled and modified from Oliveira (1992), Cavalcante et al. (2003), Delgado et al. (2003), Angelim et al. (2006), Van Schmus et al. (2008), Oliveira and Medeiros (2012). Insert: Figure 4.7. …………………………….. 30

Figure 4.2: Airborne geophysical surveys covering the Borborema Province (BP) and its boundaries with the Paleozoic Parnaíba Basin and São Francisco Craton (A). Geophysical maps: total magnetic intensity (TMI) (B); reduced to pole magnetic anomaly (RTP) (C); K (D), eTh (E), and eU (F) radioelements. ……………………………..…………… 33

Figure 4.3: Analytic signal amplitude map of the Borborema Province (BP), showing the location of the samples collected and the magnetic susceptibility measurements (colored dots). Insert: Figure 12. ………………………………………………………….. 35

Figure 4.4: Training of the "seed-vectors" and their neighbors toward the input sample marked "x". The solid lines represent the situation before the training and the dashed lines correspond to the positions after training. The blue and red circles represent seed-vectors and trained best-matching units (BMUs), respectively. The QER is the distance between the sample (x) and the nearest trained red dot (BMU). The black vectors show the movement of the seed-vectors. ……………………………………….…………….. 39

Figure 4.5: Self-organized map outputs computed using the BP training area data: (A) U-Matrix; - where warm colors represent high dissimilarity and cool colors high similarity between adjacent nodes. Component Plan Plots are shown on (B) RTP; (C) ASA; (D) K; (E) eTh; and(F) eU, where warm colors represent high contribution, and cool colors represent low contributions to the SOM. Black ellipses indicate areas with high values of RTP, ASA and K correlate with high contribution in U-matrix. Purple circles display areas with high values in eTh, eU and U-matrix plots. ………………………………... 40

Figure 4.6: Davies-Bouldin index (y axis) for the K-means clustering (x axis). Seven was chosen as an optimum number of clusters (red circle) as it was the lowest number of clusters with the first lowest Davies-Bouldin index value. ………………..………… 41

Figure 4.7: Geological and geophysical data (location in Fig. 4.1) used as input to the SOM training: geological map modified from Cavalcante et al. (2003) (A); RTP (B) and ASA magnetic variables (C); K (D), eU (E), and eTh (F) radioelements. Shear zones: OR – Orós; SP – Senador Pompeu. ………………………………………………………….. 42

Figure 4.8: Comparison between the SOM classification of clustered populations in the training area, considering two alternative datasets: only magnetic data (A) with 4 classes of clustered populations; and magnetic and gamma-spectrometric data with 4 (B), 7 (C), 9 (D), 11 (E), and 22 (F) classes of clustered populations. ……………………………. 45

Figure 4.9: SOM solution map of the training area, displaying each sample coded by its population color. The black lines represent the geological features shown in Figure 4.7A………………………………………………………………………….……….... 49

Figure 4.10: Typical exposures of the Rio Ceará-Mirim Dyke Swarm (RCM), showing the contact between the dyke and its host rock (sandstone) on the ground (A) or forming small hills (B); and displaying onionskin weathering. ………………………………… 51

Figure 4.11: Distribution of SOM-derived clustered populations (1 - yellow and 6 - orange) related to mafic dyke swarm occurrence in the Borborema Province, Paleozoic Parnaíba Basin and São Francisco Craton computed from airborne geophysical data (A). Comparison between previously mapped dykes (bold black lines) and those suggested by SOM solutions (B and C). Sedimentary basins: IG – Iguatu; RP – Rio do Peixe. Shear zones: OR – Orós; PA – Patos; PE – Pernambuco; SP – Senador Pompeu. Dyke swarms: Rio Ceará-Mirim – RCM; Canindé – CD; Riacho do Cordeiro – RC........................... 52

Figure 4.12: Comparison between ASA map (left), SOM solutions related to mafic dykes (middle), and the comparison between SOM-derived dykes and previously mapped dykes and geological structures (right) in distinct regions of the Borborema Province (A, B and C). Locations in Figure 4.3. ……………………………………………………………… 53

Figure 5.1: Schematic reconstruction map of the West Gondwana, showing the main cratonic areas – Amazonian, São Francisco (SF) - Congo, São Luís - West African and Kalahari (A) and the Borborema Province (BP); Pre-drift reconstitution of the main geological features of the NE Brazil and the west African counterpart, modified from Ngonge et al. (2016) (B); Simplified geological map of the Borborema Province (BP) (C). Main structures and magmatic events were compiled and modified from Oliveira (1992),

Cavalcante et al. (2003), Delgado et al. (2003), Angelim et al. (2006), Van Schmus et al. (2008), Oliveira and Medeiros (2012), Hollanda et al. (2019) and Melo et al. (2021). 70

Figure 5.2: Airborne geophysical surveys covering the Borborema Province and its southern boundary with the São Francisco Craton and Parnaíba Basin (A); Data processing workflow applied for each survey (location in Figure 2A) (B). See Tab. 4.1 for specifications about airborne geophysical surveys. ……………………………... 77

Figure 5.3: Gamma-spectrometric maps: K (A), eTh (B), eU (C), RGB (D), and CMY (E) ternary composition. Shear zones and sedimentary basins are well marked on ternary maps; Iguatu basin in black and Orós shear zone in white color (F); Iguatu basin in white color and Orós shear zone in black color (G). ………………………….……… 79

Figure 5.4: Magnetic anomaly maps of the Borborema Province: total magnetic intensity (A); total magnetic intensity reduced to magnetic pole (RTP) (B); analytical signal amplitude of the RTP anomalies (RTP_ASA), with the location of the samples collected and the magnetic susceptibility measurements (colored dots) (C). Matched Filter maps for equivalent source layers: DMS - magnetic anomaly of deep sources, related to structures in the deep upper crust (D); IMS1 - magnetic anomaly of intermediate sources 1, related to upper crust features (E); IMS2 - magnetic anomaly of intermediate sources 2, related to dykes within the province (F); SMS magnetic anomaly of shallow sources, related to near-surface magnetic sources and residual data noise (G); and analytical signal amplitude of intermediate 2 magnetic anomaly (IMS2_ASA) (H). Zoomed IMS2 (I) and IMS2_ASA (J) maps of the Iguatu Basin illustrate details of the magnetic patterns of sedimentary basins, shear zones and dykes. ………………………………………… 82

Figure 5.5: Typical exposure of the Rio Ceará-Mirim Dyke Swarm (RCM). Outcrop showing RCM alignment (A); phaneritic texture (basaltic) in a rock sample (B); aphanitic texture in a rock sample (C); Outcrop displaying dyke with spheroidal weathering (D). …………………………………………………………………………………..….. 87

Figure 5.6: Spatial distribution of dyke swarms in the Borborema Province and surrounding areas (NE Brazil), based in our qualitative interpretation. Dotted lines show dykes interpreted from the aeromagnetic maps by Melo et al. (2021). Solid lines denote dykes mapped based on magnetic anomalies, but also visible in Google Earth™ satellite images data and validated by field work. …………………………………………… 89

Figure 5.7: Rose diagrams of the dyke directions mapped in the Borborema Province (NE Brazil). Red – Rio Ceará-Mirim (RCM), Green – Canindé (CD) and blue – Riacho do Cordeiro (RC). ……………………………………………………….......................... 90

Figure 5.8: Thin dykes well marked on Google Earth™ satellite images (A), which are not detected on aeromagnetic maps (analytical signal of the IMS2 magnetic anomaly - B), probably due to self-demagnetization. Dykes interpreted from Google Earth™ satellite images, geophysical maps and field work (C). …………………..………… 92

Figure 5.9: Total magnetic intensity (A, A'); Analytical signal of the IMS2 magnetic anomaly (B, B'); and Dykes interpreted from Google Earth™ satellite images, geophysical maps, and field work (C, C') of two areas across the Rio Ceará-Mirim dyke swarm (RCM), whose locations are shown in Fig. 5.6. ………………………………. 93

Figure 5.10: Spatial density of mapped dykes in the Borborema Province (NE Brazil). Contour lines represent number of dykes for 50 km cells. …………………………….. 96

Figure 5.11: Paleostress trajectories of dykes in the Borborema Province (NE Brazil) derived from dyke spatial distribution. ………………..……………………….….. 100

LISTA DE TABELAS

Tabela 2.1:Classificação de Rickwood (1990), considerando espessura e comprimento de diques. 9

Table 4.1: Airborne geophysical survey specifications. Survey: 1027 – Borda Sul da Bacia do Parnaíba, 1042 – Norte da Chapada Diamantina, 1067 – Pernambuco/Piauí (PE/PI), – Médio São Francisco, 1074 – Novo Oriente, 1079 – Borda Leste do Planalto da Borborema (RN, PB, PE, AL), 1086 – Norte do Ceará, 1087 – Médio São Francisco, 1091 – Pernambuco/Paraíba, 1092 – Paraíba/Rio Grande do Norte, 1101 – Centro-Sudoeste do Ceará, 1102 – Estado de Sergipe, 1103 – Oeste de Tucano, 1104 – Paulo Afonso/Teotônio Vilela, BP – Bacia Potiguar. CS – Company Survey; NFH – nominal flight height; FLD – flight-line direction; FLS – flight-line spacing; TLD – tie-line direction; TLS – tie-line spacing; MFI – magnetic field inclination; MFD – magnetic field declination. (For detailed information, access the Geophysical Surveys and Associated Products of the Geological Survey of Brazil at http://geosgb.cprm.gov.br/geosgb/downloads_en.html). …………………………...… 34

Table 4.2: Reference values of magnetic (RTP and ASA) and gamma-spectrometric (K, eTh and eU) data to determine the classification of SOM variable samples. ….……… 46

Table 4.3: Medium values and classification of variables for each SOM-derived cluster population. ……………………………………………………………………….. 47

Table 5.1: Airborne geophysical survey specifications. CS – Company Survey; NFH - nominal flight height; FLD - flight-line direction; FLS - flight-line spacing; TLD - tie-line direction; TLS - tie-line spacing; MFI - magnetic field inclination; MFD - magnetic field declination. Additional information about the surveys are available in the electronic site of the Geophysical Surveys and Associated Products of the Geological Survey of Brazil at http://geosgb.cprm.gov.br/geosgb/downloads_en.html. ………..…………… 78

Table 5.2: Summary of Magnetic Susceptibility (MS in $\times 10^{-3}$ SI) of dyke rocks collected in the Borborema Province (NE Brazil). ………..…………………………….……….. 83

Table 5.3: Dyke swarm length (in km) mapped in the Borborema Province (NE Brazil). RCM – Rio Ceará-Mirim, CD – Canindé, RC – Riacho do Cordeiro. ………..…......... 88

Table 5.4: Dyke width (in meters) mapped in the Borborema Province (NE Brazil). … 91

Capítulo 1

INTRODUÇÃO

1.1. Apresentação

O presente trabalho constitui a tese de doutorado que integra os requisitos necessários para a obtenção do título de Doutora em Geodinâmica e Geofísica do Curso de Doutorado do Programa de Pós-graduação em Geodinâmica e Geofísica (PPGG) da Universidade Federal do Rio Grande do Norte (UFRN). Esta pesquisa foi desenvolvida sob a orientação do Prof. Dr. David Lopes de Castro.

Esta tese está associada ao projeto The Equatorial Atlantic Magmatic Province (EQUAMP): Identifying a new large igneous province in NE Brazil, coordenado pela Professora Maria Helena Hollanda do Instituto de Geociências (IGC) da Universidade de São Paulo (USP). Este projeto visa estudar os eventos magmáticos expostos no Nordeste do Brasil que estejam relacionadas com a evolução da margem continental atlântica durante o Cretáceo e ao desmembramento do Gondwana Ocidental. Esses eventos são representados por: (1) enxames de diques máficos arqueados (doleritos) em escala continental denominados Rio Ceará-Mirim, que atravessa um importante bloco pré-cambriano, a Província Borborema, e (2) soleiras da Formação Sardinha que intrudem a sucessão sedimentar da bacia Paleozoico do Parnaíba. Este projeto de pesquisa pretende categorizar formalmente a EQUAMP como uma nova Grande Província Ígnea (LIP) na América do Sul. Para ter sucesso em nossa iniciativa seguiremos as recomendações da LIP de modo a estudar as soleiras da Bacia do Parnaíba e os enxames de diques da Província Borborema com base nas relações de campo, geofísica, geoquímica, idade, estrutura e propriedades magnéticas.

A pesquisa desenvolvida nesta tese abordada a cartografia geofísica regional dos enxames de diques máficos da Província Borborema, utilizando dados aerogeofísicos, imagens de satélite e a técnica dos Mapas Auto-Oganizáveis (*Self-Organizing Maps* — SOM) para identificar e delinear a distribuição dos enxames de diques que ocorrem na Província Borborema. Já que o mapeamento detalhado dos enxames diques possibilita uma análise em escala regional de sua geometria e cinemática, fornecendo entendimentos sobre sua origem (pluma ou não), que deve ser posteriormente testada por geoquímica.

Na presente tese, foi efetuado um mapeamento semiautomático, empregando a técnica do SOM em dados aerogeofísicos. Objetivou-se a definição de populações de conjuntos de variáveis, que representassem os enxames de diques máficos na Província Borborema, no Nordeste do Brasil. Utilizando o *software SiroSOM*, foi possível mapear enxames de diques até então desconhecidos, revelando que os mesmos ocorrem de forma mais ampla do que se conhecia anteriormente, em toda a Província Borborema, intrudindo o Cráton São Francisco e a borda leste da Província Borborema. As análises baseadas nos mapas geofísicos demonstraram que os enxames de diques se estendem por 6,8 x 10^6 km. Os diques máficos estão agrupados em três enxames distintos com 1388 possíveis diques máficos distintos: 1135 - Rio Ceará-Mirim (RCM); 168 - Canindé (CD) 86 Riacho do Cordeiro - (RC). Esses enxames de diques mostram três orientações preferenciais E-W, NW-SE e NE-SW. Os enxames não invadiram as estruturas pré-existente do embasamento, assim como não ocorrem nas bacias rifte do Cretáceo na Província Borborema. A distribuição espacial e a análise estrutural dos diques permitiram estabelecer o campo de tensões ativo no momento da intrusão.

No processamento digital dos dados aerogeofísicos, foi utilizado o *software Oasis Montaj v.9.1*. Já o processamento dos mapas auto-organizáveis foi realizado no *software SiroSom v2.2*, desenvolvido pela *Commonwealth Scientific and Industrial Research Organisation* (CSIRO).

A partir das informações adquiridas foi produzido um artigo científico submetido ao *Journal of Applied Geophysics,* intitulado *Using Self-Organizing Maps in Airborne Geophysical Data for Mapping Mafic Dyke Swarms in NE Brazil* e um segundo manuscrito submetido ao periódico *Tectonophysics,* com o título de *Mesozoic Dyke Swarms in Borborema Province (NE Brazil): a Structural Analysis Based on Airborne Geophysical data and Fieldwork.*

1.2. Estrutura da Tese

A tese foi dividida em seis capítulos. O Capítulo 1 (Introdução) tem como finalidade apresentar a Tese, descrever seus objetivos, justificativas e localizar espacialmente o leitor em relação à área de pesquisa. Além disso, são apresentadas, de maneira resumida, as fontes dos dados aerogeofísicos utilizados neste trabalho e a sua distribuição espacial em relação à área de pesquisa. No entanto, por uma questão de objetividade, a metodologia aplicada a cada um desses dados é abordada apenas nos capítulos 4 e 5.

O Capítulo 2 reúne uma compilação das principais publicações no âmbito do contexto geológico e geofísico, respectivamente, com vistas a trazer um resumo geral sobre os aspectos gerais dos diques e dos enxames de diques.

A fundamentações teórica referente aos dados geofísicos e seu processamento são descritos no Capítulo 3. A técnica do SOM também é descrita neste capítulo.

No Capítulo 4, é apresentado o manuscrito "*Using Self-Organizing Maps in Airborne Geophysical Data for Mapping Mafic Dyke Swarms in NE Brazil*", submetido no dia 4 de maio de 2020 ao periódico *Journal of Applied Geophysics*. Aceito para publicação em 14 de maio de 2021. Esse manuscrito aborda a aplicação do SOM, utilizando dados aerogeofísicos para o mapeamento de enxames diques máficos no Nordeste do Brasil.

O Capítulo 5 compreende o manuscrito "*Mesozoic Dyke Swarms in Borborema Province (NE Brazil): a Structural Analysis Based on Airborne Geophysical data and Fieldwork*" submetido ao periódico *Tectonophysics* em maio de 2021. O trabalho proposto promove o mapeamento regional dos enxames de diques, possibilitando uma análise estrutural, integrando padrões geofísicos, dados de campo e uma compilação de mapas geológicos anteriores para descrever a distribuição detalhada dos enxames de diques na Província de Borborema.

No Capítulo 6, estão reunidas as considerações finais da tese com a síntese integradora das principais conclusões discutidas nos artigos científicos submetidos. E para finalizar, encontram-se as referências bibliográficas citadas nos capítulos que antecedem os artigos, permanecendo as referências dos artigos listados nos mesmos.

1.3. Justificativa

O estudo de diques máficos é de fundamental importância para a compreensão da geologia estrutural e da evolução geotectônica (Halls, 1982; Ernst, 2014). A distribuição temporal e espacial e o mecanismo de alojamento de enxames de diques máficos estão diretamente relacionados ao campo de tensão tectônico e à evolução crustal (Halls, 1982). A orientação dos enxames de diques fornece evidências sobre a paleotensão, cinemática crustal e regime geotectônico atuante durante a sua intrusão (Anderson, 1951; Halls, 1982; Delaney et al., 1986). Sendo assim, os enxames de diques representam importantes marcadores de tempo, que fornecem informações cronológicas sobre o processo geodinâmico, cinemática de rifteamento, atividade magmática e gênese de grandes províncias ígneas (*Large Igneous Provinces* – LIP's) (Ernst et al., 1996; Ernst, 2014; Demarco et al., 2020). Portanto, o mapeamento de enxames de diques máficos, especialmente aqueles de extensão regional, integrado com litogeoquímica, química mineral, geocronologia de alta resolução (K-AR, Ar-Ar, U-Pb) tornou-se uma fonte de dados imprescindível para pesquisas relacionadas a atividade de plumas do manto, grandes províncias ígneas (LIP's) e a tectônica de placas (Ernst e Buchan, 2001; Ni et al., 2018).

Mapear enxames de diques em escala regional é uma excelente abordagem para reconhecer os movimentos das placas, que podem culminar em ruptura continental, especialmente nas fases iniciais da extensão crustal, na reconstituição do estilo tectônico, assim como as forças atuantes durante o processo de rifteamento (Halls, 1982; Reeves, 2000; Ernst e Buchan, 2001; Zaineldeen, 2012). Entretanto, mapear enxames de diques em escala regional é uma tarefa difícil. O levantamento clássico de diques com base em trabalho de campo é demorado, custoso, além de ser dificultoso pelo fato de grande parte dos diques não serem aflorantes (Jessel, et al., 2015; Ni et al., 2018; Demarco et al., 2020).

Para auxiliar o mapeamento de diques são utilizados dados aerogeofísicos, especialmente aqueles que utilizam sensores magnéticos e gamaespectrométricos, para cartografia geológica e correlação com mapas geológicos prévios (Trumbull et al., 2004; Xiong et al., 2016; de Castro et al., 2018). No entanto, interpretar uma grande quantidade de dados e compreender a complexidade das interrelações entre o campo magnético, a distribuição de radioelementos e as unidades geológicas criam uma excelente oportunidade para o uso de técnicas de otimização para melhorar a eficiência e a eficácia da interpretação conjunta de múltiplos dados geofísicos.

Este problema pode ser objetivamente abordado usando técnicas de aprendizagem de máquina (*machine leanning*), que trabalhem no hiperespaço multivariado, usando parâmetros que quantificam características geológicas vistas em dados geofísicos, petrológicos, geoquímicos e geocronológicos. O SOM consiste em uma técnica não supervisionada desenvolvida para a análise integrada e mapeamento semiautomático, que funciona como uma ferramenta de análise e visualização de dados em espaço n-dimensional, baseada em princípios de quantização vetorial (VQ) e medidas de similaridade de vetor (VS) (Kohonen, 1982, 2001). Esta técnica tem sido utilizada com sucesso no mundo, inclusive no Brasil, para otimizar o mapeamento de unidades geológicas e geofísicas usando dados de múltiplas origens (Fraser e Dickson, 2007; Carneiro et al., 2012; de Castro et al., 2018).

1.4. Localização da área de estudo

A pesquisa foi realizada em uma área que abrange toda a Província Borborema (PB), que corresponde a um domínio geológico-estrutural localizado no Nordeste do Brasil. A PB tem uma extensão de aproximadamente 380.000 km² (Almeida et al., 1981) e é limitada a sul pelo Cráton São Francisco, a oeste pela Bacia do Parnaíba e a norte e leste pelas bacias costeiras (Fig. 1.1). Compreende uma vasta unidade geotectônica da plataforma sul-americana (Almeida et al., 2000) e consiste em um complexo mosaico de blocos crustais de diferentes idades, do Arqueano ao Proterozóico, amalgamados no último evento orogênico que afetou o território brasileiro, a Orogenia Brasiliana. Este período de colisão continental generalizado se desenvolveu desde o final do Neoproterozoico até o início do Fanerozoico, no contexto da construção do supercontinente Gondwana Oeste (Brito Neves e Cordani, 1991; Neves et al., 2000).

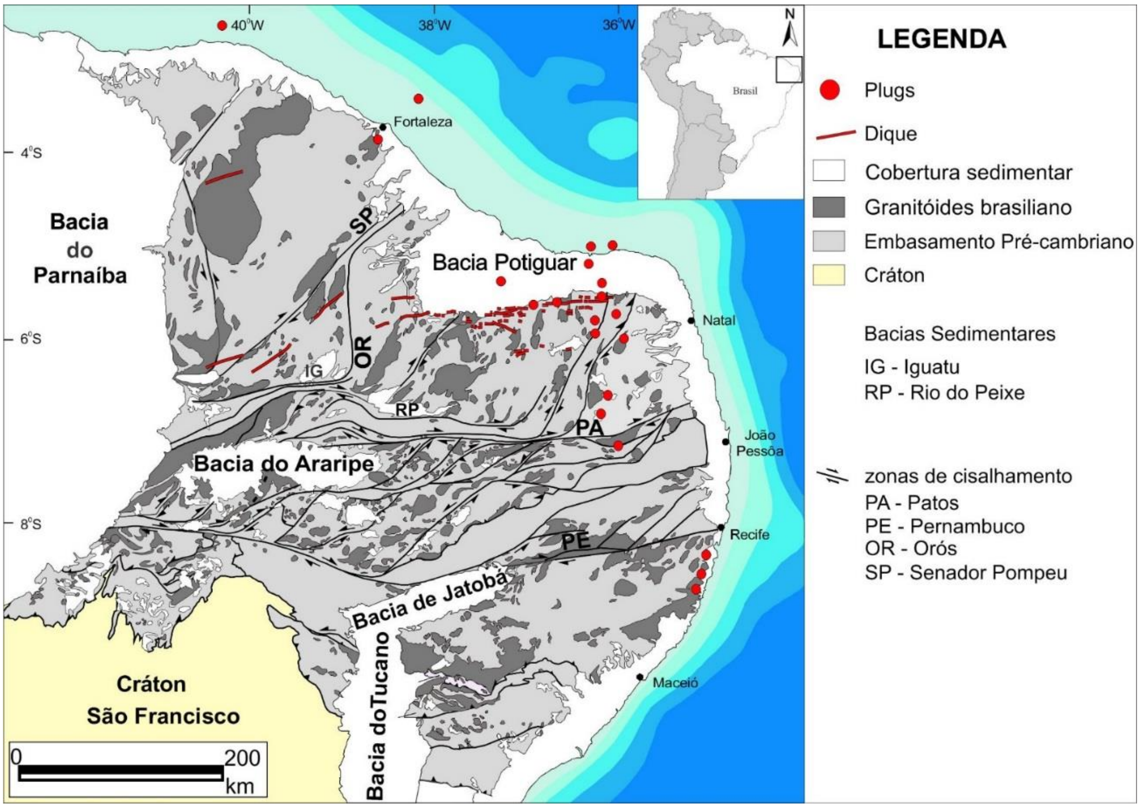

Figura 1.1: Mapa geológico simplificado da Província Borborema. As principais estruturas e eventos magmáticos foram compilados e/ou modificados de Oliveira (1992), Cavalcante et al. (2003), Delgado et al. (2003), Angelim et al. (2006), Van Schmus et al. (2008), Oliveira e Medeiros (2012).

1.5 Objetivos

O objetivo principal desta pesquisa é fazer o mapeamento regional dos enxames de diques, encontrar e estabelecer suas relações entre orientação, mecanismo de alojamento e controle estrutural. Para tanto, empregou-se uma técnica semiautomática para mapear os enxames de diques com base em conjuntos de dados aerogeofísicos e avaliar sua eficácia em atingir esse objetivo. Além de promover uma interpretação integrada de dados aerogeofísicos (gama-espectrométricos e magnéticos), análises estruturais dos mapas geofísicos, trabalho de campo e compilação de dados geológicos anteriores para analisar os enxames de diques da Província Borborema.

Para isto, enumeram-se os seguintes objetivos específicos:

- Desenvolver uma rotina semiautomática para identificar diques máficos, otimizando tempo de interpretação;
- Mapear os diques nos mapas geofísicos;
- Estabelecer relações geométricas capazes de promover interpretações morfológicas e geométricas dos diques;
- Determinar o padrão de esforços tectônicos atuante no momento da intrusão;

Com isso, este trabalho vem a preencher uma lacuna científica no que diz respeito ao mapeamento e à análise de diques máficos na Província Borborema, contribuindo para uma melhor compreensão do papel dos enxames de diques e sua evolução tectônica nos períodos Mesozoico e Cenozoico.

Capítulo 2

ASPECTOS GERAIS DOS DIQUES

2.1. Diques Máficos

Diques podem ser definidos como intrusões ígneas de forma tabular, de tamanhos variados, com comprimento muitas vezes maior que a largura e que cortam verticalmente ou sub-verticalmente discordante à estratigrafia de uma sequência ou de um outro corpo rochoso, estratificado ou não (Holmes, 1944; Mckenzie, 1984). Os diques representam uma expressão de processos distensivos da litosfera, desenvolvem-se em qualquer ambiente rúptil, alojando-se em diversos níveis crustais. São considerados como sendo os principais condutores de material mantélico para a crosta superior (Halls e Fahrig, 1987; Ernst e Buchan, 2001).

Os diques podem ocorrer isoladamente ou como enxames de diques, quando eles ocorrem em conjunto de diques subparalelos contemporâneos, exibindo uma geometria linear, radial ou semiradial (Ernst e Buchan, 2001). Os enxames de diques possuem proporções consideráveis em área, sendo são considerados excelentes indicadores de processos distensionais (Halls, 1982; Gudmundsson, 1990). Os enxames de diques máficos estão presentes em todos os continentes, com idades variando do Arqueano ao Recente (Halls, 1982; Halls e Fahrig, 1987).

Em geral, os diques apresentam uma relação de comprimento/largura máxima de 100:1 e mínima de 1:100. De acordo com Rickwood (1990), os diques podem ser classificados em função das suas dimensões, considerando comprimento e espessura (Tab. 2.1).

Tabela 2.1: Classificação de diques por Rickwood (1990), considerando suas espessuras e comprimentos.

Classificação	**Largura**	**Comprimento**
Microdique	< 1 cm	< 2 m
Minidique	1 – 10 cm	1 – 20 m
Dique	10 – 50 m	0,1 – 50 km
Macrodique	50 – 250 m	50 -250 km
Megadique	> 250 m	> 250 km

2.2. Morfologia de diques

A intrusão de um dique ocorre quando o magma sob pressão litostática abre caminho pela crosta através da propagação de uma fratura ou sistemas de fraturas. A direção de propagação dos diques depende da pressão exercida pelo magma e do campo de tensão regional atuante durante sua intrusão (Delaney et al., 1986). Por isso, a atitude dos diques é utilizada para determinar o paleotensão associado aos critérios cinemáticos da rocha encaixante e de fluxo de magma, juntamente com dados geocronológicos.

A direção de um dique é perpendicular ao eixo de menor esforço (σ_3), alojando-se no plano de distensão máxima, sendo esta correspondente à direção de abertura. A direção de propagação de um dique é determinada pela geometria dos seus segmentos. Em geral, a propagação de diques ocorre paralelamente ao eixo mais extenso do segmento (Anderson, 1951; Pollard, 1987). Entretanto, pode ocorrer abertura de diques com componentes de movimentação (dextrais ou sinistrais). Através da análise das bordas dos segmentos dos diques, nos contatos com a rocha encaixante, também é possível identificar qual foi o regime tectônico atuante durante a sua intrusão e propagação, podendo ser distensivo, transtensional ou transpressional (Rickwood, 1990).

Quanto a morfologia dos diques, as denominações mais comuns de segmentos de diques são ponte, salto, degrau e chifre (Fig. 2.1). Existe também uma geometria específica denominada *en-échelon*, que ocorre quando diques que se propagam a partir de uma estrutura prévia, ou quando a força da intrusão do corpo magmático – juntamente com distúrbios locais na rocha encaixante – provoca pequenas fraturas escalonadas provocando a rotação do esforço mínimo a medida que o dique se aproxima da superfície crustal (Rickwood, 1990; Oliveira, 1992).

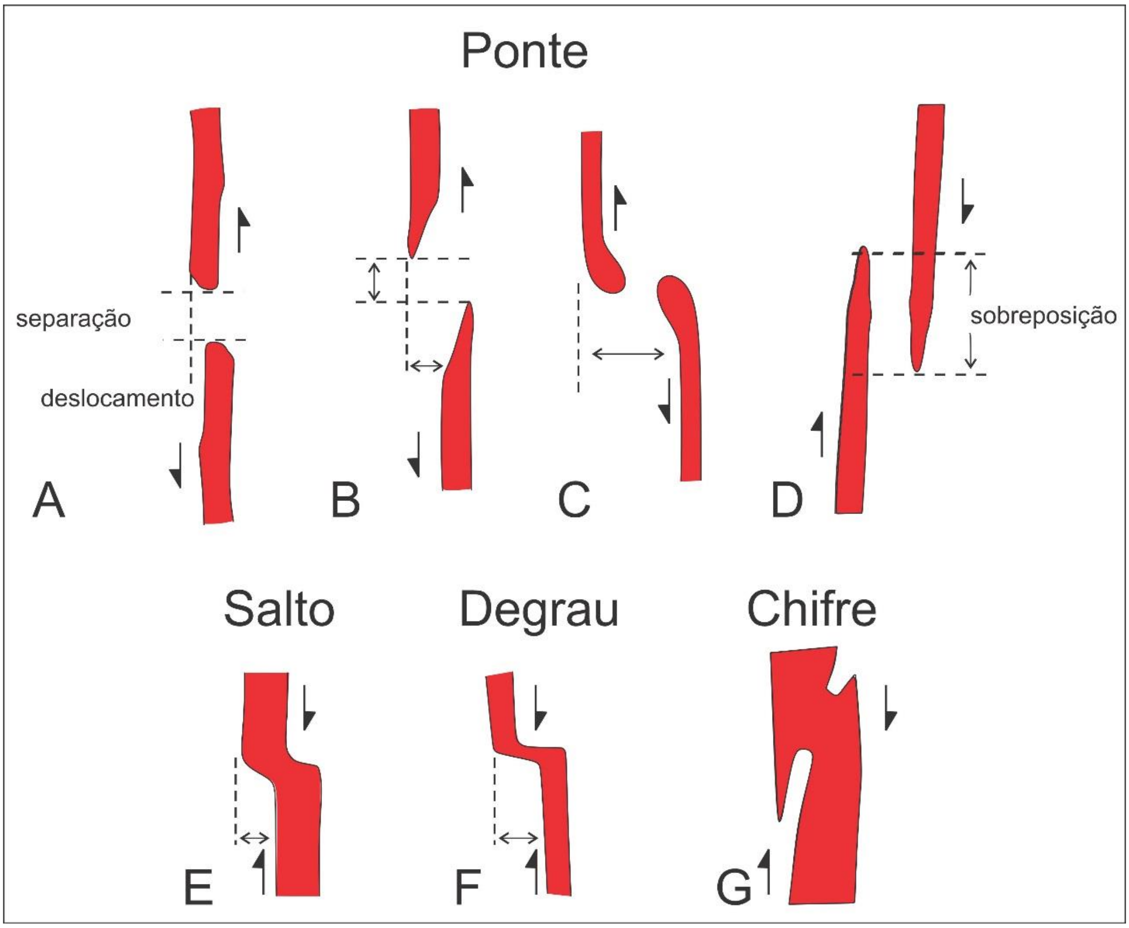

Figura 2.1: Morfologia de alojamento de diques. As ilustrações mostram casos em que há o desmembramento e a movimentação dextral ou sinistral dos segmentos de diques para a formação de morfologias do tipo Ponte (A, B, C e D); Salto (E); Degrau (F) e Chifre (G). Compilado de Rickwood (1990).

2.3. Geometria dos Enxames de Diques

A geometria e a estrutura de um enxame de diques podem sugerir um modelo tectônico de intrusão dos diques, tanto em limites divergentes como em zonas de riftes. Os enxames de diques concentram-se em zonas, de forma paralela ou subparalela, o que indica que foram submetidos a uma tensão constante, que atuou sobre uma vasta área.

Baseados na observação da geometria, disposição e extensão de enxames de diques gigantes (> 300 km de extensão), Ernst e Buchan (1997) propuseram um modelo para explicar a origem da formação dos diques, que, posteriormente, foi aprimorado em Ernst (2014). Nesses trabalhos, são descritos enxames de padrões lineares, arqueados e radiais (Fig. 2.2).

Os enxames de diques gigantes podem ser agrupados em seis grupos com base em sua geometria, de acordo com Ernst e Buchan (1997, 2001) (Fig. 2.2). Três dessas geometrias (Figs. 2.2A, B e C) exibem um padrão radial, ou seja, os diques irradiam de um ponto comum. A Figura 2.2A exibe um padrão de diques contínuos em leque. Esse tipo de geometria pode ser observada no Enxame de Diques de Mackenzie, localizado no nordeste da América do Norte (Ernst e Buchan, 1997). Os diques distribuidos em um padrão de leque, subdividido em subenxames da Figura 2.2B podem ser encontrados no Enxame de Diques Matachewan, também na América do Norte. Já o padrão de diques em subenxames de forma subparalela, em direções distintas (Fig. 2.2C) ocorre comumente associado ao riftemaento continental, como no caso dos diques do Paraná-Etendeka Ernst e Buchan (2001).

Os enxames de diques do tipo paralelos e semiradiais (Fig. 2.2D, E e F), podem ser interpretados como uma representação da porção distal dos enxames de diques observados nas Figuras 2.2A, B e C. O padrão do tipo semiradial pode ser observado na Figura 2.2D. Já a geometria para os enxames de diques representados nas Figuras 2.2E e F demostra uma distribuição linear, sendo os diques da Figura 2.2E subparalelos e ocorrendo em uma zona mais ampla, já os diques mostrados na Figura 2.2F se distribuem em uma área mais restrita (Ernst e Buchan, 1997, 2001).

No geral, os enxames lineares são correlacionados a processos de rifteamento, enquanto os enxames em forma de arco demonstram que ocorreram mudanças no campo de esforços regional durante o processo de intrusão dos diques. Já o padrão radial ou semiradial é indicativo de atividade de plumas mantélicas e/ou ruptura crustal a partir de junção tríplice (Ernst e Buchan, 1997, 2001).

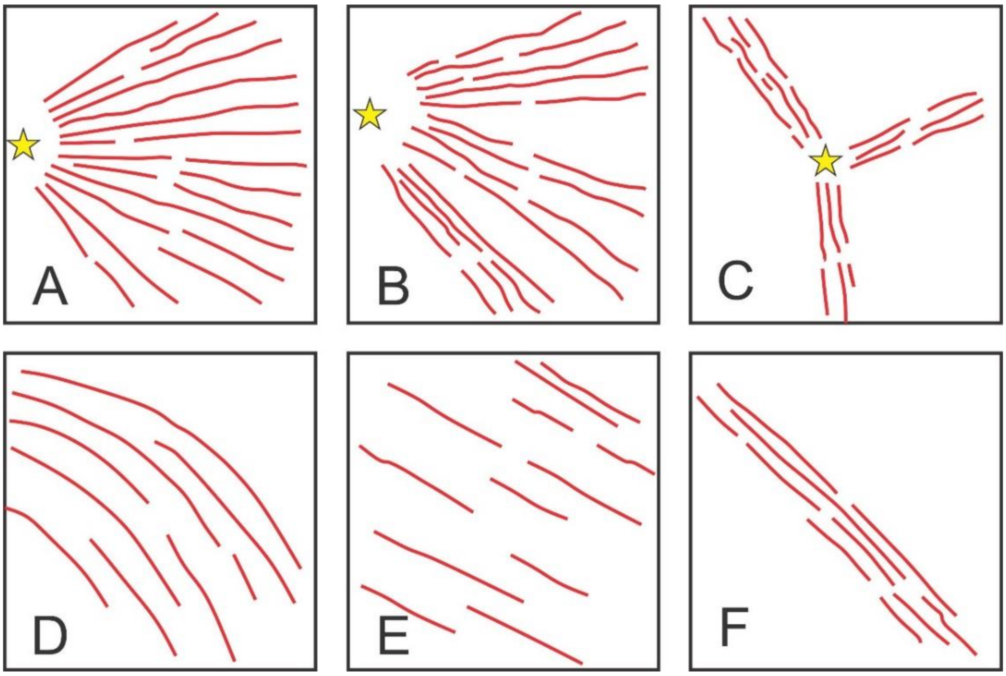

Figura 2.2: Geometria dos grandes enxames de diques. Padrão linear de leque contínuo (A); Padrão em leque subdividido em subenxame (B); Subenxames em diques paralelos, que irradiam de um ponto comum (C); Padrãos semiradial (D); Diques subparalelos espalhados por uma área (E); Diques subparalelos em uma zona restrita (F). As estrelas indicam a localização da pluma. Compilado de Ernst e Buchan (1997, 2001).

2.4. Grandes Províncias Ígneas (LIPs)

Grandes Províncias Ígneas (*Large Igneous Province* – LIP's) foram definidas como enormes intrusões magmáticas, predominantemente máficas e extrusivas, que tem sua origem desvinculada do espalhamento oceânico (Coffin e Eldholm, 1994; Foulger, 2007; Bryan e Ernst, 2008). As LIP's abrangem uma área com no mínimo 0,1 Milhões de km^2, possuem volumes ígneos superiores a 0,1 Milhões de km^3 e com uma duração total de no máximo 50 Ma. São caracterizadas por pulsos ígneos de curta duração (~1 - 5 Ma) entre os pulsos, durante os quais uma grande proporção do volume ígneo total (> 75%) é produzida. As LIP's que ocorrem em regiões intraplaca, no geral estão localizadas próximas das bordas de crátons, estendendo-se em zonas de rifte ou por descontinuidades pretéritas à intrusão do magmatismo (Fig. 2.3).

As LIP's continentais Mesozoicas – Cenozoicas estão relacionadas à processos de rifteamento continental, desenvolvimento de margens continentais, formação de bacias oceânicas e de sistemas de espalhamentos de dorsais mesoceânica. Entretanto, a instalação inicial da LIP ocorre anterior à formação da bacia oceânica, e a composição magmática da LIP é, do ponto de vista geoquímico, distinta do magma gerado nas bordas de placas divergentes (Coffin e Eldholm, 1994).

A maioria das LIP's é predominantemente máfica (< 56% de SiO_2), sendo o principal tipo de rocha os basaltos toleiíticos. Todavia, há algumas LIP's silicáticas, de composições variada, com componentes extrusivos e intrusivos, desde basaltos a riolitos.

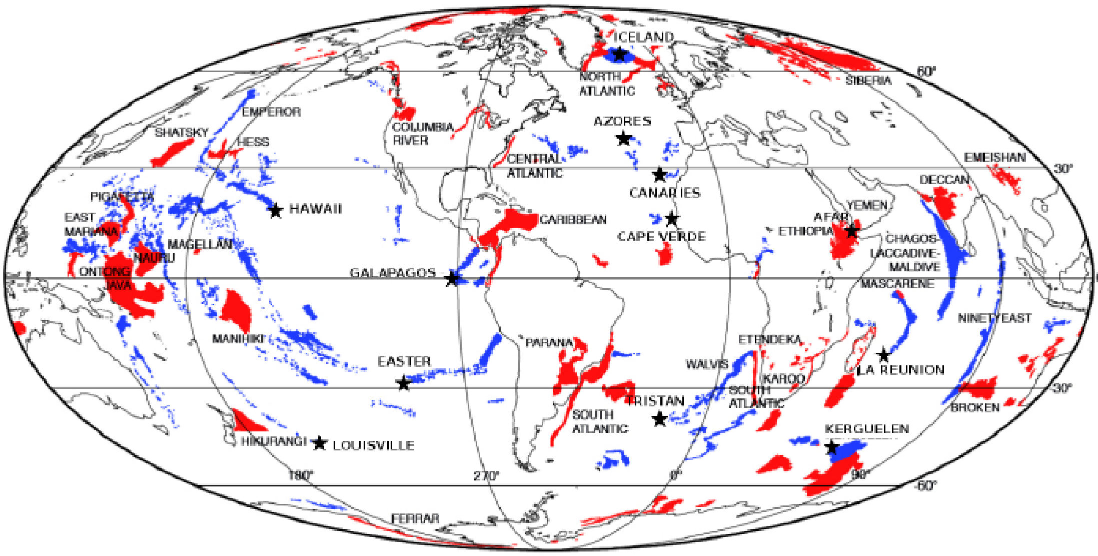

Figura 2.3: As estrelas representam a distribuição global das LIP's. Em vermelho: LIP's geradas por uma cabeça de pluma transitória. Em azul: LIP's geradas por uma cauda de pluma persistente. Compilado de Coffin e Eldholm (1994) e Cinzia e Hofmann (2011).

Capítulo 3

FUNDAMENTAÇÃO TEÓRICA

3.1. Anomalias Magnéticas de Rochas Ígneas

Devido a sua natureza alóctone, corpos ígneos, como diques, soleiras, fluxos de lava e rochas vulcânicas, apresentam, via de regra, contrastes de suas propriedades físicas e químicas com as rochas encaixantes. Associa-se ao fato de seus contatos serem abruptos, fazendo com que estas unidades rochas sejam fontes de expressivas anomalias geofísicas, especialmente gravimétricas, magnéticas e, por vezes, gama-espectrométricas. Nestes casos, levantamentos geofísicos aerotransportados podem ser um procedimento eficaz para mapear corpos ígneos em escala regional, especialmente aqueles não aflorantes, sendo essenciais para estimar o tamanho original e a extensão de grandes províncias magmáticas.

A Magnetometria auxilia na delimitação de unidades litológicas através do contraste das propriedades magnéticas de um pacote rochoso em relação às unidades vizinhas, bem como na identificação de feições estruturais, tais como falhas, zonas de cisalhamento e contatos. Em bacias sedimentares, cujo preenchimento rochoso tem baixa magnetização, as anomalias magnéticas mais expressivas estão relacionadas a rochas cristalinas do embasamento ou a corpos ígneos inseridos nas camadas sedimentares, como *plugs*, diques, soleiras e rochas vulcânicas.

As anomalias magnéticas são causadas por minerais magnéticos contidos nas rochas. O aumento do conteúdo ferromagnesiano em rochas ígneas máficas intensifica sua susceptibilidade magnética e, por conseguinte, as amplitudes do sinal magnético (Kearey et al., 2009). Porém, não é possível identificar com certeza a litologia causativa da anomalia com base apenas nas anomalias magnéticas (Xiong et al., 2016). As fontes de anomalias magnéticas locais não podem ser muito profundas porque as temperaturas abaixo de 20 km de profundidade (cerca de 580^{o}C) ultrapassam a temperatura de Curie, ponto em que as rochas perdem suas propriedades magnéticas (Kearey et al., 2009).

A susceptibilidade magnética é um dos principais parâmetros no método magnético. Materiais, como as rochas e minerais, que possuem grande susceptibilidade quando expostos a um campo magnético externo, tendem a magnetizar-se mais fortemente do que materiais com baixa susceptibilidade. A Figura 3.1 traz os valores típicos da susceptibilidade magnética das rochas.

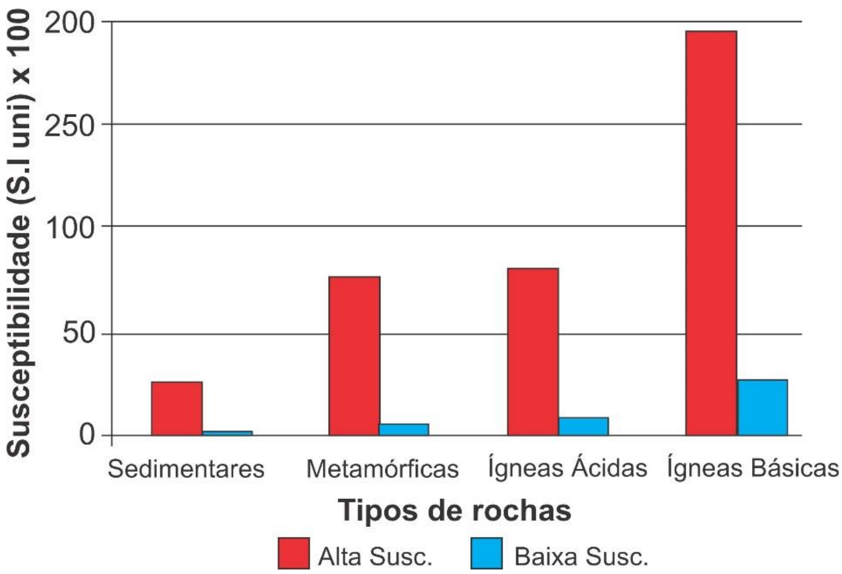

Figura 3.1: Valores médios de susceptibilidade magnéticos para os principais tipos de rocha. Modificado de Kearey et al. (2009).

3.2. Processamento dos Dados Magnéticos

Um mapa de anomalia magnética é a resultante da soma de uma série de anomalias causadas por diferentes tipos de fontes causativas, rasas e profundas. As fontes magnéticas profundas estão associadas a corpos e estruturas geológicas regionais. As fontes rasas podem ser de interesse prospectivo, como depósitos minerais, que ocorrem nos níveis rasos da crosta. A separação do efeito dessas fontes requer uma série de processamentos que permitam ao intérprete adequá-las para o processo de interpretação e integração geológica, bem como, para sua modelagem e quantificação. Muitas dessas transformações são, por vezes, empregadas para eliminar ruídos e / ou na manipulação da forma da anomalia para posicioná-la mais precisamente sobre a sua fonte e realçar características específicas das fontes, como contatos laterais e profundidades relativas. Numerosas técnicas de realce de anomalias estão disponíveis na literatura para auxiliar na interpretação dos mapas magnéticos, como a Redução ao Polo, *Matched-Filter* e Amplitude do Sinal Analítico. Este fluxo de processamento foi aplicado a cada levantamento aeromagnético separadamente, sendo depois integrados com a ferramenta Gridknit do *software* Oasis Montaj. Tais levantamentos aéreos e detalhes do seu processamento serão descritos nos capítulos 4 e 5.

3.2.1. Redução ao Polo

A Redução ao Polo (RTP) envolve a conversão das anomalias magnéticas em suas formas equivalentes como ocorrem no polo norte magnético (Blakely, 1996). As vantagens são o posicionamento correto da anomalia sobre a sua fonte, e a facilidade na sua interpretação, pois, nesse caso, transforma uma anomalia de caráter dipolar em uma anomalia monopolar. Este filtro desloca o máximo da anomalia, fazendo com que se localize exatamente em cima do corpo causador (Fig. 3.2) (Baranov e Naudy, 1964; Kearey et al., 2009).

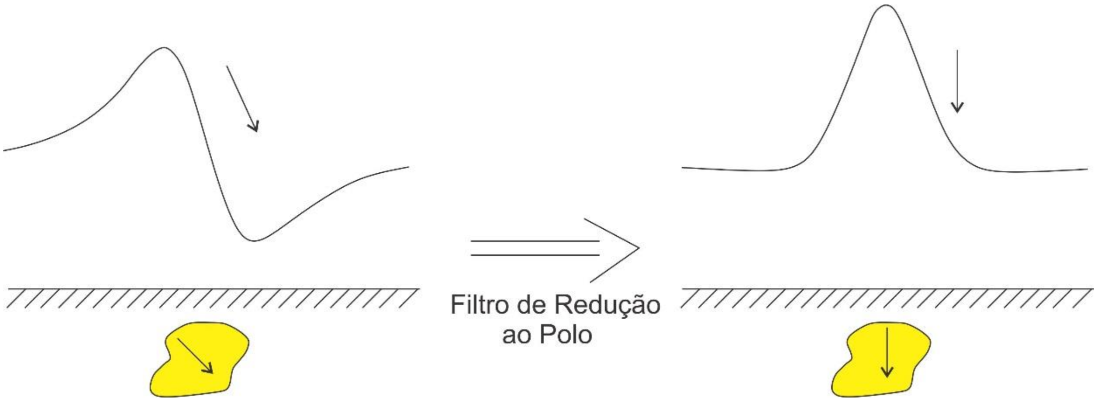

Figura 3.2: Ilustração da aplicação do filtro de redução ao polo. Adaptado de Blakely (1996).

A Redução ao Polo é uma operação instável para baixa latitudes magnéticas (±20°), gerando alta amplitudes na direção da declinação magnética. Porém, a introdução de uma pseudo-inclinação magnética (Ia) permite corrigir a fase da anomalia, sem amplificar erroneamente sua amplitude. A equação para a aplicação deste filtro no domínio da frequência é apresentada abaixo, onde I é a inclinação geomagnética da região na época do levantamento, Ia é a pseudo-inclinação, D é a declinação do campo geomagnético da região na época do levantamento e θ é a latitude A pseudo-inclinação para a correção de amplitude é, geralmente, calculada empiricamente como sendo o complemento da inclinação magnética (Ia = 90 - I).

$$RTP = \frac{[\sin(I) - i\cos(I)\cos(D-\theta)]^2}{[\sin^2(Ia) + \cos^2(Ia)\cos^2(D-\theta)].[\sin^2(I) + \cos^2(I)\cos^2(D-\theta)]}$$

3.2.2. Matched Filter

A técnica do *Matched Filter* (MF) propõe, através do uso de filtros passa-banda e azimutais otimizados por um algoritmo de inversão (Fig. 3.3), proporcionar um melhor ajuste do espectro de potência do sinal geofísico para separar o conteúdo do sinal para diferentes profundidades médias das fontes a partir do princípio das camadas equivalentes (Phillips, 2001). A técnica permite a separação de anomalias com base nos seus diferentes comprimentos de onda baseada na premissa das fontes de anomalias profundas serem representadas por sinais de baixa frequência, enquanto fontes de anomalias rasas apresentam conteúdo de alta frequência (Spector e Grant, 1970).

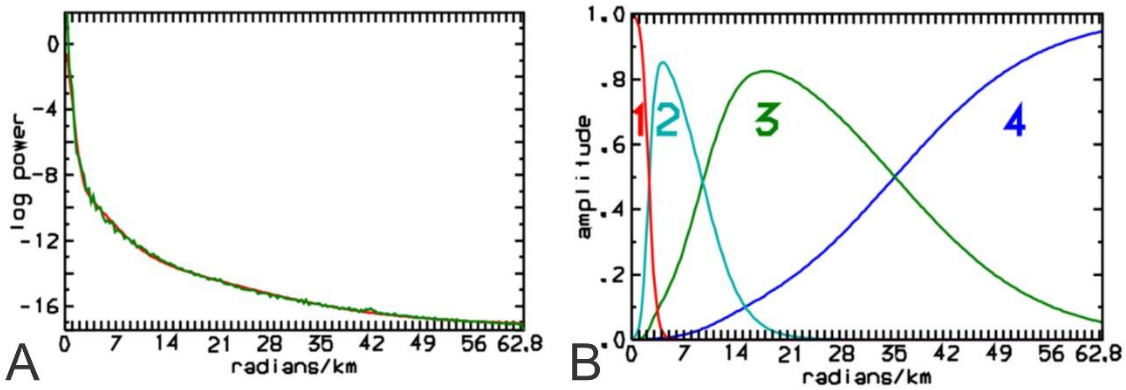

Figura 3.3: Espectro de potência dos dados magnéticos (em verde) e o espectro de quatro camadas equivalentes (em vermelho) (A). Os filtros passa-banda correspondem às quatro camadas equivalentes (B). Compilado de Phillips (2001).

O MF opera no domínio da frequência por meio da transformada de Fourier a partir da análise espectral do sinal. Os sucessivos filtros passa-banda eliminam os conteúdos de frequência indesejados do sinal para o conjunto de fontes relacionados à camada equivalente específica. A operação do MF é dada pela equação abaixo, onde kx e ky são os números de onda nas direções preferenciais dos vetores unitários **i** e **j**, |k| = $[(kx)^2+ (ky)^2]$ ½ e B é uma constante proporcional à amplitude de ruído de magnetização ou contraste de densidade dentro da camada.

$$|F(k_x,k_y)| = |F(|k|)| = B|k|^n e^{-|k|z}$$

3.2.3. Amplitude do Sinal Analítico

O filtro de Amplitude do Sinal Analítico (ASA) é um filtro útil para o mapeamento de bordas de corpos e feições estruturais. Realçando corpos com largura partir de 20 cm, e de comprimento que variam de poucos centímetros a dezenas de quilômetros. Segundo Blakely (1996), o ASA consiste na combinação dos gradientes horizontal e vertical da anomalia. Seus resultados são dependentes da profundidade, extensão e ângulo de mergulho do corpo, além da direção do campo magnético da Terra. O efeito da amplitude do sinal analítico é realçar as bordas das fontes das anomalias e é muito útil no caso de dados magnéticos que contenham influência de magnetização remanescente ou medidos a baixas latitudes. Os picos do sinal analítico são simétricos e ocorrem diretamente sobre toda a extensão das bordas dos corpos e no centro do limite do mesmo. Interpretações do sinal analítico podem fornecer indicações da geometria das fontes magnéticas, sendo possível inferir o tamanho do corpo. Se as fontes dos picos forem contatos magnéticos verticais, a largura da anomalia é proporcional a sua profundidade (Nabighian, 1972). A Amplitude do Sinal Analítico é dada pela equação abaixo, onde A são os valores do campo magnético anômalo.

$$ASA = \sqrt{\left(\frac{\partial A}{\partial x}\right)^2 + \left(\frac{\partial A}{\partial y}\right)^2 + \left(\frac{\partial A}{\partial z}\right)^2}$$

3.3. Fundamentos da Gamaespectrometria

A gamaespectrometria mede as contagens e/ou concentrações dos elementos radioativos potássio (K), urânio (U) e tório (Th) nos primeiros 30-40 cm da superfície da Terra, por meio da detecção da radiação gama (γ) emitida pela desintegração desses elementos. Essa desintegração ocorre devido à instabilidade do núcleo do átomo radioativo, ocasionando a liberação de energia pela emissão de partículas alfa (α), beta (β) e gama (γ) (Dickson e Scott, 1997; Minty, 1997).

A aerogamaespectrometria mede os valores relativos dos radioelementos através da interação da energia emitida com o gamaespectomêtro que detecta o efeito causado pelos pulsos energéticos que são gerados. Estes pulsos são amplificados e discriminados no analisador multicanal, gerando um espectro. Esta quantificação é possível a partir do ajuste das energias dos espectros com uma fonte padrão, pois os comprimentos de onda são específicos para cada elemento e suas intensidades são proporcionais à concentração do elemento na amostra, sendo expressa a partir da conversão das energias detectadas em contagem por segundo para unidade de massa (Minty, 1997) (Fig. 3.4).

A energia é dada em elétron-volt (eV), que é equivalente à energia cinética adquirida por um elétron sob a ação do potencial de um volt. Os raios gama possuem frequências de 10^{19} a 10^{25} s^{-1}, com comprimento de onda de 10^{-11} a 10^{-13}m, sua energia varia de 40KeV a 4 4MeV.

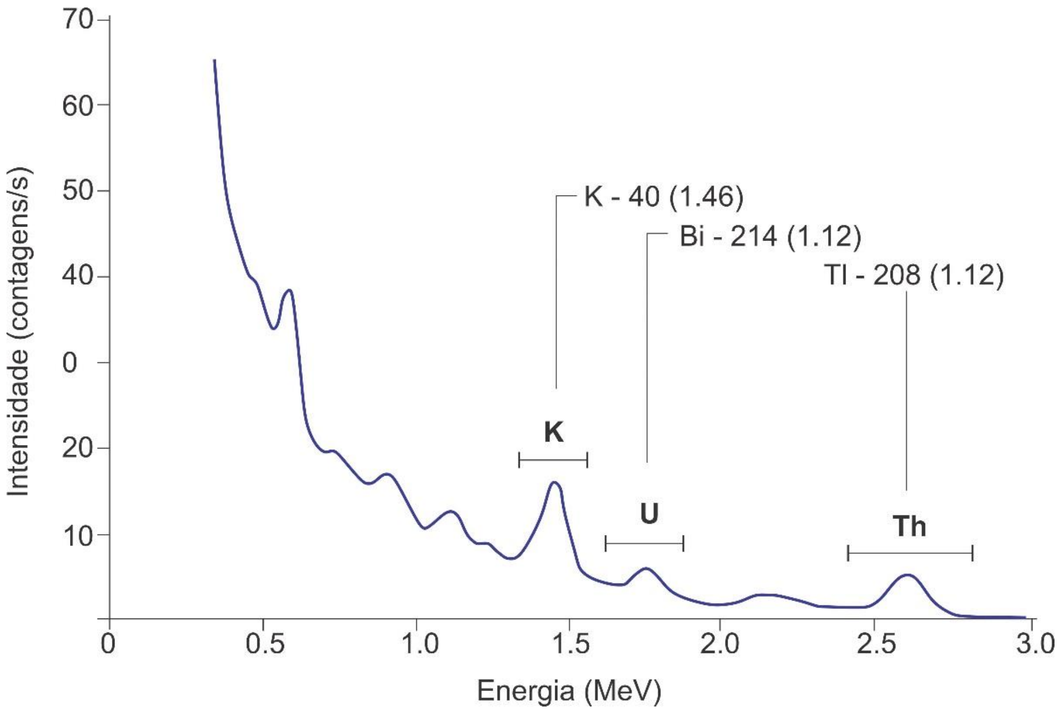

Figura 3.4: Espectro típico da radiação gama indicando as janelas energéticas convencionais do potássio (K), urânio (U) e tório (Th). Modificado de Minty et al. (1997).

3.3.1. Radioelementos

O potássio é o principal responsável pela emissão de radiação gama dos radioisótopos primários presente na crosta. Segundo Minty (1997), o potássio é identificado e quantificado através da absorção de uma energia de 1,46 MeV (Fig. 3.4), correspondente ao único isótopo natural (^{40}K), o qual representa 0,012 % do K total dos outros isótopos, ^{39}K e ^{41}K, ademais, eles não são radioativos e representam, respectivamente, 93,26% e 6,73% do K total. O K é medido diretamente pelo pico correspondente ao decaimento de isótopos de 40K, que emite raios γ, pois decai para ^{40}Ar, que, devido a sua maior abundância crustal, tem a concentração normalmente expressa em percentagem (dag kg^{-1} K).

O tório natural é essencialmente composto pelo isótopo ^{232}Th, seus produtos de decaimento representam 100% do Th total, sendo identificado pelo pico do tálio (^{208}Tl), correspondente a uma energia de absorção de 2,62 MeV (Fig. 3.4). A série radioativa do Th termina no isótopo estável 208Pb (Minty, 1997).

O U ocorre naturalmente como radionuclídeo ^{238}U e ^{235}U, e sua série radioativa termina nos isótopos estáveis ^{206}Pb e $^{20}7Pb$, respectivamente. O urânio é detectado pela energia de 1,76 MeV, correspondente à absorção do bismuto (^{214}Bi) da série do ^{238}U, utilizada para identificar e quantificar o urânio natural (Fig. 3.4) (Minty, 1997).

A determinação dos teores de Th e U são mais complexas do que o K, uma vez que ^{232}Th e ^{238}U apresentam decomposição por meio de uma série de nuclídeos filhos até atingirem isótopos estáveis de Pb. Por isso, as concentrações de Th e U são geralmente expressas em partes por milhão (equivalentes a eU e eTh), o que indica que suas concentrações são inferidas a partir de elementos filhos em sua cadeia de decaimento (Minty, 1997).

3.3.2. Imagens Ternárias (RGB e CMY)

Os mapas ternários dos elementos radiométrico são utilizados para ressaltar contrastes entre áreas com diferentes concentrações dos três elementos radioativos (K, Th e U). Esses mapas são gerados a partir da associação de cores para cada um dos radioelementos. O padrão RGB associa as cores vermelho, verde e azul (*red, green, blue*) ao potássio (em %), tório e urânio (em ppm), respectivamente. Já o padrão CMY utiliza as cores ciano, magenta e amarelo (c*yan*, *magenta, yellow*) como base para composição do mapa. Em ambos os casos, as cores são associadas a cada um dos vértices de um triangulo equilátero, com gradações das cores variando de acordo com o teor de cada um dos elementos considerados. A cor branca representa altas contagens dos três elementos. Enquanto a cor preta é associada às baixas contagens dos mesmos (Ribeiro et al., 2013).

3.4. Mapas Auto-Organizáveis (*Self-Organizing Maps* — SOM)

O SOM é um tipo de rede neural artificial que foi proposta e se difundiu na década de 1980, pelo professor finlandês Teuvo Kohonen. Por isso, as técnicas baseada no SOM também são referidas como mapas de Kohonen (Kohonen e Somervuo, 1998). Essa técnica de mapeamento semiautomático fornece meios para se analisar e interpretar relações entre conjuntos de dados distintos, espacialmente localizados de maneira iterativa. Este método classifica cada dado de entrada em grupos distintos (ou *clusters*), de acordo com suas similaridades e comportamento (Fraser e Dickson, 2007).

O SOM se apresenta como uma técnica de análise de dados que funciona agrupando variáveis com características comuns de forma automática, ou seja, não supervisionada. Sendo assim, não é necessário nenhum conhecimento prévio sobre a natureza e o número de *clusters* dos dados, baseando-se apenas em medidas de similaridade vetorial. O SOM tem a capacidade de considerar todos os dados independentemente do seu tipo, eles podem ser geofísicos, geológicos e geoquímicos, tendo apenas que ser espacialmente relacionados.

Os princípios envolvidos na análise de dados multivariados com o SOM são a quantificação de vetores e medidas de similaridade entre vetores (Fraser e Dickson, 2007). A aplicação desta técnica tem como objetivos extrair informações do banco de dados para reconhecimento de classes com características semelhantes e encontrar associação entre as variáveis através da formação de agrupamentos (*clusters*).

A ideia básica de um SOM é mapear os padrões de dados em uma malha n-dimensional. Este mapeamento tenta preservar as relações topológicas, ou seja, padrões que são próximos no espaço de entrada serão mapeados para unidades que estão próximas no espaço de saída, e vice-versa. Os dados de saída são bidimensional (x e y), e a maioria das implementações do SOM usam uma grade retangular de medidas (Bação et al., 2005).

A associação de classes de um SOM é amplamente definida pelos padrões de entrada, que compartilham recursos comuns. Assim, a rede poderá identificar esses recursos em toda a gama de padrões de entrada. Uma classe de um sistema não supervisionado baseia-se na aprendizagem competitiva, em que os vetores de saída competem entre si para serem ativados, com o resultado que apenas um é ativado a qualquer momento (D’Urso et al., 2014).

O treinamento de uma análise SOM é realizado, primeiramente, usando uma estratégia de aprendizagem chamada *winner-take-all* (Penn, 2005). O SOM começa por combinar um grupo de vetores vizinhos. Este processo é baseado em uma medida de similaridade vetorial (Fraser e Dickson, 2007) e, uma vez que o vetor vencedor é encontrado, suas propriedades são modificadas por um percentual para que suas características se assemelhem mais àquelas da amostra de entrada mais próxima. No segundo passo, que é conhecido como o passo cooperativo, todos os vetores dentro de um determinado raio do vetor vencedor também são modificados para que suas propriedades também sejam alteradas por uma porcentagem para mais perto assemelharem-se à amostra de entrada em questão. Este procedimento é então repetido para a próxima amostra de entrada. Ao reduzir o raio de influência e alterar a modificação percentual aplicada para os vetores durante cada iteração, os vetores se tornam treinados para representar a estrutura dos dados de entrada (Fig. 3.5). Isso pode envolver a execução de centenas ou milhares de iterações dos procedimentos acima em cada amostra de entrada.

O mapa auto-organizado é uma representação ordenada e 2D de um complexo conjunto de dados de múltiplos parâmetros. É uma estrutura ideal para subsequente visualização e interpretação, após o treinamento dos vetores para representar a estrutura dos dados de entrada, agora chamados de *seed-vectors.* Todos os dados de entrada original mais próximas desse *seed-vectors* são representados por um mapa 2D. A característica principal deste mapeamento é que preserva o relativo relacionamento (topologia) entre os *seed-vectors*. Isso é, os *seed-vectors* que estão próximos no espaço nD têm nós que estão próximos no mapa 2D. Os dados de entrada originais são agora representados por nós no mapa auto-organizado, e estes podem formar um grupo ou *cluster*.

O SOM calcula automaticamente, para cada dado do arquivo de entrada, o erro de quantização (QER). Este erro consiste numa medida da distância entre uma amostra do seu *seed-vectors* (Fraser e Dickson, 2007). Os dados com alto erro de quantização representam os valores anormais do conjunto de dados. Essas amostras são consideradas anômalas em comparação com a maioria das amostras. Essas amostras de QER altas representam variáveis anômalas descorrelacionadas ou pouco correlacionadas com as demais (Carneiro et al., 2012), que também podem representar as bordas ou limites dentro de um conjunto de dados, o que, para a geologia, pode ser interpretado como contatos litológicos ou bordas de corpos (Bação et al., 2005).

Os Mapas de Componentes (*Component Plots*) são outra possibilidade de visualização do SOM. Como cada *seed-vectors* é um vetor no hiperespaço de dados definido pelas variáveis de entrada. É possível visualizar a contribuição de cada *seed-vectors* e exibir os valores usando uma escala de temperatura de cor, na qual os valores de alta dissimilaridade são exibidos em azul e os alta similaridade em vermelho (Bierlein et al., 2008).

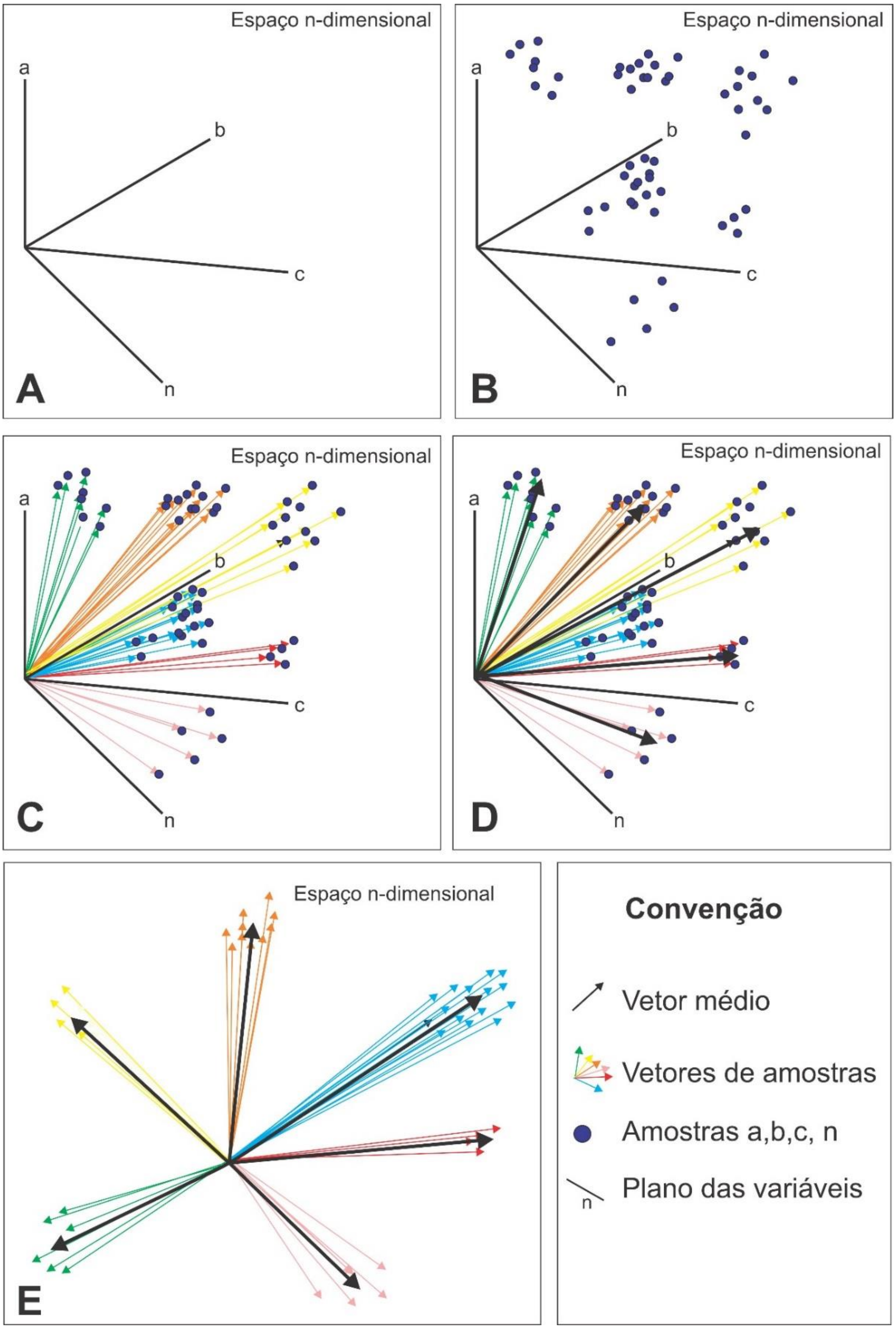

Figure 3.5: Síntese das etapas de uma análise em ambiente de Self-Oganizing Maps. Espaço n-dimensional (A). Definição de *seed-vectors* (B). Etapa competitiva, a amostra original é comparada com os *seed-vectors* (C). Determinação do vetor representativo o mais similar (D). Definição dos *Best Matching Units* (BMU's). Adaptado de Carneiro (2010).

Capítulo 4

*USING SELF-ORGANIZING MAPS IN AIRBORNE GEOPHYSICAL DATA FOR MAPPING MAFIC DYKE SWARMS IN NE BRAZIL**

* Este manuscrito foi submetido ao *Journal of Applied Geophysics* em 28 de abril de 2020.

Using Self-Organizing Maps in Airborne Geophysical Data for Mapping Mafic Dyke Swarms in NE Brazil

Alanny Christiny Costa de Melo[a*], David Lopes de Castro[a,b], Stephen James Fraser[c,d], Antomat Avelino Macêdo Filho[e]

[a] Programa de Pós-Graduação em Geodinâmica e Geofísica, Departamento de Geologia, Universidade Federal do Rio Grande do Norte, Campus Universitário S/N, Lagoa Nova, 59.078- 970 Natal – RN, Brazil.
[b] Departamento de Geologia, Universidade Federal do Rio Grande do Norte, Campus Universitário S/N, Lagoa Nova, 59.078-970 Natal – RN, Brazil.
[c] VectORE Pty Ltd, PO Box 588 Annerley QLD 4103, Australia.
[d] WH Bryan Mining and Geology Research Centre, Sustainable Minerals Institute, The University of Queensland, University Experimental Mine, 40 Isles Rd, Indooroopilly QLD 4068, Australia.
[e] Instituto de Geociências, Universidade de São Paulo, São Paulo 05508–080, Brazil.

Highlights

- An unsupervised data mining approach for mapping mafic dykes.
- Prediction of dyke swarms using self-organizing maps.
- Integrated spatial analysis and classification of airborne geophysical data.
- Optimization of geophysical and geological mapping.

ABSTRACT

Mapping widespread dyke swarms shed light on the tectonic processes that culminate in continental fragmentation, especially in the early phases of the crustal extension and magma emplacement. Airborne magnetic data are an effective geophysical tool to clarify the extent of dyke swarms in continental-scale areas due to the expressive magnetic contrast between magmatic bodies and host rocks. However, many geological features display similar magnetic patterns, making the qualitative interpretation of magnetic anomaly maps quite subjective and ambiguous. To improve and optimize the predictive mapping of dyke swarms, this research presents a multivariate analysis of airborne geophysical surveys, applying a Self-Organizing Map (SOM) approach using two magnetic and three gamma-spectrometric variables. This semiautomatic technique has allowed an integrated spatial analysis and the classification of the lithological units based on their magnetic and gamma-spectrometric signatures. We applied the SOM method to investigate a set of mafic dyke swarms that intruded in the Neoproterozoic Borborema

Province (BP), Parnaíba Basin (PB) and the São Francisco Craton (SFC) in NE Brazil. These dykes are part of a large magmatic event associated with the continental breakup, which formed the Equatorial Atlantic Ocean in the Early Cretaceous, denominated EQUAMP. First, the SOM parameters were defined by running the algorithm in a representative area in the central part of the BP. This training test area worked as a SOM template through which all data from the area were processed. The SOM analysis identified seven different populations, according to responses found in the five geophysical input variables. Two of these populations were associated with the mafic dykes, reducing the ambiguity of the magnetic anomaly interpretation. These populations represent high SOM quantization error, which means that these groups are the most anomalous data, evidenced in airborne magnetic data. These results were checked during fieldwork, revealing that dyke swarms occur more widely than were previously known, throughout the BP intruding the SFC, and showing some occurrences embedded in the sedimentary infill of the eastern border of the PB.

Key Words: Airborne Geophysics, Self-Organizing Maps (SOM), Mafic Dykes.

4.1. Introduction

The investigation of magmatic events grants understanding the mechanisms that initiate and corroborate with the development of rupture processes in the lithosphere (Hill, 1991; Bleeker and Ernst, 2006; Hawkesworth et al., 2016). Therefore, mapping dyke swarms at a regional scale is an excellent approach for acknowledging the plate motions that culminated in the continental breakup, especially in the early phases of the crustal extension, in the reconstitution of the tectonic style, the driven forces during the development of continental fragmentation and drift (Halls, 1982; Reeves, 2000; Ernst and Buchan, 2001; Zaineldeen, 2013). Mapping mafic dyke swarms also provides subsidies for a more comprehensive understanding of the mechanisms involved in the rifting process, shedding light on the ancient continental-scale stress field. Furthermore, the presence of dykes is useful to estimate the volume of magma and helps the analysis of the temporal relations about the duration of magmatic events (Halls, 1982; Ernst and Buchan, 2001; Jessel et al, 2015).

Mapping dyke swarms is a difficult task. The classical survey of dykes based on fieldwork is time-consuming, and hampered by the vast areas affected by them, their width are restricted to a few dozens to hundreds of meters and a large part of the dykes are not exposed on the surface (Ni et al., 2019). To overcome this limitation, airborne geophysical surveys, especially those using magnetic and gamma-spectrometric sensors, are one of several remote sensing methods available to assist the geological cartography and correlated with previous geological maps (Trumbull et al., 2004; Xiong et al., 2016). However, the large quantity of data and the complexity of the interrelationships between magnetic field, radioelements distribution and geological units create a requirement for the use of optimization techniques to improve the efficiency and effectiveness of joint interpretation of multiple geophysical data.

Regarding mafic dykes, the strong magnetic susceptibility allows their identification by high-amplitude magnetic anomalies with short wavelengths and large extensions. Nevertheless, continental geological boundaries with expressive contrast in magnetic properties, such as deep-seated crustal shear zones, faults, and geological contacts, display similar magnetic patterns (e.g., Ross et al., 1994), which commonly causes uncertainty and misinterpretation. Gamma-spectrometric data can make the identification of dykes more accurate, but they can also conduct a more complex and subjective interpretation process. This problem can objectively be addressed using data-mining methods that work in multivariate hyperspace using parameters that quantify geological features seen in geophysical, petrological, geochemical, and geochronological data through a suite of deterministic calculations performed on a computer. Self-Organizing Mapping (SOM) an unsupervised technique developed for the integrated analysis and semi-automated mapping, which works as a tool for analysis and visualization of data in n-dimensional space, based on principles of vector quantization (VQ) and measures of vector similarity (VS) (Kohonen, 1982; Kohonen, 2001). Boschetti et al. (2003) were the pioneers to apply SOM in geophysical data. Also, this technique has been used to optimize the mapping of geological and geophysical units using airborne geophysical data (Fraser and Dickson, 2007; Carneiro et al., 2012; de Castro et al., 2018).

The Neoproterozoic Borborema Province (BP) in NE Brazil (Fig. 4.1) is an excellent area to analyze the performance of the SOM method to map dyke swarms at a continental scale using airborne geophysical data. Furthermore, this area is considered a key region to understand the formation of the West Gondwana and its subsequent fragmentation, during the opening of the Equatorial Atlantic Ocean (Brito Neves and Cordani, 1991; Matos, 1992; Oliveira and Medeiros, 2018). A previous analysis of the magnetic and gamma-spectrometric data of the BP indicates three fundamental aspects that favor the mapping of mafic dykes with airborne geophysical surveys. Firstly, extensive magnetic anomalies with high amplitude and short wavelength stand out in the smoother magnetic pattern of the Precambrian crystalline basement. Secondly, the fact that the NE region of Brazil has a semi-arid climate, with a thin soil layer, low vegetation cover, sparse sedimentary basins and vast exposure of rocks favors the use of radiometric data. Finally, some dykes are close enough to the ground surface that gamma-spectrometric data are capable to detect them.

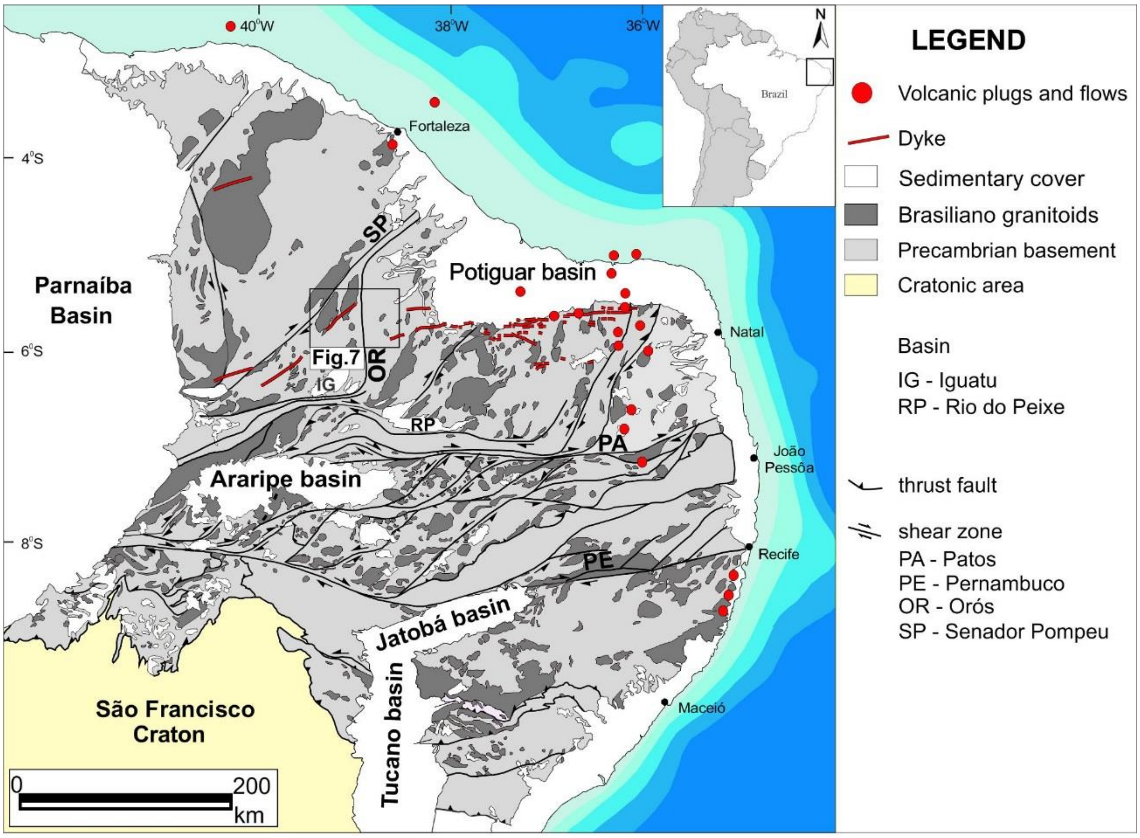

Figure 4.1. Simplified geological map of the Borborema Province (BP), NE Brazil. Main structures and magmatic events were compiled and modified from Oliveira (1992), Cavalcante et al. (2003), Delgado et al. (2003), Angelim et al. (2006), Van Schmus et al. 2008. Insert: Figure 4.7.

The main aim of this study is to adjust a semi-automatic technique to map extensive dyke swarms in a large Precambrian fold belt based on multi-variable geophysical datasets and evaluate its effectiveness in achieving this objective. The SOM method was initially trained over a target area to optimize the mapping process of extensive swarms of dyke in the entire BP. It is noteworthy that the introduction of gamma-spectrometric data in the multi-variable approach increases the success of the SOM method to identify dyke swarms. Our SOM analysis approach identified seven different clustered populations according to their geophysical similarities. Mafic dyke swarms are assigned to two populations (1 and 6). The choice of these clusters was defined by specific geophysical patterns displayed by the dykes. These SOM derived populations exhibited high degrees of intend validity, based on their geophysical characteristics, and were associated with three main dyke swarms in BP. Field survey confirmed the presence of dykes predicted by the SOM analysis. As a striking result, we estimate a substantial increase of the area affected by swarms (80%) in the BP compared to what was previously known.

4.2. Geological Setting

The Borborema Province (BP) encompasses a vast geotectonic unit of the South American platform in NE Brazil (Fig. 4.1) (Almeida et al., 2000; Brito Neves et al., 2014). It consists of a complex mosaic of crustal blocks of different ages, origin, and evolution, amalgamated in the last orogenic event that affected the West Gondwana continent, the Brasiliano/Pan-African Orogeny. Its collisional plate motions have come to an end between the Neoproterozoic and early Phanerozoic ages (~540 Ma), in the context of the Gondwana supercontinent construction. The BP congregates large areas of gneissic-migmatite, metasedimentary, metavolcanic, and granitic rocks ranging from Archaean to Neoproterozoic. The BP is bordered to the south by the São Francisco Craton (SFC), to the west by the Paleozoic Parnaíba Basin and to the north and east by the Mesozoic-Cenozoic sedimentary cover of the continental coastal basins.

During the Mesozoic and Cenozoic eras, NE Brazil was the scenario of several intrusive and extrusive magmatic events of predominantly basic rocks that were partially synchronous with the setup and evolution of a series of intracratonic rift basins in the BP (Fig. 4.1). The BP begun to rupture along an NW-SE oriented axis with a rotational component to N-S (Szatmari et al., 1987; Almeida et al., 1988). The roughly NE-S-W oriented trend of aborted small and extensive rifts, from Tucano basin (south) to Potiguar basin (north), occupies a 500-km wide belt throughout the BP (Matos, 1992).

The NE part of the BP was also affected by different magmatic episodes in the Mesozoic and Cenozoic (Almeida et al., 1988). Using geochronological data K-Ar, Mizusaki et al. (2002), grouped these events in three distinct events: a) Early Cretaceous – represented by a series of tholeiitic dykes with E-W and NE-SW directions (Fig. 4.1), preceding the first rifting stage of the Potiguar Basin evolution (Matos, 1992). The Rio

Ceará-Mirim dyke swarm (RCM) presents geochronological ages of 132.2 ± 1 Ma (Souza et al. 2003); b) Late Cretaceous – related to a magmatic event that occurred as dykes, plugs, and sills in the Cretaceous clastic sequences of the Potiguar Basin with Ar-Ar ages between 93.1 Ma (Souza et al., 2003); and c) Cenozoic Magmatism – distributed over a wider area at NE border of the BP (Fig. 4.1), showing recurrence along the Cenozoic. Its main representatives are volcanic plugs and flood basalts with ages between 70-65 and 9-6 Ma, with peaks between 48.9 ± 2.9 and 31.4 ± 1.5 (Silveira, 2006; Knesel et al., 2011).

The RCM consists of tholeiitic basalts and dolerites with plagioclase, clinopyroxene (± olivine), Fe-Ti oxides and pigeonite (Ngonge, et al., 2016) and has an extension of approximately 350 km in length in the E-W direction (Bellieni et al, 1992; Oliveira, 1992; Archanjo and Launeau, 2004). To the west of the 39º W, the tholeiitic dykes change their orientation to the NE-SW direction (Fig. 4.1). In the western part of the BP, these dykes become nearly parallel to the NE-SW trending Early Cretaceous rift system (Potiguar, Iguatu, and Araripe basins).

Based on paleomagnetic data, the RCM was divided in sub-swarms, exhibiting different directions of magnetization. It indicates that the dykes were emplaced at different times, and probably cooled with different rates (Ernesto et al., 1991; Bellieni et al., 1992). The RCM magmatism correlates to both the Central Atlantic Magmatic Province (CAMP) (Marzoli et al., 1999) and the Paraná-Etendeka Magmatism (Hollanda et al., 2006), which is contemporaneous to the basaltic and rhyolitic flows in the Northern Benue Trough (Bellieni et al., 1992; Maluski et al., 1995), the African counterpart of the Potiguar Rift. In addition, the Geological Survey of Brazil has systematically carried out airborne geophysical surveys all over the BP in the last decade, improving the geological knowledge of this Precambrian fold belt. Previous analyses of the vast amount of data have revealed that dyke swarms can be spread by a much larger region than already mapped. This present study aims to better estimate the real dimension for the dykes of these magmatic events using a SOM analysis.

4.3. Data and Methods

4.3.1. Airborne Geophysical Database

The fourteen airborne geophysical surveys covering the BP (Fig. 4.2 and Table 4.1) were provided by the Geological Survey of Brazil (SBG) and Brazilian Petroleum

Agency (ANP). The magnetic data were previously corrected for diurnal variation, and leveling errors and the International Geomagnetic Reference Field (IGRF) was removed. The directional cosine filter was applied to attenuate noise along the flight lines. The gamma-spectrometric data were also corrected for non-geological radiation sources (instrumental, atmospheric, and cosmic effects) and random noise. A detailed description of reduction procedures applied to airborne gamma-spectrometric surveying is provided by Minty et al. (1997). The K data are expressed in percentage, while the eU and eTh data are expressed in micro-equivalents. We interpolated the magnetic data using the bi-directional method (Geosoft, 2013) and the radiometric data using minimum curvature (Briggs, 1974) (Fig. 4.2). We adopted a cell size of 250 m, which represents half of the distance between flight lines of the most airborne surveys (Table 4.1). The surveys were merged in a single grid using the Gridknit tool (Geosoft, 2010). This suture method automatically estimates errors, defines the best suture path, and smooths the contact between each grid.

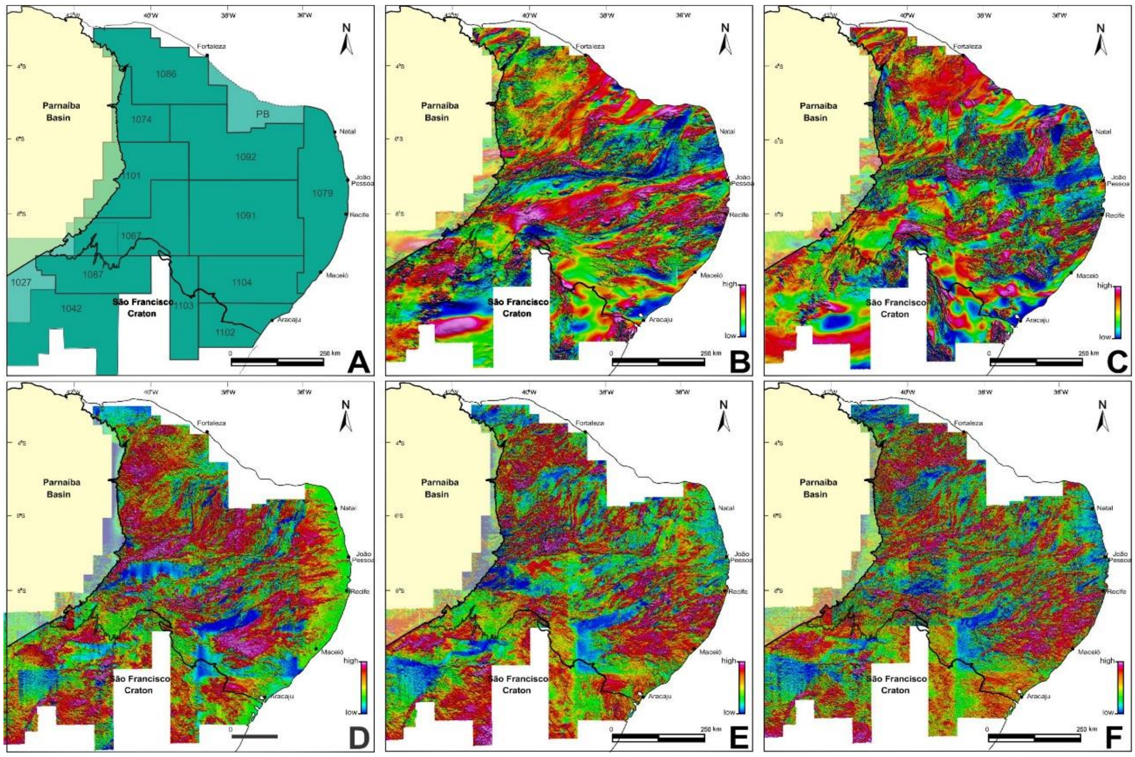

Figure 4.2. Airborne geophysical surveys covering the Borborema Province (BP) and its boundaries with the Paleozoic Parnaíba Basin and São Francisco Craton (A). Geophysical maps: total magnetic intensity (TMI) (B); reduced to pole magnetic anomaly (RTP) (C); K (D), eTh (E), and eU (F) radioelements.

Table 4.1: Airborne geophysical survey specifications. Survey: 1027 – Borda Sul da Bacia do Parnaíba, 1042 – Norte da Chapada Diamantina, 1067 – Pernambuco/Piauí (PE/PI), – Médio São Francisco, 1074 – Novo Oriente, 1079 – Borda Leste do Planalto da Borborema (RN, PB, PE, AL), 1086 – Norte do Ceará, 1087 – Médio São Francisco, 1091 – Pernambuco/Paraíba, 1092 – Paraíba/Rio Grande do Norte, 1101 – Centro-Sudoeste do Ceará, 1102 – Estado de Sergipe, 1103 – Oeste de Tucano, 1104 – Paulo Afonso/Teotônio Vilela, BP – Bacia Potiguar. CS – Company Survey; NFH – nominal flight height; FLD – flight-line direction; FLS – flight-line spacing; TLD – tie-line direction; TLS – tie-line spacing; MFI – magnetic field inclination; MFD – magnetic field declination. (For detailed information, access the Geophysical Surveys and Associated Products of the Geological Survey of Brazil at http://geosgb.cprm.gov.br/geosgb/downloads_en.html).

Survey	Year	CS	NFH (m)	FLD	FLS (m)	TDL	TLS (m)	MFI	MFD
1027	1976	CPRM	100	N-S	500	E-W	10,000	-5.85	-8.78
1042	1979	CPRM	100	N-S	500	E-W	10,000	-10.56	-20.91
1067	2006	CPRM	100	N-S	500	E-W	10,000	-19.05	-22.14
1074	2007	CPRM	100	N-S	500	E-W	10,000	-14.24	-21.63
1079	2008	CPRM	100	N-S	500	E-W	10,000	-30.43	-21.33
1086	2009	CPRM	100	N-S	500	E-W	10,000	-14.16	-21.38
1087	2009	CPRM	100	N-S	500	E-W	10,000	-27.84	-22.59
1091	2010	CPRM	100	N-S	500	E-W	10,000	-21.74	-22.05
1092	2010	CPRM	100	N-S	500	E-W	10,000	-19.8	-21.83
1101	2010	CPRM	100	N-S	500	E-W	10,000	-19.17	-22.11
1102	2011	CPRM	100	N-S	500	E-W	10,000	-28.76	-23.04
1103	2011	CPRM	100	N-S	500	E-W	10,000	-26.26	-22.85
1104	2011	CPRM	100	N-S	500	E-W	10,000	-26.89	-22.78
BP	1981	ANP	500	N70W	400	N60E	20,000	-11.89	-21.80

Before merging, each grid was processed separately to obtain a comprehensive compilation of magnetic anomalies in the whole studied area. The processing routine includes downward continuation, reduction to the magnetic north pole (RTP), and analytical signal amplitude calculation (ASA). Due to the difference in flight height of some surveys (Table 4.1), the magnetic grids were continued for the same height of 100 m, applying the downward continued filter followed by a Butterworth low-pass filter (Geosoft, 2013) to obtain a consistent database. Moreover, we applied the RTP, aimed to centralize the magnetic anomaly on its sources (Blakely, 1996). We operated the RTP transformation for each magnetic survey separately, using magnetic inclinations and declinations given by the IGRF (Fig. 4.2C). The ranges of magnetic inclination and declination vary from -30.43° to -5.85° and from -23.04° to -8.78°, respectively. We adopted a pseudo-inclination of the magnetic field from 60° to 85° to stabilize the results of this filter, which causes instabilities in regions at low magnetic latitudes (<±20°). In addition, we applied the ASA to the RTP anomalies to produce maxima amplitudes on the highest magnetic gradients (Nabighian, 1972), highlighting geological contacts and structural features, especially the dyke swarms (Fig. 4.3).

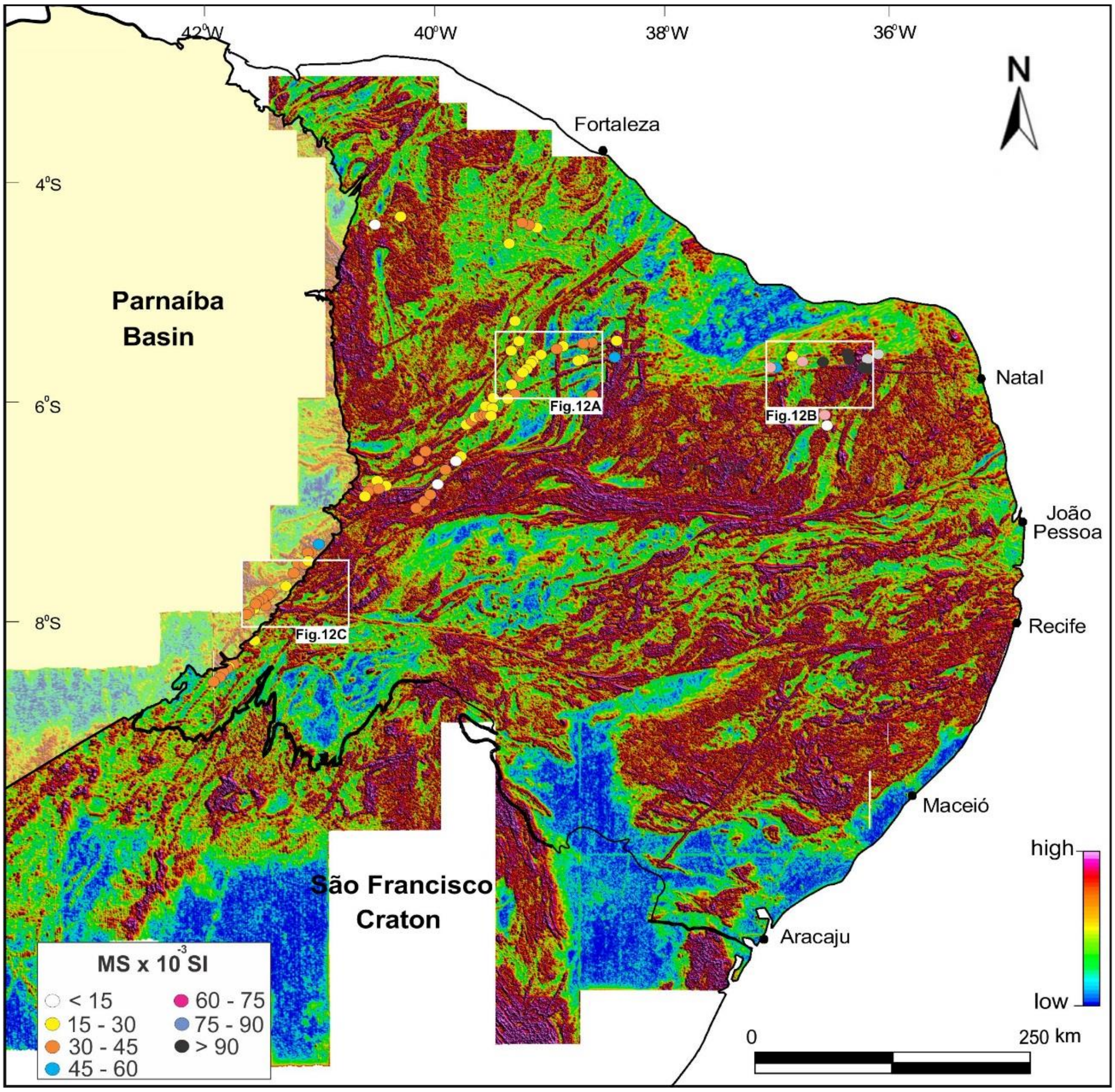

Figure 4.3. Analytic signal amplitude map of the Borborema Province (BP), showing the location of the samples collected and the magnetic susceptibility measurements (colored dots). Insert: Figure 4.12.

Also, the magnetic susceptibility (MS) of dykes and their host rocks were systematically measured in the PB, using a portable MS meter KT-10 v2 (*Terraplus Inc.*). This equipment can measure MS of rock samples with a high sensitivity of 1.0 × 10^{-6} SI units. The MS of the dolerite dykes varies from 8.4 to 103.8 × 10^{-3} SI units, with an average value of 32.5 × 10^{-3} SI. Higher MS dolerites are concentrated in the E-W-oriented segment of the RCM dyke swarm south of the Potiguar Basin. While dykes display lower MS along the NE-SW trending swarm segment (Fig. 4.3). The average MS of the sedimentary and basement host rocks are much lower, ranging from 0.4 × 10^{-3} SI to 3.2 × 10^{-3} SI, respectively. These expressive MS contrasts should be the responsible factor by the high amplitude magnetic anomalies related to the dolerite dykes in the PB.

4.3.2. Self-Organizing Map (SOM)

The SOM technique facilitates and accelerates the speed at which data can be analyzed and interpreted for improving the routine preparation of geological maps to enable quick identification of natural domains, prospecting targets and highlighting potential hazards for academic research, exploration, mining and processing (Fraser and Dickson, 2007; Fraser and Hodgkinson, 2009). SOM provides means to analyze and promote interrelationships between disparate datasets, spatially localized in an iterative way (Bação et al., 2005).

Fundamentally, a SOM approach aims to visualize and identify complex multidimensional data as nodes (vector) on a 2D representation of the original multidimensional data set. In an iterative process, seed vectors are trained to represent the patterns within the original data set. The mapping from multidimensional space to 2D space attempts to preserve topological relationships, which means samples that are similar in the input space will be mapped and visualized as close on the resulting output self-organized 2D map (Bação et al., 2005). The processes involved in data analysis with SOM are vector quantization (treating each input sample as a vector in a dataspace defined by input variables) and vector similarity to determine the dissimilarity between samples (Fraser and Dickson, 2007). The SOM approach aims to extract relationships, find patterns, and identify outliners from a database essentially by recognizing samples with similar features or attributes.

The output visualization of most SOM implementations is a rectangular grid of trained vectors, also called Best Matching Units (BMUs), that represents the internal patterns and complexities within a data set. SOM analysis is unsupervised, which means no prior knowledge is required as to the nature or number of groupings within the data set (Mikula et al., 2008). A limitation of the SOM is that it scales all the input variables to the range [0,1], therefore, it is not possible to set weights for the importance of different inputs (Torppa et al., 2015).

4.4. SOM Analysis

We used the SiroSOM software, developed by the Commonwealth Scientific and Industrial Research Organization (CSIRO, Australia) for this analysis. One advantage of SiroSOM is that it can be operated in both non-supervised and supervised modes. SiroSOM makes it possible to create a SOM framework or model from a key area, then to process other data through that pre-computed model. Such an approach was used in this analysis of the magnetic and gamma-spectrometric datasets to map mafic dyke swarms in the BP and surroundings geological units (Figs. 4.1 to 4.3). The magnetic variables, RTP and ASA anomalies; and the gamma-spectrometric variables K, eTh and eU were input to this analysis.

In a typical SOM analysis, the data space defined by the input variables is seeded randomly by dummy vectors. These “seed-vectors” are then trained via an iterative process which involves both competitive and collaborative learning and decreasing spheres of influence, to represent the patterns and structures within the input data cloud. Once trained, the seed-vectors are known as “best matching units” (BMUs); and these may represent numbers of input samples or none at all. Ultimately, these BMUs or code-vectors are transformed to be displayed as nodes or cells on the “self-organized map”. In an attempt to preserve the relationships between BMUs in nD space, when projecting to either 2D or 3D space, the SOM procedure employs the concept of a “global” shape/surface for the nD data-cloud (equivalent to a sheet, cylinder or toroid) and a local lattice structure (rectangular or hexagonal) for 3D or 2D positioning, analysis and visualization. Self-organized “maps” are typically rectilinear and composed of either rectangular or hexagonal nodes that represent the BMUs, which are positioned so that the relationships between the nodes in nD space are preserved (as best as possible) on the 2D map. Hence one or more nodes on a 2D self-organized map may represent natural populations of self-similar samples (Fraser and Dickson, 2007).

In this study, we used the following parameters for our analysis: a 70x50 element sized grid (the number of seed vectors); a random initiation; a Gaussian neighborhood function; a toroidal geometry for the data cloud; and a local hexagonal lattice for the final map display. These parameters were chosen after exhaustive experimentation using the training area.

Numerous trial runs were used to determine an optimum size for this SOM analysis. Our premise being that the SOM size must be large enough to have some nodes with no input data attached to them. It means the SOM is large enough to display all the variance in the data set (Fraser and Dickson, 2007). The size of the map dictates the number of seed-vectors (BMUs or nodes) nodes or BMUs that will be used. We subsequently selected a 70x50 map size (3500 node-vectors). Once trained, the node-vectors represent the structure of the input data, all the original input samples closest to that node-vector are represented by that node on the 2D map.

A random initialization of the seed vectors was chosen to remove bias; hence group positions and population colors are unique to each SOM run. The seed vectors were trained using large numbers of iterations. Once trained, the now BMUs, or code-vectors became the nodes on our self-organized map. Each node may represent a group of similar samples, or no samples at all. The distance of a sample is away from its BMU is the sample's QER. This is a useful metric that indicates how anomalous that sample is compared to the other samples assigned to that particular BMU (Fig. 4.4).

These trained vectors in multi-dimensional space are then projected onto an enveloping plane or surface that sits outside the boundaries of our multidimensional data set. It can be a hyper-plane, hyper-cylinder, or hyper-toroid. In our case, we used the hyper-toroid due to the advantage that they wrap in both x and y; planes do not wrap at all.

Given that we cannot readily visualize hyper-dimensional surfaces, the BMUs are then transformed to either a lesser 3D or 2D space. This process forces/squashes our BMUs to become adjacent on the lesser dimensional grid and we use a local hexagonal lattice to facilitate this. During this step, the nD topological relations are maintained, as best possible, so that BMUs, which are close in nD space, continue to be close in 3D or 2D space.

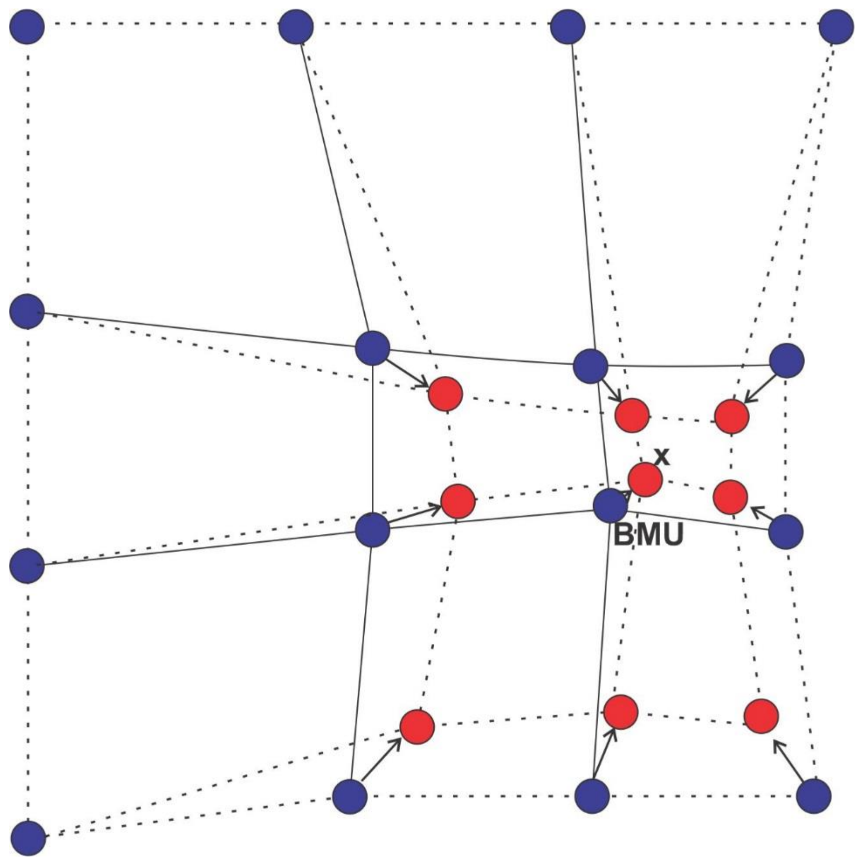

Figure 4.4. Training of the "seed-vectors" and their neighbors toward the input sample marked "x". The solid lines represent the situation before the training and the dashed lines correspond to the positions after training. The blue and red circles represent seed-vectors and trained best-matching units (BMUs), respectively. The QER is the distance between the sample (x) and the nearest trained red dot (BMU). The black vectors show the movement of the seed-vectors.

Once the 3D/2D self-organized maps are computed, various enhancements and parameters may be used to assist in understanding and interpreting the self-organized map data. The Unified-Distance Matrix (U-Matrix) is a visualization to color a given node based on the average distance in nD space between that node and its six neighboring nodes (Ultsch, 2003). Typically, a color-temperature scale is used to color the nodes with lower temperature colors indicating closeness (similarity), and hotter temperatures. The hexagonal node lattice and the output U-matrix are displayed in Figure 4.5A.

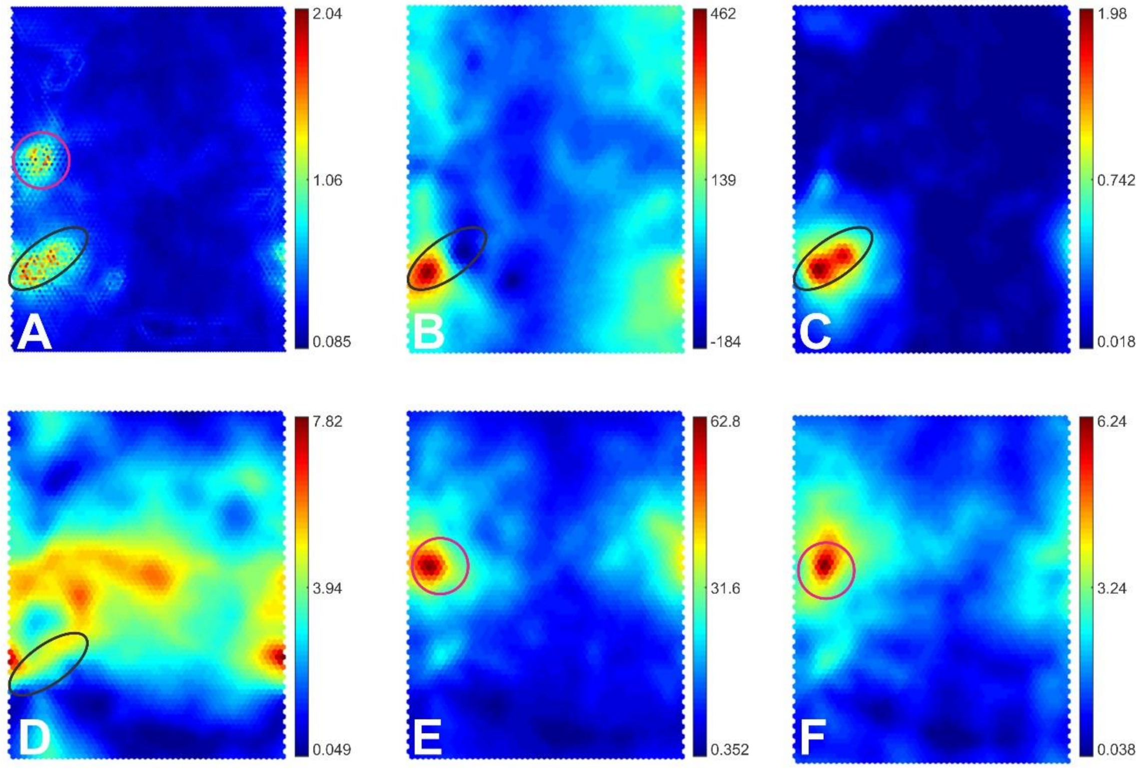

Figure 4.5. Self-organized map outputs computed using the BP training area data: (A) U-Matrix; - where warm colors represent high dissimilarity and cool colors high similarity between adjacent nodes. Component Plan Plots are shown on (B) RTP; (C) ASA; (D) K; (E) eTh; and(F) eU, where warm colors represent high contribution, and cool colors represent low contributions to the SOM. Black ellipses indicate areas with high values of RTP, ASA and K correlate with high contribution in U-matrix. Purple circles display areas with high values in eTh, eU and U-matrix plots.

Component Plots essentially show the input values per node for a given variable across the map (for each node) (Fig. 4.5). They are colored using a color-temperature scale to indicate low contribution (blue) or high contribution (red) they are to adjacent nodes. Correlations and contributions among these variables can be useful to understand the relationships between the input variables. Some of these relationships can be described as high values of RTP, ASA and K, showing the high contribution for U-matrix (black ellipses in Fig. 4.5), another specific area with high values in U-matrix is coincident in the eTh and eU plots (purple circles in Fig. 4.5).

To discover the relationships between the nodes on a 2D SOM visualization, we performed a K-means clustering of the node values. K-means clustering is a method of vector quantization that aims to partition N samples into k clusters, in which each observation belongs to the cluster with the nearest mean (Torppa et al., 2015). However, because K-Means requires the input of a pre-determined number of clusters (a supervised machine learning approach), we use the Davies-Bouldin (DB) index (Davies and Bouldin, 1979) to assist in estimating the number of clusters/natural populations present. The DB index results from a comparison of the variances within and between cluster means for a range of cluster numbers. The idea being to minimize the within and maximize the cluster variances to estimate the number of clusters as input to the K-means process. In this study, the DB analysis estimated there were 7 populations with a DB index of 1.1 (Fig. 4.6).

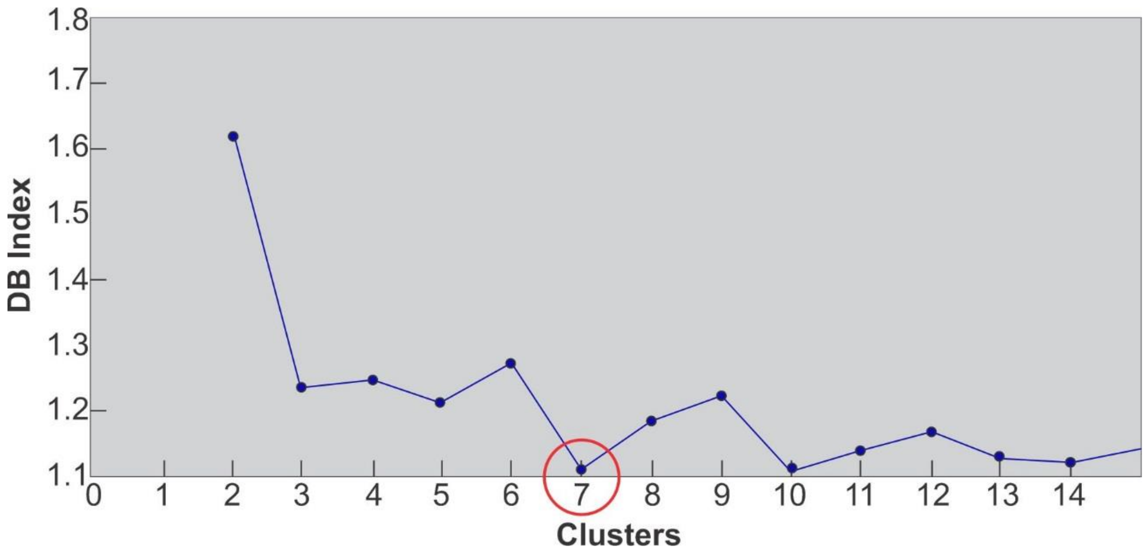

Figure 4.6. Davies-Bouldin index (y axis) for the K-means clustering (x axis). Seven was chosen as an optimum number of clusters (red circle) as it was the lowest number of clusters with the first lowest Davies-Bouldin index value.

4.4.1. SOM Training Test Area

Initially, we tried to undertake a SOM analysis overall of the BP. However, due to the size of the area and its geological complexity, (its lithologic heterogeneity in particular), the process to identify populations related to geological units was not satisfactory. This approach was not able to establish similarity patterns within the large dataset of airborne geophysical data. So, we decided to train the SOM over a 100 x 65 km representative area in the central part of the BP (Fig. 4.7, location in Fig. 4.1). We used this area as an exemplar to create a SOM framework to pass through all data corresponding to the entire studied area. The BMUs determined for the region in Figure 4.7 were used to categorize the data sets for all PB.

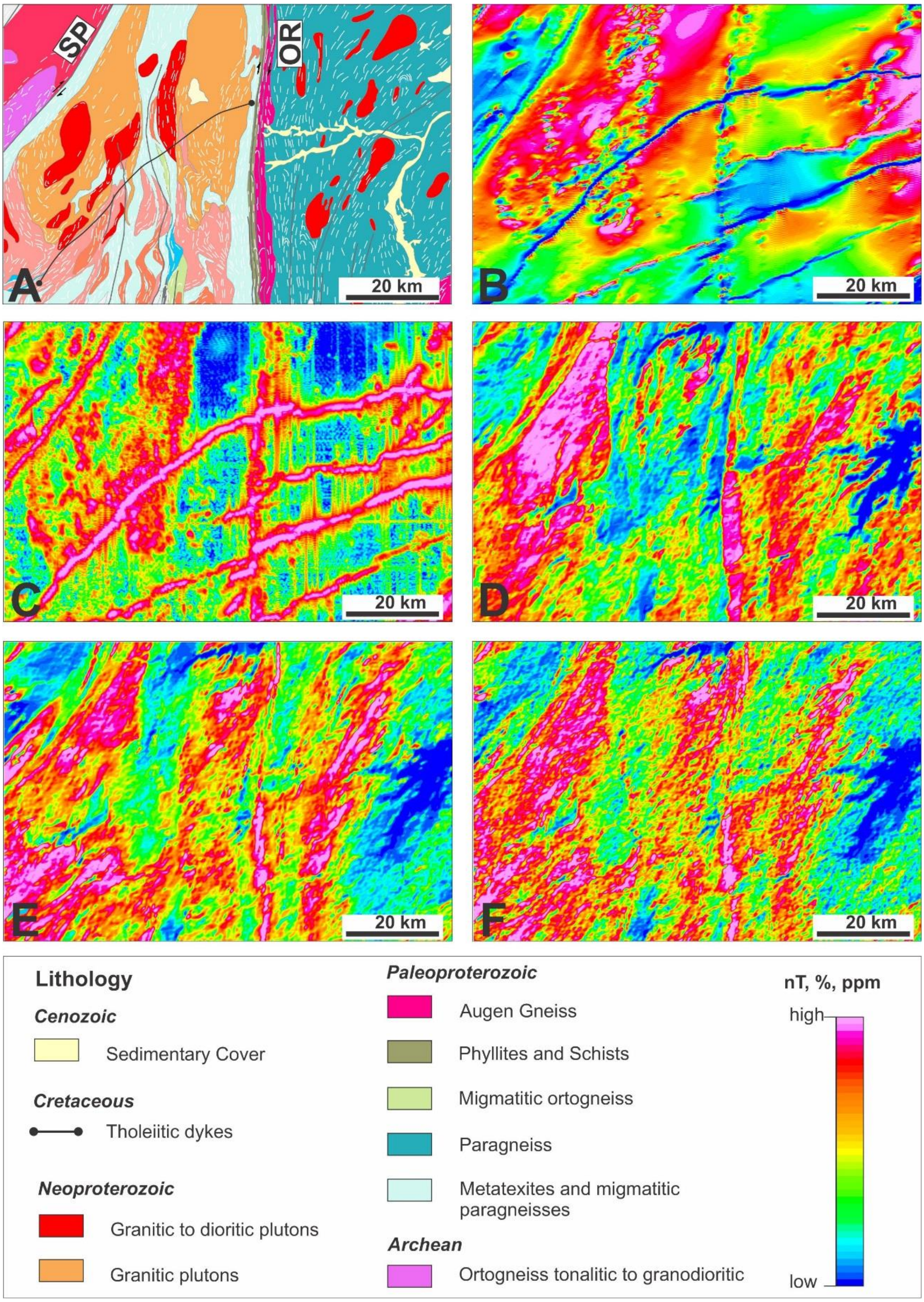

Figure 4.7. Geological and geophysical data (location in Fig. 4.1) used as input to the SOM training: geological map modified from Cavalcante et al. (2003) (A); RTP (B) and ASA magnetic variables (C); K (D), eU (E), and eTh (F) radioelements. Shear zones: OR - Orós.

The selected area presents rocks and lithology ranging from the Archean to the Cenozoic (Cavalcante et al., 2003), comprising the main geological elements of the BP exposed in this region, i.e. Precambrian basement, Neoproterozoic granitoids, shear zones, and the Cretaceous dyke swarms (Fig. 4.7A). In this area, the occurrence of dykes was already mapped using airborne magnetic data, so it was possible to establish a pattern of similarities that characterized and recognized this pattern whenever it occurred in the rest of the BP. The extension of the dykes ranges from dozens to hundreds to kilometers along the NNE-SSW oriented Precambrian grain, forming a set of four curved dyke lineaments. High-amplitude magnetic anomalies reveal their location, even those that do not outcrop, as verified by fieldwork. After running the SOM in this test area, the trained parameters were then adopted for the SOM analysis throughout the entire BP.

In the local geological setting (Fig. 4.7A), the Archean eon is represented by tonalitic to granodioritic orthogneisses (Cavalcante et al., 2003). Augen-gneisses, phylites and schists, migmatitic orthogneisses, paragneisses and metatexites comprise the Paleoproterozoic basement units. The Neoproterozoic orogenic cycle is represented by granitic to dioritic plutons. The Early Cretaceous rifting that prevailed the crustal breakup of the Pangea supercontinent is marked by NE-SW oriented dyke swarms and a small, aborted rift basin, anchored on the Neoproterozoic shear zones (de Castro et al., 2008). Finally, the Cenozoic is characterized by sedimentary covering.

The five geophysical variables selected as input to the SOM procedure are shown in Figure 4.7: the magnetic data, RTP and ASA anomalies, and the gamma-spectrometric data, Potassium (K), Thorium equivalent (eTh) and Uranium equivalent (eU) counts. This airborne dataset is part of the project 1092 (Fig. 4.2A, Table 4.1) and consists of 294,696 samples. The data were combined to make a single CSV file, in which each point in space within the dataset has a value for each variable. Due to the low magnitude and variation of the analytic signal, logarithmic values were used to produce a better definition in the SOM analysis.

4.4.2. Semi-automatic Mapping of the Test Area

Several alternative datasets were used as input to SOM. Some approaches were computed considering only the magnetic data. The K-means clustering computed only four populations (Fig. 4.8A). In this case, we did not obtain a satisfactory mapping of the mafic dyke swarms because the SOM analysis was unable to clearly discriminate mafic dykes from other geological units and features, as lineaments, faults, and extensive shear zones. Moreover, the SOM procedure produced no significant number of clustered populations that accurately represented the local surface geology. In fact, plenty of SOM solutions were attributed to other types of causative sources with high amplitude and short wavelength magnetic patterns (Fig. 4.8B). To overcome these excessive solutions not correlated with dykes, we ran the SOM analysis introducing gamma-spectrometric data, whose typical low radioelement counts of basic dykes facilitated differentiating them from felsic rocks and other geological features. The combination of magnetic and gamma-spectrometric data provided a larger number of clustered populations, promoting better geological discrimination (Fig. 4.8C).

Although the DB analysis suggested an optimal K-means cluster of seven populations (Fig. 4.6), we tested the SOM analysis using higher numbers of SOM-derived K-means clusters. From several DB analyses, we chose those that estimated different quantities of clustered populations (9, 11, and 22) for comparison purpose. The increase in the population number makes the map of solutions more and more detailed (Figs. 4.8D to F). However, the recognition of mafic dykes does not show any visible improvement for populations larger than seven. Then, we chose the K-means cluster, which produced seven clustered populations with the best geological compromise (Figs. 4.8C and 4.9). The reference values derived from the complete dataset to classify the contribution of each SOM-derived cluster component are shown in Table 4.2. The cluster output values were gridded using the "nearest neighbor" resampling procedure for discrete data and the spatial distribution of input samples color-coded by their SOM-derived cluster number is displayed in Figure 4.9.

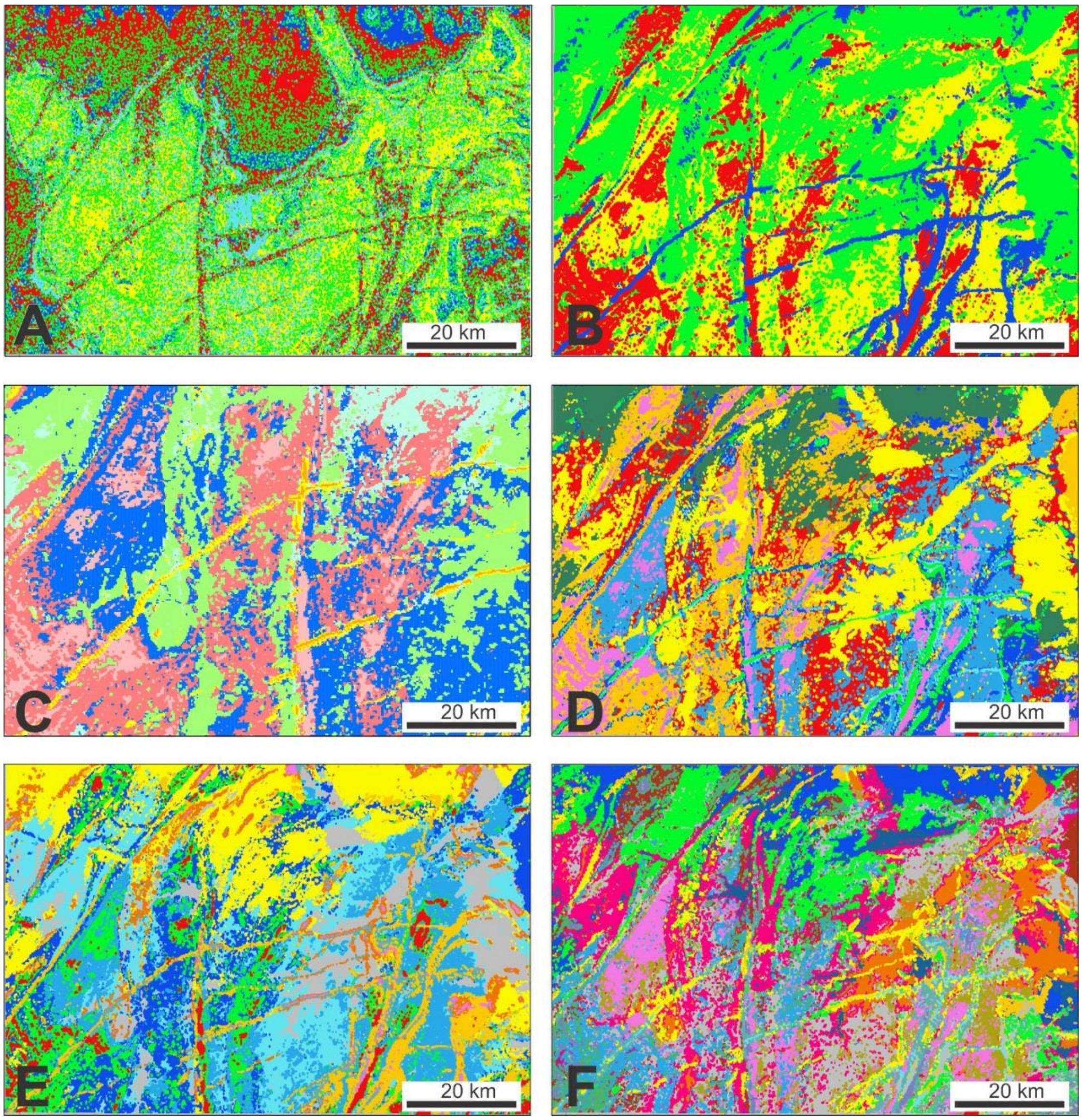

Figure 4.8. Comparison between the SOM classification of clustered populations in the training area, considering two alternative datasets: only magnetic data (A) with 4 classes of clustered populations; and magnetic and gamma-spectrometric data with 4 (B), 7 (C), 9 (D), 11 (E), and 22 (F) classes of clustered populations.

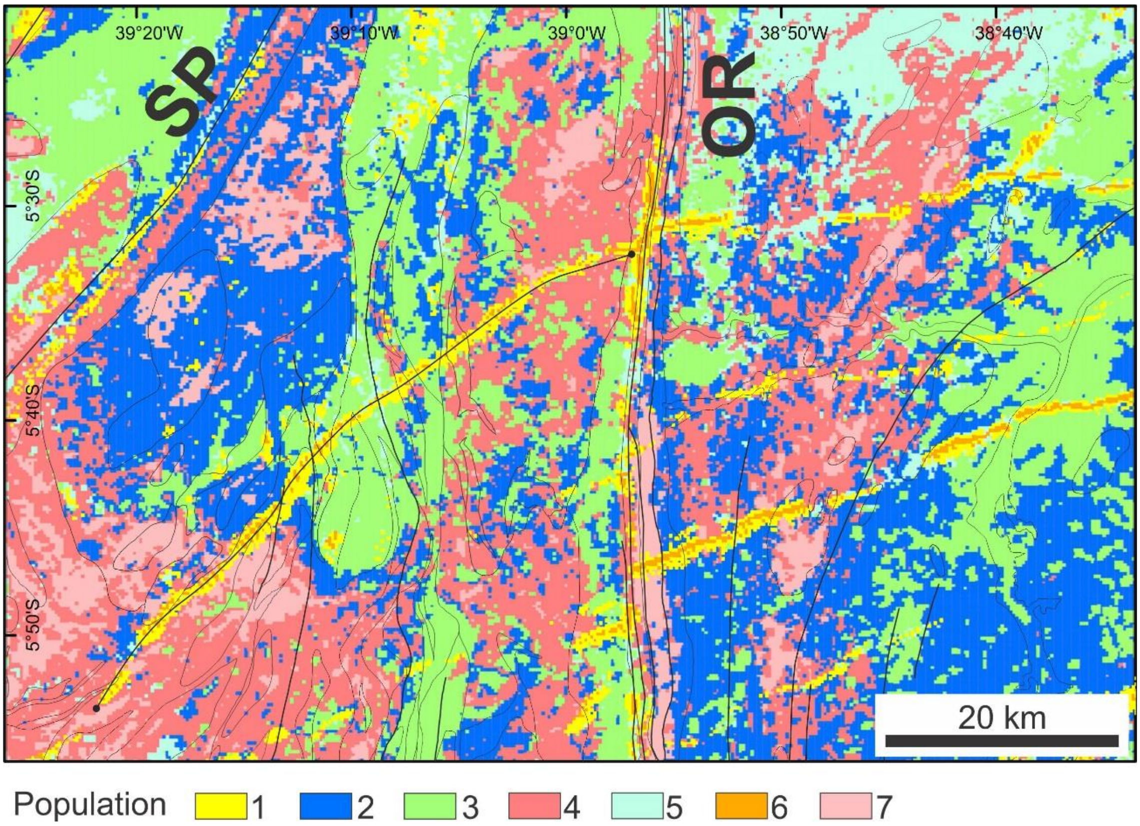

Figure 4.9. SOM solution map of the training area, displaying each sample coded by its population color. The black lines represent the geological features shown in Figure 4.7A.

Table 4.2. Reference values of magnetic (RTP and ASA) and gamma-spectrometric (K, eTh and eU) data to determine the classification of SOM variable samples.

	RTP (nT)	ASA (nT/m)	K (%)	eTh (ppm)	eU (ppm)
Minimum	-3639.18	0.0001	0	0	0
Maximum	1589.75	28.32	15.25	767.15	93.45
Average	95.10	0.088	1.89	14.68	3.32
Median	88.91	0.037	1.43	12.28	3.06
Standard deviation	103.76	0.173	1.52	10.06	1.51
Classification					
Low values	<51.684	<0.465	<5.057	<255.718	<31.150
Medium values	51.684 — 103.369	0.465 — 30.232	5.057 — 10.114	255.718 — 511.436	31.150 — 62.300
High values	>103.369	>30.232	>10.114	>511.436	>62.300

The statistical parameters (Table 4.2) were calculated for each variable of the original data set for comparison with the SOM-derived cluster results of SOM training in the test area. A broad classification was obtained based on the median value for each input variable to find the optimal reference values. Table 4.3 shows the contribution from each variable for each population group. The reference variable values were divided into three classes for each variable, including the QER results: (1) high values; (2) medium values; and (3) low values. These results are discussed in the next chapter.

Table 4.3: Medium values and classification of variables for each SOM-derived cluster population.

Population	QER	RTP (nT)	ASA (nT/m)	K (%)	eTh (ppm)	eU (ppm)
1	0.847 (High)	-2.839 (Low)	0.637 (High)	3.367 (High)	12.278 (Medium)	1.569 (Low)
2	0.373 (Low)	-46.200 (Low)	0.077 (Medium)	4.010 (High)	11.772 (Medium)	1.493 (Low)
3	0.306 (Low)	-43.281 (Low)	0.075 (Medium)	1.376 (Medium)	5.756 (Low)	0.807 (Low)
4	0.405 (Low)	3.773 (Low)	0.053 (Low)	2.698 (Medium)	18.730 (Medium)	2.065 (Medium)
5	0.362 (Low)	68.338 (Medium)	0.086 (Medium)	1.925 (Medium)	7.759 (Low)	0.981 (Low)
6	1.134 (High)	251.509 (High)	1.021 (High)	3.221 (High)	11.938 (Medium)	1.560 (Low)
7	0.699 (Medium)	-10.185 (Low)	0.087 (Medium)	4.291 (High)	32.559 (High)	3.230 (Medium)

4.4.3. Correlation of the SOM Solutions with the Surface Geology in the Test Area

The SOM solutions were grouped in seven different populations based on the geophysical signatures of the near surface geological units and structural features in the trained area (Figs. 4.7 and 4.9). However, it does not mean that each geological unit is directly related to a specific SOM population. Indeed, different lithologies with slightly diverse compositions may be included in the one population. For all populations identified by the SOM analysis, we considered possible contamination of SOM solutions by high-frequency noise due to short spatial sampling along the flight lines. However, it is a low-amplitude coherent noise equally spread over the entire geophysical signal, which apparently does not compromise the good results obtained by SOM analysis. To validate this premise, we correlated the SOM-derived cluster populations and the outcropping geological units previously mapped (Fig. 4.7A) and carried out fieldwork in the trained area. This comparison was then expanded to the entire tectonic province. Moreover, SOM solutions for mafic dykes were also checked throughout the whole studied area.

The mafic dykes are recognized in populations 1 and 6. These populations show similar geophysical signatures (Figs. 4.7 and 4.9). The related magnetic anomalies display E-W and NE-SW orientations, short wavelength, high magnetic amplitudes, and polarity alternation of the magnetic anomalies (Fig. 4.7B), which reflects inversion of the magnetic field between different magmatic events. Furthermore, the populations 1 and 6 exhibit high amplitude of the analytic signal (ASA), and high K (%) and medium eTh values. While eU counts are low for these cluster populations (Fig. 4.7E and Tables 4.2 and 4.3). Although similar, these two clusters have been differentiated by the SOM classifier due to the averages of RTP values. The population 1 shows lower average amplitudes of the RTP anomalies than population 6.

The magnetic anomalies display evidently the NE-SW to E-W trending mafic dykes (Figs. 4.7B and 4.7C) due to their strong and contrasting magnetic signatures with the host rocks, including the ones that outcrop and those in the subsurface. Both SOM populations show high QER (Table 4.3), which represents anomalous vectors, which are mainly evidenced in magnetic patterns and give a general overview of the anomalous features in the data. However, there are N-S-oriented SOM solutions included in populations 1 and 6 (Fig. 4.9) that are related to the Orós shear zone (OR in Figs. 4.1 and 4.7A). Its magnetic signature is very similar to the mafic dykes, but this structure is easy to be recognized and differentiated from the dykes. In this case, the dykes present a different structural trend, orthogonally crossing the shear zone. Likewise, the Senador Pompeu shear zone (SP in Fig. 4.7A) that occurs in the northwestern part of the trained area shows a set of SOM solutions belonging to populations 1 and 6. This is easily recognized, although it presents the same structural trend as the dykes. This demonstrates that a small amount of SOM solutions is mistakenly classified as dykes. The inclusion of other variables in the semi-automatic mapping process (for example, remote sensors such as Lidar systems and satellite imagery), in addition to field survey, are necessary to validate the SOM solutions in these cases.

The other clustered populations not related to mafic dykes are briefly described as followed: a) population 2 exhibits high levels of K radioelement, contrasting with the medium and low levels of all the other variables. To the west, a large granitic pluton can be easily identified on the maps in Figures 4.7A and 4.9. This population is also associated to another lithotype (paragneiss) that occurs in the eastern part of the area; b) the characteristics of population 3 consist of medium levels of ASA and K, and low levels of RTP, eTh, and eU. This population represents granitic rocks with associated alkalis, gneiss, metatexites, migmatitic paragneisses, which may relate to weakly magnetic and radioelements content; c) population 4 comprises low levels for the magnetic variables, RTP and ASA, and medium values of gamma-spectrometric variables, K, eTh and eU. These characteristics suggest a diversified lithologic composition. According to the geological map (Fig. 4.9A), this population of clusters can also be mainly associated with metamorphic rocks as metatexites, paragneisses and orthogneisses; d) population 5 occurs predominantly in the northeastern corner of the trained area. We find no consistent correlation between the clustering promoted by the SOM analysis and neither a specific geological unit or rocky assembly. The geophysical characteristics of the population 5 consist of medium levels of RTP, ASA and high radioelement counts, which contrast with the low values of all the other gamma-spectrometric variables. These features can be related to rocks with low alkali-feldspar content and moderate magnetic susceptibility. Accordingly, granodiorite occurs in the areas of this cluster and may be associated with it; and e) population 7 is the only population to show medium values of QER owing to the high values of K and eTh, while presenting medium values of eU and ASA, and low values of RTP. This population appears more frequently in the southwestern and the central parts of the trained area. The first occurrence is associated with paragneiss and, in the last case, the population looks like an elongated form represented by the outcropping augen-gneiss intrusive suite (Fig. 4.7A).

4.4.4. SOM Solution Validation

The effectiveness of the SOM method to properly identify dyke swarms using magnetic and gamma-spectrometric datasets was assessed based on published geological maps and an extensive field survey. We compiled diverse geologic maps of the BP (e.g., Oliveira, 1992; Cavalcante et al., 2003; Delgado et al., 2003; Angelim et al., 2006; Van Schmus et al., 2008), which indicate dyke occurrences especially at the southern edge of the Potiguar basin and isolated dykes close to the Parnaíba basin (Fig. 4.1). After comparing the compiled geological map and the SOM solutions derived map expanded to the entire BP, we eliminate those solutions that are clearly not inserted in the geological context of the dike swarms. In fact, clouds of solutions that do not have an extensive linear pattern and preferential orientations along known or projected swarm trends are discarded. After removing of spurious solutions, target areas for the validation of predictive dyke mapping were selected. Even situations where previous maps indicate geological structures not directly related to mafic dykes, but which present SOM solutions, were visited to confirm the absence of magmatic bodies in those areas.

The field excursions were carried out in the BP between 2016 and 2018 to access the dyke swarms. We recovered more than 1000 km along the E-W, NW-SE, and NE-SW branches of the predicted dyke swarms, guided by the spatial distribution of the SOM solutions. We visited 127 sites and located 100 exposures of magmatic bodies or superficial evidence of their outcrop presence (Fig. 4.10), such as high morphology, weathered blocks, and reddish soil. Furthermore, magnetic susceptibility (MS) was measured, and the samples of igneous rocks were collected for further geochemical analysis (Fig. 4.3). As a result of the field survey, it has been found that the SOM methodology was more than 90% successful in detecting dolerite dykes in a semi-automatic fashion, after removing clouds of solutions visually not related to the dykes.

Figure 4.10. Typical exposures of the Rio Ceará-Mirim Dyke Swarm (RCM), showing the contact between the dyke and its host rock (sandstone) on the ground (A) or forming small hills (B); and displaying onionskin weathering.

4.5. SOM Analysis of Dyke swarms in NE Brazil

SOM analysis classifies the multivariable dataset into distinct groups (or natural populations), according to their similarities and behavior (Fraser and Dickson, 2007). After the SOM training in the test area (Figs. 4.7 and 4.9), we expanded the SOM classification to the whole studied area (Fig. 4.2), using all the airborne geophysical data, which cover the BP, eastern edge of the Paleozoic Parnaíba Basin and the northern border of the São Francisco Craton to obtain an optimized mapping of the mafic dyke swarms that emplaced during the early rifting phase of the Brazilian Equatorial margin in Cretaceous. It is noteworthy that during the SOM analysis of the entire studied area, into seven clustered populations, populations 1 and 6 were always related to the mafic dykes. However, the other populations comprise geological units that vary within the different tectonic domains of the province and have no genetic relationship between them. As the scope of this study is the mapping of dyke swarms, the characterization of the host rocks was disregarded. Likewise, solutions from populations 1 and 6 are clearly unrelated to the dykes were also disregarded. The final SOM solutions for dyke swarms in the BP and neighboring tectonic domains are shown in Figure 4.11.

We selected 3 areas in the BP (Fig. 4.3) to assess the improvement provided by the semi-automatic mapping based on the airborne magnetic and gamma-spectrometric data. The selection criteria were: a) the number of new dykes identified by SOM analysis in comparison with previous geological maps; and b) the SOM method's ability to separate the dykes from other geological features with the same magnetic response.

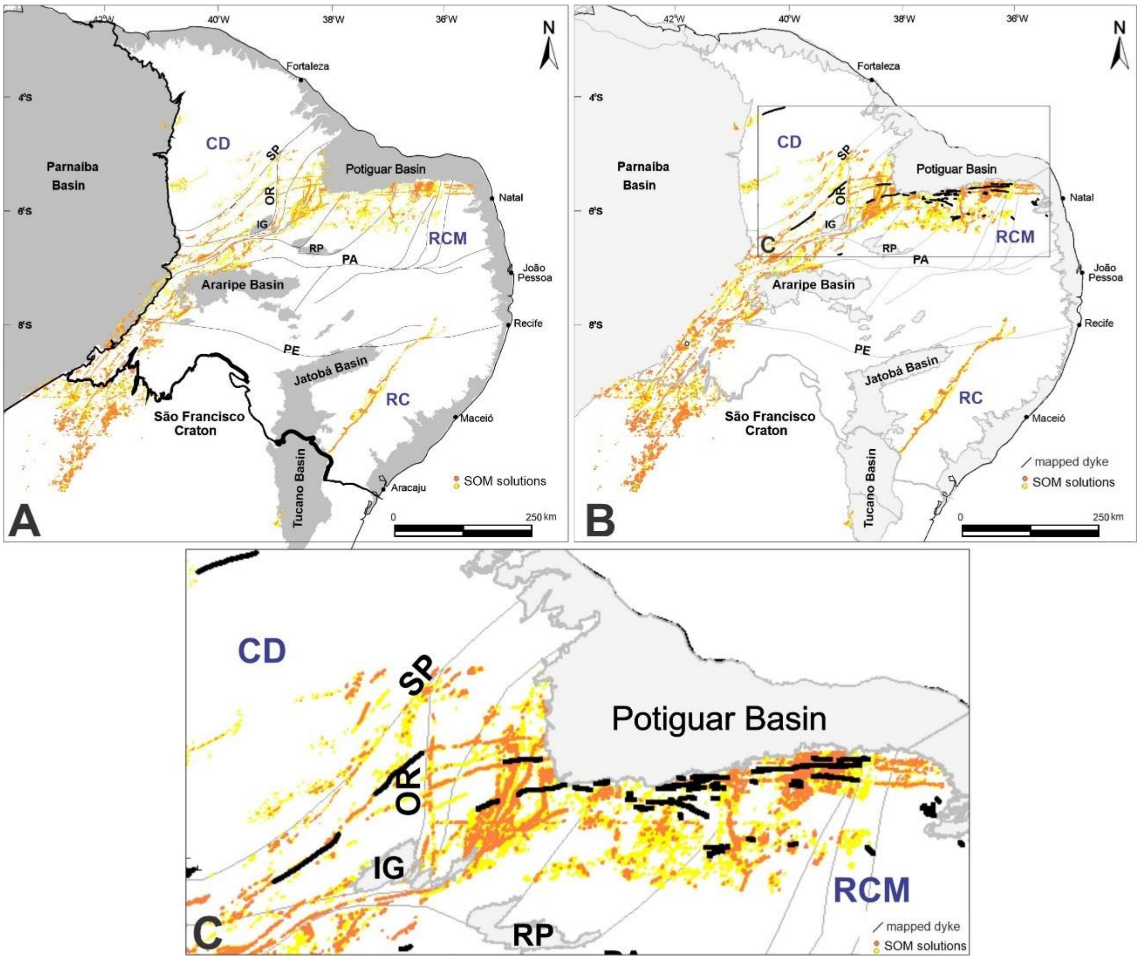

Figure 4.11. Distribution of SOM-derived clustered populations (1 - yellow and 6 - orange) related to mafic dyke swarm occurrence in the Borborema Province, Paleozoic Parnaíba Basin and São Francisco Craton computed from airborne geophysical data (A). Comparison between previously mapped dykes (bold black lines) and those suggested by SOM solutions (B and C). Sedimentary basins: IG – Iguatu; RP – Rio do Peixe. Shear zones: OR – Orós; PA – Patos; PE – Pernambuco; SP – Senador Pompeu. Dyke swarms: Rio Ceará-Mirim – RCM; Canindé – CD; Riacho do Cordeiro – RC.

In the first area, which corresponds to the training area for the SOM analysis, there are four sets of dykes already identified by Cavalcante et al. (2003), using magnetic data (Fig. 4.6A). In this case, the SOM solutions correctly classified the dykes and differentiated them from shear zones that cross the area (Figs. 4.11 and 4.12A). This differentiation would not be so clear if only magnetic anomalies were considered, due to similar magnetic patterns. In this area, it is also possible to see that the dykes exhibit displacements of a few kilometers, where they cross the N-S trending shear zones (Fig. 4.12A), suggesting that the shear zone was reactivated at some point after the dyke intrusion.

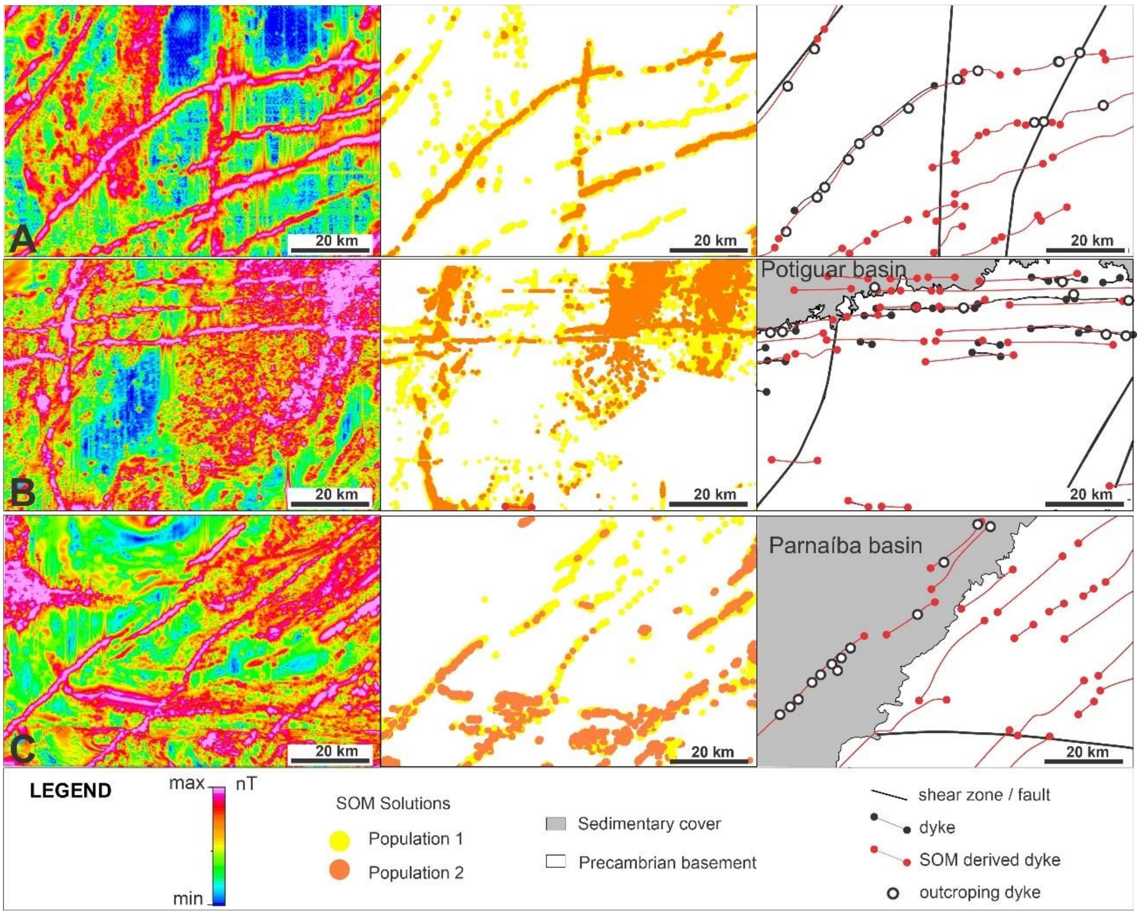

Figure 4.12. Comparison between ASA map (left), SOM solutions related to mafic dykes (middle), and the comparison between SOM-derived dykes and previously mapped dykes and geological structures (right) in distinct regions of the Borborema Province (A, B and C). Locations in Figure 3.3.

In the area south of the Potiguar Basin (Figs. 4.1 and 4.12B), the SOM solutions show a considerable increase in the number of previously mapped dykes, but the same success has not been achieved in differentiating the magnetic signature of the E-W oriented dyke swarms from geological units with high-amplitude ASA anomalies as in the training area described above (Fig. 4.12B). The Precambrian fabric and many Cenozoic igneous bodies that occur in this region (Mizusaki et al., 2012; Knesel et al., 2011) generate clouds of SOM solutions, roughly oriented in the N-S direction. In this case, it is evident the need for an extra analysis of the geological context to eliminate solutions not directly associated with the dykes. However, the SOM analysis greatly reduces the target areas for later field recognition.

And finally, in the area in the SW portion of the BP (Figs. 4.3 and 4.12C), the SOM solutions were able to reveal dykes that are not mapped on the most recent geological maps, encompassing even the Paleozoic units of the Parnaíba Basin. In this case, the SOM analysis correctly differentiates the dykes from regional-scale geological features, especially E-W shear zones. As in the test area (Fig. 4.12A), the SOM derived dykes reveal that the NE-SW swarms cross the E-W shear zones at high angles (40-45°).

The SOM method applied to the geophysical dataset in this study demonstrates that the occurrences of mafic dyke swarms, outcrops and non-outcrops, in the BP associated to the West Gondwana Breakup breakup and the Equatorial Atlantic opening (Bellieni et al., 1992; Marzoli et al., 1999; Hollanda et al., 2019), have greater extension than was previously known (Fig. 4.1). Furthermore, the SOM allowed us to identify three groups of dyke swarms with different structural directions. The main and most expressive dyke swarm has an extension of approximately 350 km in length and E-W direction at the southern boundary of the Potiguar Basin. It is also possible to distinguish four parallel sub-swarms, which change their orientation to NE-SW westward from 39º W meridians, defining an arched geometric pattern for all swarm complex, whose longitudinal extension reaches about 1000 km (Figs. 4.9 and 4.11). The great extension and the orientation change of the dyke sub-swarms classify them as an arcuate giant swarm according to the definition given by Ernst and Buchan (1997).

In this case, we correlated the clustered populations 1 and 6 to the Rio Ceará-Mirim dyke swarm (RCM). The SOM solutions with the directions E-W and NE-SW are coincident with the dykes previously mapped by Cavalcante et al., (2003) and Angelim et al. (2006) (Figs. 4.1, 4.7 and 4.12). Furthermore, SOM analysis predicted that these dyke swarms, which we correlated to the RCM have much greater extent than reported in previous studies (e.g., Bellieni et al., 1992; Archanjo and Launeau, 2004; Ngonge et al., 2016). It is even possible to clearly identify SOM solutions that occur at the western border of the BP with NE-SW direction, crossing the Patos and the Pernambuco shear zones (PA and PE in Fig. 3.11). We even identified some occurrences of dykes 200-km far away in the southwestern part of the Parnaíba Basin and others that extend southward into the São Francisco Craton.

Matos (1992) associated the emplacement of the RCM to the first syn-rift stage of the evolution of the Potiguar Basin. Our semi-automatic mapping also presents solutions for the already known dykes that occur in the Potiguar Basin in additional to NE solutions attributed to the dykes that occur on the edges of other aborted cratonic rifts such as Iguatu and Rio do Peixe basins (IG and RP in Fig. 4.11). The NE-SW oriented dykes have not yet been studied in geochemical, geochronological, and structural terms. In general, these dykes cross the shear zones at high angles, which demonstrates the influence of the paleostress field active during the emplacement of dykes. The SOM solutions showed that the pattern of conditioning efforts of the swarm intrusion remains unchanged during the igneous event, but the regime that was acting in an area could be more extensive than that related by Matos (1992). The author proposed that the variation in the trend of the structures can be explained by the differentiated tectonic behavior in the portions above the Patos shear zone, due to a rotation of the extensional axis from NW-SE to N-S during the South American and African breakup.

The SOM analysis also recognized another set of dykes, named Canindé dyke swarm (CD in Fig. 4.12) (Hollanda et al., 2019), originated from the same magmatic event as the RCM, in the NW sector of the BP, in the Ceará Central domain west of the Senador Pompeu shear zone (SP in Fig. 4.11). Within this geological domain, Cavalcante et al. (2003) mapped dykes with different orientations, NE-SW and NW-SE. However, the SOM analysis shows well-defined solutions only for the NE-SW dykes. This may have happened due to the low magnetic susceptibility of the NW-SE dykes and their smaller dimensions compared with dykes of the RCM.

A new set of dykes was predicted by SOM analysis in the southeastern portion of BP. Hollanda et al. (2019) suggest that this dyke swarm, called Riacho do Cordeiro (RC in Fig. 4.12), is part of the same magmatic event of the RCM based on an unpublished local K-Ar age of 119 ± 2.0 Ma. SOM solutions present two distinct segments, a 0.3-km long segment in the southwestern boundary of the Tucano basin and a much longer group of solutions, which has up to 300 km to the east of the Tucano and Jatobá basins until crossing with the Pernambuco shear zone northwards (Fig. 4.11). SOM analysis shows no cluster population within the sedimentary basins, just outside its borders. This may have happened due to the presence of a ~6.0 km thick, low magnetic sedimentary infill (Costa et al., 2007), which attenuates the magnetic anomalies from supposed dykes deep-seated in the basement. The RC magmatism can be related to the syn-rift stage of these basins, just as RCM is for the evolution of the Potiguar Basin as pointed out by Matos (1992).

4.6. Conclusions

An unsupervised semi-automated mapping technique based on a SOM approach, was applied to airborne geophysical data to map extensive mafic dyke swarms, associated with the Equatorial Atlantic opening, and emplaced in a Neoproterozoic fold belt and in adjacent cratonic domains in NE Brazil. In this study, we use five variables, derived from magnetic and gamma-spectrometric data, to classify them in distinct populations and to associate some populations with geophysical patterns related to the mafic dyke swarms. At first, a test area was selected to train SOM parameters (BMU's) and then, the adjusted SOM analysis was replicated for the entire studied area to preserve the same solutions pattern for the variables that were used. Since we assume the same trained BMU's for all areas and the geophysical signatures of the dykes are similar throughout the region where they occur, we did not notice any significant differences in the SOM solutions for the different airborne surveys.

The SOM approach identified seven distinct populations, of which two populations (1 and 6) were directly associated with the mafic dykes, while the other populations were correlated to different geological units, according to the geophysical signatures of each rock type or structural feature. The mafic dyke populations demonstrate similar characteristics as short wavelength and high amplitudes of the magnetic data, causing high quantization error in these groups. Also, they show high K (%), medium and low values of eTh and eU, respectively. Field surveys confirmed the presence of dykes in the areas indicated by the SOM solutions. In addition, the effectiveness of the SOM analysis in identifying mafic dykes was evaluated by comparing its solutions with previous geological maps and with qualitative interpretation only of magnetic anomalies. The introduction of gamma-spectrometric data reduced the ambiguity in the identification of dykes.

The SOM results expanded the area of occurrence of the Rio Ceará-Mirim dyke swarm (RCM) from merely 350 km to more than 1000 km, crossing the entire Borborema Province and affecting the adjacent cratonic region and Paleozoic basin. Two new Riacho do Cordeiro (RC) and Canindé (CD) dyke swarms were identified by the SOM analysis, in regions where the presence of dykes was little known or even unknown. With these results, a new large magmatic province (LIP) is being proposed for the region. Field surveys have already confirmed the presence of dykes in the locations indicated by the SOM solutions. In addition, the SOM solutions were able to assign to the RCM magmatism two sets of dyke swarms with E-W and NE-SW directions in the NE and SW borders of the Borborema Province, respectively. The RC is also successfully mapped by SOM analysis, revealing the occurrence of another swarm of dyke coeval to the RCM. To the best of our knowledge, this dyke swarm was poorly described in previous studies. Nevertheless, the SOM solutions display no consistent results for CD. Due to the thin thickness of those dykes, they have probably no expressive geophysical responses. The tectonic implications of the real dimension of the magmatic events responsible for dyke emplacement in BP is beyond the scope of this article and will be the aim of a future study.

Acknowledgments

The authors thank the Dr. Colin Farquharson and the anonymous reviewers for the suggestions that greatly improved the previous version of this article. ACCM would like to thank Programa de Formação de Recursos Humanos PRH-PB 229 (FUNPEC/UFRN/PETROBRAS) for her PhD scholarship (project 672013) and the Coordenação de Aperfeiçoamento de Pessoal de Nível Superior (Capes) for supporting a sandwich PhD scholarship at the Australian Commonwealth Scientific and Industrial Research Organization (CSIRO) and The University of Queensland (UQ; Process N. 88881.188664/2018-01). DLC thanks Conselho Nacional de Desenvolvimento Científico e Tecnológico (CNPq) for his PQ grants. AAMF thanks Fundação de Amparo à Pesquisa do Estado de São Paulo (FAPESP) for his PhD scholarships at the University of São Paulo (USP; grants 2017/13130–0) and the Research Internships Abroad Program (BEPE / FAPESP) for his scholarship at the UQ (grant 2018/24769–5). We also thank the Geological Survey of Brazil (SGB) for providing the geophysical data; CSIRO Mineral Resources Flagship, located at the "Queensland Centre for Advanced Technologies"

(QCAT) in Brisbane, for the provision of the SiroSOM software and for the facilities to execute the SOM analysis; Professors Maria Helena Hollanda and Carlos Archanjo from USP for all the support during the fieldwork and general discussions; Professors Rick Valenta and Paul Gow from the UQ for their contributions. This work is part of the ACCM PhD dissertation and the Instituto Nacional de Ciência e Tecnologia em Estudos Tectônicos (INCT-ET) and corresponds to the contribution no. 3 of the EQUAMP LIP Project (grant 2017/08423-9).

REFERENCES

Almeida, F.F.M., Brito Neves, B.B., Dal Ré Carneiro, C., 2000. The origin and evolution of the South American Platform. Earth-Science Reviews 50, 77–111. https://doi.org/10.1016/S0012-8252(99)00072-0

Almeida, F.F.M., Carneiro, C.D.R., Machado Jr., D., Dehira, L., 1988. Magmatismo Pós-Paleozóico no Nordeste Oriental do Brasil. Revista Brasileira de Geociências 18, 451–462.

Angelim, L.A.A., Medeiros, V.C., Nesi, J.R., 2006. Programa Geologia do Brasil – PGB. Projeto Geologia e Recursos Minerais do Estado do Rio Grande do Norte. Mapa geológico do Estado do Rio Grande do Norte. Escala. 1:500.000. Recife: CPRM/FAPERN, 2006. 1mapa color.

Archanjo, C.J., Launeau, P., 2004. Magma flow inferred from preferred orientations of plagioclase of the Rio Ceará-Mirim dyke swarm (NE Brazil) and its AMS significance. Geological Society, London, Special Publications 238, 285–298. https://doi.org/10.1144/gsl.sp.2004.238.01.17

Bação, F., Lobo, V., Painho, M., 2005. The self-organizing map, the Geo-SOM, and relevant variants for geosciences. Computers and Geosciences 31, 155–163. https://doi.org/10.1016/j.cageo.2004.06.013

Bellieni, G., Macedo, M.H.F., Petrini, R., Piccirillo, E.M., Cavazzini, G., Comin-Chiaramonti, P., Ernesto, M., Macedo, J.W.P., Martins, G., Melfi, A.J., Pacca, I.G., De Min, A., 1992. Evidence of magmatic activity related to Middle Jurassic and Lower Cretaceous rifting from northeastern Brazil (Ceará-Mirim): K/Ar age, palaeomagnetism, petrology and Sr/1bNd isotope characteristics. Chemical Geology 97, 9–32. https://doi.org/10.1016/0009-2541(92)90133-P

Blakely, R.J., 1996. Potential Theory in Gravity and Magnetic Applications, Program. https://doi.org/10.1017/CBO9780511549816

Bleeker, W., Ernst, R., 2006. Short-lived mantle generated magmatic events and their dyke swarms: The key unlocking Earth's palaeogeographic record back to 2.6Ga. Dyke Swarms - Time Markers of Crustal Evolution - Proceedings of the 5th International Conference, IDC-5 3–26.

Boschetti, F., Wijns, C., Moresi, L., 2003, Effective exploration and visualization of geological parameter space. Geochemistry, Geophysics and Geosystems, 4(10), 1086, https://doi:10.1029/2002GC000503

Briggs, I.C., 1974. Machine Contouring Using Minimum Curvature. Geophysics 39, 39–48. https://doi: 10.1190/1.1440410

Brito Neves, B.B., Cordani, U.G., 1991. Tectonic evolution of South America during the Late Proterozoic. Precambrian Research 5, 23–40. https://doi:10.1016/0301-9268(91)90004-T

Brito Neves, B.B., Fuck, R.A., Pimentel, M.M., 2014. The Brasiliano collage in South America: a review. Brazilian Journal of Geology 44, 493-518. https://doi: 0.5327/Z2317-4889201400030010

Carneiro, C.D.C., Fraser, S.J., Crósta, A.P., Silva, M., Eduardo, C., Barros, D.M., 2012. Semiautomated geologic mapping using self-organizing maps and airborne geophysics in the Brazilian Amazon. Geophysics 77, 17-24. https://doi.org/10.1190/GEO2011-0302.1

Cavalcante, J.C. , Vasconcelos, A.M., Mederios, M.F., Gomes, I., 2003. Mapa geológico do estado do Cear. Escala 1:500.000. Fortaleza: CPRM, 2003.

Costa, I.P., Milhomem, P.S., Bueno, G.V., Lima e Silva, H.S.R., Kosin, M. D., 2007. Sub-Bacias de Tucano Sul e Central. Boletim de Geociências da Petrobrás, Rio de Janeiro, 15, 2, 433-443.

Davies, D.L., Bouldin, D.W., 1979. A Cluster Separation Measure. IEEE Transactions on Pattern Analysis and Machine Intelligence PAMI-1, 224–227.

https://doi.org/10.1109/TPAMI.1979.4766909

de Castro, D.L., Bezerra, F.H.R., Castelo Branco, R.M.G., 2008. Geophysical evidence of crustal-heterogeneity control of fault growth in the neocomian iguatu basin, NE Brazil. Journal of South American Earth Sciences, 26, 271-285.

de Castro, D.L., Oliveira, D.C., and Hollanda, M.H.B.M., 2018. Geostatistical Interplay Between Geophysical and Geochemical Data: Mapping Litho-Structural Assemblages of Mesozoic Igneous Activities in the Parnaíba Basin (NE Brazil). Surveys in Geophysics, 1–31, https://doi: 10.1007/s10712-018-9463-5

Delgado, I.M., Souza, J.D., Silva, L.C., Silveira Filho, N.C., Santos, R.A., Pedreira, A.J., Guimarães, J.T., Angelim, L.A.A, Vasconcelos, A.M., Gomes, I.P., Lacerda Filho, J.V., Valente, C.R., Perrotta M.M. and Heineck, C.A., 2003. Geotectônica do Escudo Atlântico, in: Bizzi, L.A., Schobbenhaus, C., Vidotti, R.M. and Gonçalves, J.H. (Eds.), Geologia, Tectônica e Recursos Minerais do Brasil. CPRM, Brasília, pp. 227-334.

Ernesto, M., Furtado, M.H., Macedo, J. W. P., Martins, G., 1991. Paleomagnetism of the Ceará-Mirim dyke swam, northeastern Brazil. Boletim Instituto de Geociências USP, 10, 85-89.

Ernst, R.E., Buchan K.L., 2001. The use of mafic dike swarms in identifying and locating mantle plumes. In: Mantle plumes: their identification through time. Special Paper of the Geological Society of America 352, 247-265. https://doi: 10.1130/0-8137-2352-3.247

Fraser, S. H., Dickson, B.L., 2007. A new method of data integration and integrated data interpretation: Self-organizing maps, in B. Milkereit, ed., Proceedings of Exploration 07: Fifth Decennial International Conference on Mineral Exploration, 907–910.

Fraser, S.J., Hodgkinson, J.H., 2009. An Investigation Using SiroSOM for the Analysis of QUEST Stream-Sediment and Lake-Sediment Geochemical Data. Geoscience BC 2009-14 CSIRO–E&M, Report 2009/283, 43p.

Geosoft, 2010. Montaj GridKnit. Grid stitching extension for Oasis Montaj V7.1. Tutorial and users guide. Geosoft Incorporation.

Geosoft, 2013. Applying standard filters. Applying filter with montaj Geophysics. Geosoft Corporation.

Halls, H.C., 1982. The importance and potential of mafic dyke swarms in studies of geodynamic processes. Geoscience Canada 9, 145–154.

Hawkesworth, C.J., Cawood, P.A., Dhuime, B., 2016. Tectonics and crustal evolution. GSA Today 26, 4–11. https://doi.org/10.1130/GSATG272A.1

Hill, R., 1991. Starting Plumes and continental breakup. Earth and Planetary Science Letters 104, 938-416. https://doi:10.1016/0012-821X(91)90218-7

Hollanda, M.H.B.M., Archanjo, C.J., Macêdo Filho, A.A., Fossen, H., Ernst, R.E., de Castro, D.L., Melo, A.C.C., Oliveira, A.L., 2019. Dyke Swarms of the World: A Modern Perspective, in: Srivastava, R.K., Ernst, Richard E., Peng, P. (Eds.), Dyke Swarms of the World: A Modern Perspective, Springer Geology, Springer Geology. Springer Singapore, Singapore, pp. 87–110. https://doi.org/10.1007/978-981-13-1666-1

Hollanda, M.H.B.M., Pimentel, M.M., Oliveira, D.C., Jardim de Sá, E.F., 2006. Lithosphere-astenosphere interaction and the origin of Cretaceous tholeiitic magmatism in Northeastern Brazil: Sr-Nd-Pb isotopic evidence. Lithos 86, 34-49, https://doi: 10.1016/j.lithos.2005.04.004

Jessell, M.W, Santoul, J., Baratoux, L., Youbi, N., Ernst, R.E., Metelka, V., Miller, J., Perrouty, S., 2015. An updated map of West African mafic dykes. Journal of African Earth Sciences, 112 (2), 440-450. https://doi:10.1016/j.jafrearsci.2015.01.007

Knesel, K. M., Souza, Z. S., Vasconcelos, P. M., Cohen, B.E., Silveira, F. V., 2011. Young volcanism in the Borborema Province, NE Brazil, shows no evidence for a trace of the Fernando de Noronha plume on the continent. Earth and Planetary Science Letters, 302 (1-2), 38-50. https://doi:10.1016/j.epsl.2010.11.036

Kohonen, T., 1982. Analysis of a simple self-organizing process. Biological Cybernetics 44, 135-140, https://doi:10.1007/BF00317973

Kohonen, T., 2001. Self-Organizing Maps, Third edit. ed. Berlin, Heidelberg: Springer Berlin Heidelberg, Berlin, Heidelberg. https://doi: 10.1007/978-3-642-56927-2

Maluski, H., Coulon, C., Popoff, M., Baudin, P., 1995. 40Ar/39Ar chronology, petrology and geodynamic setting of Mesozoic to early Cenozoic magmatism from the Benue trough, Nigeria. Journal of th Geological Society, 152, 311–326, https://doi:

10.1144/gsjgs.152.2.0311

Matos, R.M.D., 1992. The Northeast Brazilian Rift System. Tectonics 11, 766–791. https://doi.org/10.1029/91TC03092

Marzoli, A., Renne, P.R., Piccirillo, E.M., Ernesto, M., Bellieni, G., De Min, A., 1999. Extensive 200-million-year-old continental flood basalts of the Central Atlantic Magmatic Province. Science 284, 616–618. https://doi.org/10.1126/science.284.5414.616

Mikula, P.A., Fraser, S.J., Lee, M.F., 2008. Self-Organising Map Analysis of Seismicity Associated with Mining at Mount Charlotte Mine, in Y. Potvin, , J. Carter, A. Dyskin, R. Jeffrey, eds., Proceedings of the First Southern Hemisphere International Rock Mechanics Symposium, Australian Centre for Geomechanics, 653–666. https://doi.org/10.36487/ACG_repo/808_103

Minty, B.R.S., 1997. Fundamentals of airborne gamma-ray spectrometry. AGSO Journal of Australian Geology & Geophysics, 17 (2), 39–50.

Mizusaki, A.M.P., Thomaz Filho, A., Milani, E.J., Césero, P., 2002. Mesozoic and Cenozoic igneous activity and its tectonics control in northeastern Brazil. Journal of South American Earth Sciences 15, 183–198. https://doi: 10.1016/S0895-9811(02)00014-7

Nabighian, M.N., 1972. The analytic signal of two dimensional magnetic bodies with polygonal cross-section: It's properties and use for automated anomaly interpretation. Geophysics, 37, 507-517. https://doi: 10.1190/1.1440276.

Ngonge, E.D., de Hollanda, M.H.B.M., Archanjo, C.J., de Oliveira, D.C., Vasconcelos, P.M.P., Munhoz, P.R.M., 2016. Petrology of continental tholeiitic magmas forming a 350-km-long Mesozoic dyke swarm in NE Brazil: Constraints of geochemical and isotopic data. Lithos 258–259, 228–252. https://doi.org/10.1016/j.lithos.2016.04.008

Ni, N., Chena, N., Ernstb, R.E., Yanga, S., Chend, J., 2019. Precambrian Research. 329, 262-272, https://doi: 10.1016/j.precamres.2018.05.020

Oliveira, D. C., 1992. O papel do Enxame de Diques Rio Ceará Mirim na evolução tectônica do nordeste oriental (Brasil): implicações na formação do Rifte Potiguar. Ms.

C. Dissertation, Univ. Fed. de Ouro Preto, Ouro Preto, Brazil.

Oliveira, R.G., Medeiros, W.E., 2012. Evidences of buried loads in the base of the crust of Borborema Plateau (NE Brazil) from Bouguer admittance estimates: Journal of South American Earth Sciences, 37, 60–76, https://doi: 10.1016/j.jsames.2012.02.004

Oliveira, R.G., Medeiros, W.E., 2018. Deep crustal framework of the Borborema Province, NE Brazil, derived from gravity and magnetic data. Precambrian Research 315, 45–65. https://doi.org/10.1016/j.precamres.2018.07.004

Reeves, C.V., 2000. The geophysical mapping of Mesozoic dike swarms in south Africa and their origin in the disruption of Gondwana. Journal of African Earth Science 30, 3, 449-513. https://doi: 10.1016/S0899-5362(00)00035-X

Ross, G.M., Broome, J., Miles, W., 1994. Potential fields and basement structure: Western Canada Sedimentary Basin, in G.D. Mossop and Shetsen, I., Geological atlas of the Western Canada Sedimentary Basin: Canadian Society of Petroleum Geologists and Alberta Research Council, 41–46.

Silveira, F.V., 2006. Magmatismo cenoz´oico da porç˜ao central do Rio Grande do Norte, NE do Brasil. Tese (Doutorado). Natal: Programa de P´os-Graduaç˜ao em Geodinˆamica e Geofísica - UFRN.

Souza, Z.S., Vasconcelos, P.M.P., Nascimento, M.A.L., Silveira, F.V., Paiva, H.S., Dias, L.G.S., Thiede, D., Carmo, I.O., 2003. 40Ar/39Ar geochronology of Mesozoic and Cenozoic magmatism in NE Brazil. Short Papers - IV South American Symposium on Isotope Geology, Salvador, Proceedings, vol. 2, pp. 691-694. http://horizon.documentation.ird.fr/exl-doc/pleins_textes/divers17-05/010039206.pdf

Szatmari, P., Françolin, J.B.L., Zanotto, O., Wolff, S., 1987. Evolução tectônica da Margem Equatorial Brasileira. Revista Brasileira de Geociências, 17(2), 180-1 88. https://doi: 10.25249/0375-7536.1987180188

Torppa, J., Middleton, M., Lerssi, J., Fraser, S., 2015. Novel Spatial Analysis Approach for Assessing Regional-Scale Mineral 61, 87–120

Trumbull, R.B., Vietor, T., Hahne, K., Wackerle R., Ledru, P., 2004. Aeromagnetic mapping and reconnaissance geochemistry of the Early Cretaceous Henties Bay-Outjo dike swarm, Etendeka Igneous Province. Namibia. Journal of African Earth Sciences, 40,17–29. https://doi:10.1016/j.jafrearsci.2004.07.006

Ultsch, A., 2003. U*-Matrix: a Tool to visualize Clusters in high dimensional Data. University of Marburg, Department of Computer Science, Technical Report, N. 36, 12p.

Van Schmus, W.R., Oliveira, E.P., Silva Filho, A.F, Toteu, F.S., Penaye, J., Guimarães, I.P., 2008. Proterozoic links between the Borborema Province, NE Brazil, and the Central African Fold Belt. In: Pankhurst, R.J., Trouw, R.A., Brito Neves, B. B., De Wit, M.J. (eds) West Gondwana: pre-cenozoic correlations across the South Atlantic, 294, 669-99. https://doi.:10.1144/SP294.5

Xiong, S., Yang, H., Ding, Y., Li, Z., Li, W., 2016. Distribution of igneous rocks in China revealed by aeromagnetic data. Journal of Asian Earth Sciences 129, 231–242. https://doi.org/10.1016/j.jseaes.2016.08.016

Zaineldeen, U.F., 2013. Mapping the Dyke Swarms of the Neoproterozoic Basement in Southwestern Jordan Using Remote Sensing and GIS Techniques. Earth Science Research, 2, 1, 156-164, https://doi: 10.5539/esr.v2n1p156

Capítulo 5

MESOZOIC DYKE SWARMS IN BORBOREMA PROVINCE (NE BRAZIL): A STRUCTURAL ANALYSIS BASED ON AIRBORNE GEOPHYSICAL DATA AND FIELDWORK

[*]Este manuscrito foi submetido ao Tectonophysics em maio de 2021

Mesozoic Dyke Swarms in Borborema Province (NE Brazil): a Structural Analysis Based on Airborne Geophysical Data and Field Work

Melo, A.C. [a*], de Castro, D.L. [a,b], Oliveira[b], D.C., and Hollanda[c] , M.H.B.M.

[a] Programa de Pós-Graduação em Geodinâmica e Geofísica, Departamento de Geologia, Universidade Federal do Rio Grande do Norte, Campus Universitário S/N, Lagoa Nova, 59.078- 970 Natal – RN, Brazil.
[b] Departamento de Geologia, Universidade Federal do Rio Grande do Norte, Campus Universitário S/N, Lagoa Nova, 59.078-970 Natal – RN, Brazil.

[c] Instituto de Geociências, Universidade de São Paulo, São Paulo 05508–080, Brazil.

*Corresponding author: Alanny Christiny Costa de Melo (alanny.melo.079@ufrn.edu.br).

Highlight:

- Airborne geophysical data applied to map mafic dyke.
- We have produced a new map of mafic dykes across the Borborema Province, NE Brazil.
- Several new dykes are identified in the Borborema Province using magnetic and structural criteria.
- New 1388 mafic dyke are identified by magnetic anomalies.
- The areal extension of mafic dykes is at least 6.8 x10^6 km^2.
- NE trend of Rio Ceará-Mirim Dyke Swarm is better characterized.

Abstract

Mapping and analyses of mafic dyke swarms support understanding in detail the orientation, geometry, spatial distribution, geochronology, emplacement mechanism, structural control, and environments at the time of the magmatic events. Therefore, dyke swarms have become a key tool for studying mantle plume activity, large igneous provinces (LIPs), and continental breakup. Precise mapping of dykes and their grouping into swarms is essential to understand the tectonic plate movement and evolution. The high-resolution airborne geophysical data of the Neoproterozoic Borborema Province allowed constructing a new map concerning the spatial distribution of dyke swarms in the northeastern most South American platform. The main objective of this research is to promote the regional mapping of the dyke swarms and their relations between orientation, emplacement mechanism and structural control to a better understanding of the role of the Mesozoic and Cenozoic large magmatic event in its tectonic evolution. We apply anomaly enhancement techniques to magnetic data to obtain the geometry and estimate the depth of causative sources. A structural analysis was carried out integrating magnetic patterns, field data and a compilation of previous geological maps to describe the detailed distribution of the dyke swarms in Borborema Province. Our analyses demonstrated that the dyke swarms extend over 6.8 $x10^6$ km^2. The 1388 mapped mafic dykes are grouped in three distinct swarms: 1135 – Rio Ceará-Mirim (RCM); 168 – Canindé (CD); and 86 – Riacho do Cordeiro – RC. The dyke swarms show three preferential trends to E-W, NW-SE and NE-SW. The swarms intrude both the Precambrian basement units and the Cretaceous sedimentary basins. The geometry and structural analysis of the dykes allowed to establish the paleostress field active at the time of the intrusion. To the RCM, the paleostress trajectories represent an N-S extension, rotating to NW-SE in the western portion of the swarm. While for CD, the paleostress orientation shows a NW-SE extension rotating to NE-SW. As for the RC, the trajectories were similar to those traced for the RCM, showing a predominant NW-SE trend.

Keywords: Airborne Geophysical Data; Mafic Dyke Swarms; Structural Analysis; Borborema Province.

5.1. Introduction

Mafic dykes constitute an essential key for studies about structural geology and geotectonic evolution. Indeed, dyke swarms represent important time-markers, which provide chronological information about geodynamic process, rift kinematics, magmatic activity, large igneous provinces genesis (Ernst et al., 1996; Ernst and Buchan, 2013; Demarco et al., 2020). Trends of dyke swarms provide evidence about paleostress, crustal kinematics and geotectonic regime (Anderson, 1951; Halls, 1982; Delaney et al., 1986). These intrusive features can support understanding implication for the tectonic events, which still needs to be answered by displaying on their age, strike direction, composition and by classifying them in swarms (Reeves, 2000).

Previous studies indicate that mapping of dykes and their grouping into swarms is fundamental for understanding the tectonic context and the driven mechanisms that promote its emplacement within the crust and plate movements (Ernst and Buchan, 2001; Trumbull et al., 2004; Zaineldeen, 2012; Nasuti, et al. 2015). Most of dyke swarms are related to mantle plumes and typically associated with divergent continental margins (Fahrig, 1987), especially to mantle plume activity, large igneous provinces (LIPs), and continental break-up (Ernst et al., 1996; Goldberg, 2010; Kiselev et al., 2012; Ernst, 2014). Nevertheless, detecting and mapping dyke swarms in large areas is laborious and therefore expensive, particularly in areas of difficult access or without outcrops. In these cases, airborne geophysical surveys provide information on both exposed and buried rocks, which makes it possible to carry out continental-scale studies, revealing the real extent of the magmatic events (Trumbull et al., 2004; Jessel et al., 2015; Xiong et al, 2016; Demarco et al., 2020). In general, basic dykes are very expressive in magnetic anomaly maps due to its high contrast of magnetic susceptibility (de Castro et al., 2018; Reeves, 2000). Most of the dykes are thin and elongated bodies, they therefore appear as linear features in magnetic maps (Tucker and Boyd, 1987).

In NE Brazil, the Precambrian Borborema Province (BP) was intensively intruded by >1000 km-wide arched dyke swarms that extend into neighboring São Francisco Craton (SFC) and Paleozoic Parnaíba Basin (PB) (e.g., Gomes et al., 1981; Hollanda et al., 2019; Melo et al., 2021) (Fig. 5.1). The BP corresponds to a geological-structural domain, which consists of Archean to Proterozoic inliers amalgamated along volcano-sedimentary belts in the easternmost tip of the South American platform (Brito Neves et al., 2014; Neves et al., 2000) (Figs. 5.1A and 5.1B). During the Mesozoic-Cenozoic period, the NE Brazil was scene of several intrusive and extrusive magmatic events of predominantly basic rocks that prevailed and partially followed the up rise and evolution of the Equatorial and South Atlantic rift systems (Almeida et al., 1988; Matos, 1992). In this area, a series of dolerite mafic dykes, which is considered the most significant magmatic activity with a length of 350 km (Archanjo and Launeau, 2004; Ngonge et al., 2016), dated age of 132.2 ± 1 Ma (Souza et al., 2003).

The Rio Ceará-Mirim Dyke Swarm (RCM) is the main branch of basic dykes, crosscutting the Precambrian host rocks with a NE-SW trend bended to E-W direction eastwards (Fig. 5.1C). Gomes et al. (1981) were one of the first to map ~250 km of the RCM, which is only a third of its currently known extension. Since then, the area of occurrence of the dyke swarm has been expanded over time, as new field studies have identified more dyke outcrops (e.g., Bellieni et al. 1992; Oliveira, 1992; Archanjo et al. 2002; Hollanda et al., 2019). Recently, Hollanda et al. (2019) integrated the Mesozoic magmatic events related to mafic dykes and sills of the RCM and those affected the Paleozoic Parnaíba Basin to propose a new Large Igneous Province (LIP) in South America. They named it the Mesozoic Equatorial Atlantic Magmatic Province (EQUAMP), which was mapped on regional scale mainly based on magnetic anomaly enhancement and semiautomatic source detection technique adapted by de Castro et al. (2018). Melo et al. (2021) applied this approach to improve the mapping of the dyke swarms in the BP, whose results were ground-truther at field locations using petrological analysis. Pessano et al. (2020) compilated a map with mafic dyke swarms of Brazil derived from airborne magnetic data, without conducting field validation. Despite of these recent advances in the mapping of magmatic bodies, the tectonic implications of the expanded areal distribution of the dyke swarms in the PB to the South Atlantic opening remain a matter of debate and will be discussed in this study.

Thus, the main objectives of this study are the regional mapping of the dyke swarms and their relations between orientation, emplacement mechanism and structural control. We combined geophysical interpretation of airborne data (gamma-spectrometric and magnetic), structural analyses of the magnetic maps, field work and compilation of previous geological data to discriminate the main structural framework of the BP and contribute to a better understanding of the role of the dyke swarms in its tectonic evolution in the Mesozoic and Cenozoic time.

The present mapping of dyke swarms demonstrated its regional-scale geometry, location, and orientation, providing a minimum estimate for the total number of the dyke swarms in the region. Our results reveal that the dyke swarms are larger, denser, more widespread, and with a more complex geometry than initially thought. In Previously studies (eg. Bellienni, 1992; Matos, 1992; Archanjo et al., 2004), dyke swarms were related to the Atlantic Ocean opening, our work shows new extension and geometry for the dykes in suggesting a possible plume activity. In general, the dykes cut faults and shear zones of the Precambrian basement, except for a few occasions, where they take advantage of weakness zones in the host rock. Moreover, crosscutting relationships make dykes valuable stratigraphic and kinematic markers. These results will certainly help further studies using other geological tools as petrology, geochemistry, analogue modelling, and geochronology.

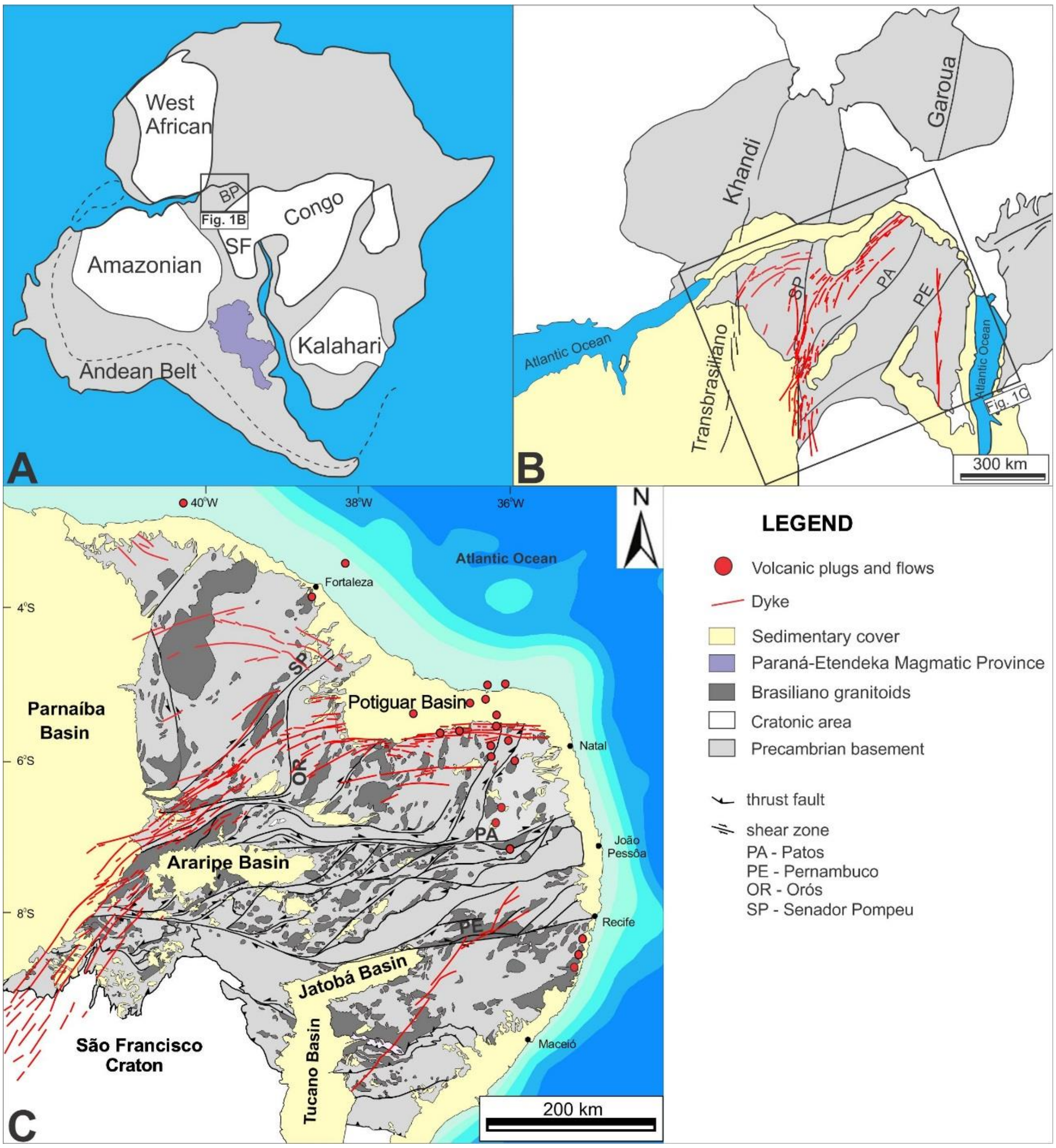

Figure 5.1. Schematic reconstruction map of the West Gondwana, showing the main cratonic areas – Amazonian, São Francisco (SF) - Congo, São Luís - West African and Kalahari (A) and the Borborema Province (BP); Pre-drift reconstitution of the main geological features of the NE Brazil and the west African counterpart, modified from Ngonge et al. (2016) (B); Simplified geological map of the Borborema Province (BP) (C). Main structures and magmatic events were compiled and modified from Oliveira (1992), Cavalcante et al. (2003), Delgado et al. (2003), Angelim et al. (2006), Van Schmus et al. (2008), Oliveira e Medeiros (2012), Hollanda et al. (2019) and Melo et al. (2021).

5.2. Regional Scale Lithostructural Host Domains

The geologic setting framework of the north easternmost area of the South American Platform, which was the scene of several igneous activity that characterizes the so-called RCM widespread dyke swarm, is characterized by a complex Neoproterozoic orogenic collage of cratonic nuclei amalgamated by fold belts along extensive ductile shear zones and partially recovered by Paleozoic intracratonic and Mesozoic marginal sedimentary basins (e.g., Brito Neves et al., 2014). The study area is composed of three distinct geological provinces: Proterozoic Borborema Province (BP), the northern sector of the São Francisco Craton (SFC) and the eastern edge of the Paleozoic Parnaíba Basin (PB) (Fig. 5.1).

5.2.1. Proterozoic Borborema Province

The BP corresponds to a Precambrian geological-structural domain located in the Northeast Brazil (Fig. 5.1), with an extension around 380.000 km² and it is characterized as a semi-arid climate (Almeida et al., 1981). It is an Archean to Proterozoic inliers amalgamated along volcano-sedimentary belts, including sedimentary basins (Brito Neves and Cordani, 1991; Neves et al., 2000). It is limited to the south by the São Francisco Craton, to the west by the Paleozoic Parnaíba Basin and to the north and east by the Mesozoic coastal basins (Potiguar, Paraíba, Pernambuco, and Sergipe Alagoas) (Fig. 5.1C).

The basement of BP is predominantly gneissic-migmatitic for all the tectonic domains, with two Archean nuclei in the middle of the Proterozoic bands. A set of extensive, NE-SW and E-W trending shear zones inherited from the overall Precambrian continental collisions represents the crustal domain boundaries (Fig. 5.1). This Precambrian geological and structural setting was completed at the final stages of the Brasiliano / Pan-African orogeny in the Neoproterozoic (Brito Neves, 1999) and, after a long period of tectonic quiescence (540-120 Ma), it was severely modified by the Cretaceous extensional tectonics that culminated in the Pangea breakup. During the Late Jurassic to Early Cretaceous occurred a series of brittle reactivations of the shear zones, forming aborted rift basins along the BP and surrounding marginal basins (Matos, 1992; Matos, 2021) (Fig. 5.1C).

The BP was segmented in three main tectonic domains (Northern, Central, and Southern sub-provinces) during the amalgamation of the Gondwana land. They are bounded by extensive transcurrent E-W Brasiliano shear zones (Patos and Pernambuco) and they are subdivided based on lithostratigraphic, structural features, geochronological data, and geophysical signatures (Delgado et al., 2003). In general, the shear zones are characterized by mylonitic rocks derived from granitoids, schist and gneiss. Furthermore, they controlled the accommodation of several granitoid bodies.

The Northern Subprovince comprises the portion of the BP located to the north of the Patos SZ (PA in Figs 5.1B and 5.1C). This area is composed of Paleoproterozoic migmatitic complexes, which are the basement of supracrustal units of Paleo-, Meso- and Neoproterozoic ages. During the Brasiliano orogeny, it was scene of intense tectonic activity that gave rise to a diverse granitoid plutonism and large N-S and NE-SW shear zones (e.g., Senador Pompeu, Orós) (Almeida et al., 1981; Brito Neves et al., 2014). The Central Subprovince corresponds to the E-W oriented crustal segment, bounded to the north and west by the Patos SZ, to the south by the Pernambuco SZ, and to the east by the coastal basins. It is structurally configured as an anastomosed system of dextral transcurrent shear zones with E-W direction and preferentially sinistral to the NE-SW direction. The Central Sub-province was affected by intense magmatism associated with final Brasiliano collisional movements (Van Schmus et al., 2003). Finally, the Meridional Subprovince represents the portion of the BP located to the south of the Pernambuco SZ, which encompasses a Mesoproterozoic domain and Neoproterozoic domains (Jardim de Sá, 1992; Brito Neves et al., 2014). This region is where the Mesozoic Tucano and Jatobá rift basins are located.

5.2.2. São Francisco Craton

The SFC is located to the south of BP, corresponding to older internal portions of the tectonic plates, which were amalgamated at the end of the Proterozoic, forming the West Gondwana Supercontinent (Almeida, 1981; Trompette, 1992; Hasui, 2012). It is associated to the Mesoproterozoic Congo Craton in West Africa. The São Francisco Craton shows a high-grade metamorphic Archaean and Paleoproterozoic terrains, Paleoproterozoic sedimentary basins and rifts, with associated supracrustal sequences and subordinate volcanism, in addition to extensive Neoproterozoic sedimentary coverings.

The SFC is subdivided, according to Souza et al. (2003), in three sectors: the western sector is strongly influenced by Transamazônico Orogenic Cycle (2,250 to 1,900 Ma); the Central sector exhibits Mesoproterozoic units; and the western sector is defined by exhibiting Neoproterozoic units. In these three sectors, it has been distinguished a large number of geological domains, also referred to as blocks (Delgado et al., 2003). The RCM swarms intrude the Archean-Paleoproterozic basement from the northwestern segment of the São Francisco Craton denominated Sobradinho Block (Fig. 5.1C). Gneiss-migmatitic, metavolcanosedimentary, and greenstone sequences compose the local host rocks for the mafic dykes.

5.2.3. Paleozoic Parnaíba Basin

The Parnaíba Basin corresponds to one of the vast Paleozoic-Mesozoic cratonic basins of the South American Platform. The basin is limited to the west by the Amazonian Craton, to the southeast by the São Francisco Craton, to the north it rests on the São Luiz Craton, and to the east it is limited by the Borborema Province (e.g., Cordani et al., 1984; de Castro et al., 2014). This area is approximately 668,858 km^2 and the thickness of the tectonic-sedimentary sequence is little more than 3,500 m (Zembruscki and Campos, 1988), which increases to about 5,000 m considering Pre-Silurian grabenlike structures anchored by the Transbrasiliano Lineament (de Castro et al., 2016).

Its Precambrian basement is represented by an Archean–PaleoProterozoic cratonic blocks, Neoproterozoic Brasiliano/Pan-African fold belts and concealed basement inliers (Cordani et al., 1984; de Castro et al., 2014). These geological domains are composed mainly of a broad assembly of magmatic/metamorphic rocks amalgamated by collisional tectonics that stabilized at the end of the Brasiliano/Pan African orogeny (Goes and Feijó, 1994).

The tectono-stratigraphic evolution of the Parnaíba basin involved a Cambrian–Ordovician aborted rift system buried by a long period of sag sedimentation (Oliveira and Mohriak, 2003; de Castro et al., 2016). Its long-term sag deposition (Silurian to Cretaceous) was preceded by two Pre-Silurian rift systems that did not evolved to continental rupture and oceanic accretion. The Riachão rift system was restricted to the central-western portion of the basin, with an approximate NW-SE direction, and the other is more prominent, distributed along the southern and eastern edges of the basin, oriented along the Transbrasiliano Lineament (de Castro et al., 2018).

In the Parnaíba Basin, the magmatic events occurred as mafic intrusions (dykes and sills) and extrusions, represented by the Mosquito and the Sardinha formations (Goes and Feijó, 1994; Macedo Filho et al., 2019). They were partially conditioned by E-W oriented structures related to the plate movements that culminated in the opening of the Equatorial and South Atlantic oceans (de Castro et al., 2018; Merle et al., 2011). The Mosquito Formation is associated with basaltic magmatic events of Early Jurassic related to the Central Atlantic Magmatic Province (CAMP) in the context of the opening of the Central Atlantic Ocean (Marzoli et al., 1999). While the tholeiitic sills of the Sardinha Formation are coeval to the Paraná-Etendeka Magmatic Province, within the context of the opening of the South Atlantic Ocean (Milani and Thomaz Filho, 2000). Hollanda et al. (2019) pointed out that mafic dykes and sills of the Sardinha Formation and the Rio Ceará-Mirim dyke swarm comprise a Cretaceous LIP, occupying an area over 700,000 km^2 in NE South America.

5.3. Giant Dyke Swams in Northeastern Brazil

Mafic dykes hosted by Precambrian geological units of the BP (Fig. 5.1C) have been subject of several studies, especially in the last decades. Moraes (1924) was the first who described the occurrence of magmatic bodies as dykes close to the southern boundary of the Potiguar basin. Throughout the 1960’s and 1980’s some cartographic surveys were carried out by Brazilian universities and oil company (Petrobras), expanding the area of dyke exposure to the SW border of the Potiguar basin and identifying some discontinuous and isolated dykes to the west in the central sector of the BP (Cavalcante et al., 1983; Santos, 1968; Sial, 1987). The remarkable evolution in the mapping of dyke swarms in Brazil can be observed by comparing the first map of mafic dykes of Brazil and Guyana published by Sial et al. (1987) with the most recent compilation promoted by Pessano et al. (2020). More specifically in the BP, the papers of Hollanda et al. (2019) and Melo et al. (2021) are the most recent contribution to the intricate spatial distribution of dyke swarms in this Precambrian structural province.

Three main mafic dyke swarms affected the BP in the Mesozoic time: Rio Ceará-Mirim (RCM), Canindé (CD) and Riacho do Cordeiro (RC). The RCM is the most expressive swarm, its name was given by Gomes et al. (1981) to differentiate it from magmatic Cenozoic bodies that also occur in the region. The range of occurrence of this dyke swarm has an approximate length of 1000 km and 130 km wide (Fig. 5.1). This magmatism occurs in terms of relative abundance, composition, kind of extrusion, and structural relationship with rift geometry.

According to Oliveira (1992), the RCM occurs continuously, from the Late Jurassic to the Early Cretaceous (Neocomian) with two main igneous pulses: K-Ar 179-161 Ma and 145-130 Ma (Bellieni, et al., 1992). The magmatic activity is synchronous to the basalt and rhyolite flows in the Northern Benue Trough (Maluski and Baudin, 1995), which is the African counterpart of the Potiguar Rift. In this context, the RCM is the response to a regime of N-S extensional processes in the lithospheric scale, which culminated in the implantation of the South Atlantic rifting system, and, above all, it is geodynamically related to the formation of the Potiguar Rift. In general, the RCM crosscuts the structural grain of the Precambrian basement at a high angle, including mylonitic rocks along NE-SW and E-W shear zones. However, Oliveira and Gomes (1996) recognized some local fault reactivation cross-cutting in high angle the E-W dykes, suggesting that the dykes are older or concomitant to the Potiguar Rift.

Bellieni et al. (1992) positioned the dykes in the Cretaceous, using lithogeochemical and isotopic data (Sr-Nd) and paleomagnetic signature. Geochronological studies dated these dykes at 135-110 Ma based on K-Ar (Oliveira, 1992) and Ar-Ar techniques (Souza et al., 2003; Ngonge et al., 2016). In addition, some paleomagnetic pole studies demonstrated good correlation with typical poles of the South America in Early Jurassic and Late Cretaceous (Guerreiro and Schult, 1983; Bucker et al., 1986; Ernesto et al., 1991; Bellieni et al., 1992). Ernesto et al. (1991) proposed a division of the RCM into five sub-swarms, each one with different magnetization characteristics. Archanjo et al. (2002) used techniques of magnetic susceptibility anisotropy (ASM) to investigate the orientation of the magmatic flow, indicating that the magmatic feeder zone is located in the eastern sector of the E-W-trending of the RCM with lateral flows.

The two other occurrence of swarms, Canindé (CD) and Riacho do Cordeiro (RC), are related to the same magmatic event that culminated in the RCM emplacement. The

CD occurs in some diffuse directions, comprising curved NW-trending dykes exposed in the NW part of the BP nearly parallel to the Equatorial Atlantic coastline (Fig. 5.1C). To the best of our knowledge, there is not petrological and age data available for these dykes. In contrast, the RC was mapped on the eastern side of the Recôncavo-Tucano-Jatobá basin by Silva Filho et al. (1981). It comprises three dyke segments, with 80 km in the total extension in the NE-trend. These dykes were modeled as an intrusive body at depth by Santos et al. (1988) and date from 104 Ma. According to Hollanda et al., 2019, the RC is also related to the Gondwana break-up in Early Cretaceous.

Marzoli et al. (1999) correlates the RCM to the Central Atlantic Magmatic Province (CAMP). While Hollanda et al. (2019) gathered the dyke swarms of the BP and the tholeiitic Sardinha sills embedded within the sedimentary infill of the neighboring Parnaíba Basin to compose a Cretaceous Large Igneous Province (LIP), named EQUAMP. Previously, the mafic dyke swarms in the northeast of Brazil were related to the Gondwana breakup, associated to the hourly rotation of the Province of Borborema, the nucleation of the Potiguar Rift and preceding the rift phase of the basins (Szatmari et al., 1987; Ernesto et al., 1991; Bellieni et al., 1992; Matos, 1992; Oliveira, 1992; Ngonge et al., 2016). However, based on the definition by Ernst and Bleeker (2010) and according to the plume position showed by Heine et al. (2013), Pessano et al. (2020) raises the possibility that EQUAMP dyke swarms originated from Santa Helena plume.

Almost simultaneously with EQUAMP, another flood basalt province, which preceded the opening of the South Atlantic Ocean, was formed: The Paraná-Etendeka Magmatic Province that occurs along the southern of Brazil (Fig. 5.1A), east Paraguay, northeastern Argentina and northwestern of Uruguay (Bellieni et al., 1986), wih 134.7 ± 1 Ma (Renne et al., 1992), 134.6 ± 0.6 Ma (Thiede and Vasconcelos, 2010).

5.4. Airborne Geophysical Database

The geophysical datasets were compiled from fourteen airborne surveys provided by the Geological Survey of Brazil (former CPRM) and the Brazilian Oil Agency (ANP) (Fig. 5.2A). The gamma-spectrometric data were corrected from the non-geological radioactivity background and leveling errors. Each magnetic dataset was previously corrected for the diurnal variations, the International Geomagnetic Reference Field (IGRF) and leveling errors.

The surveys were carried out from 1981 to 2011 with different specifications (Table 5.1). In order to obtain better results, each airborne survey was processed separately to enhance the geophysical pattern of the magmatic structures. The processing workflow (Fig. 5.2B) was performed using the software Oasis Montaj 9.3.

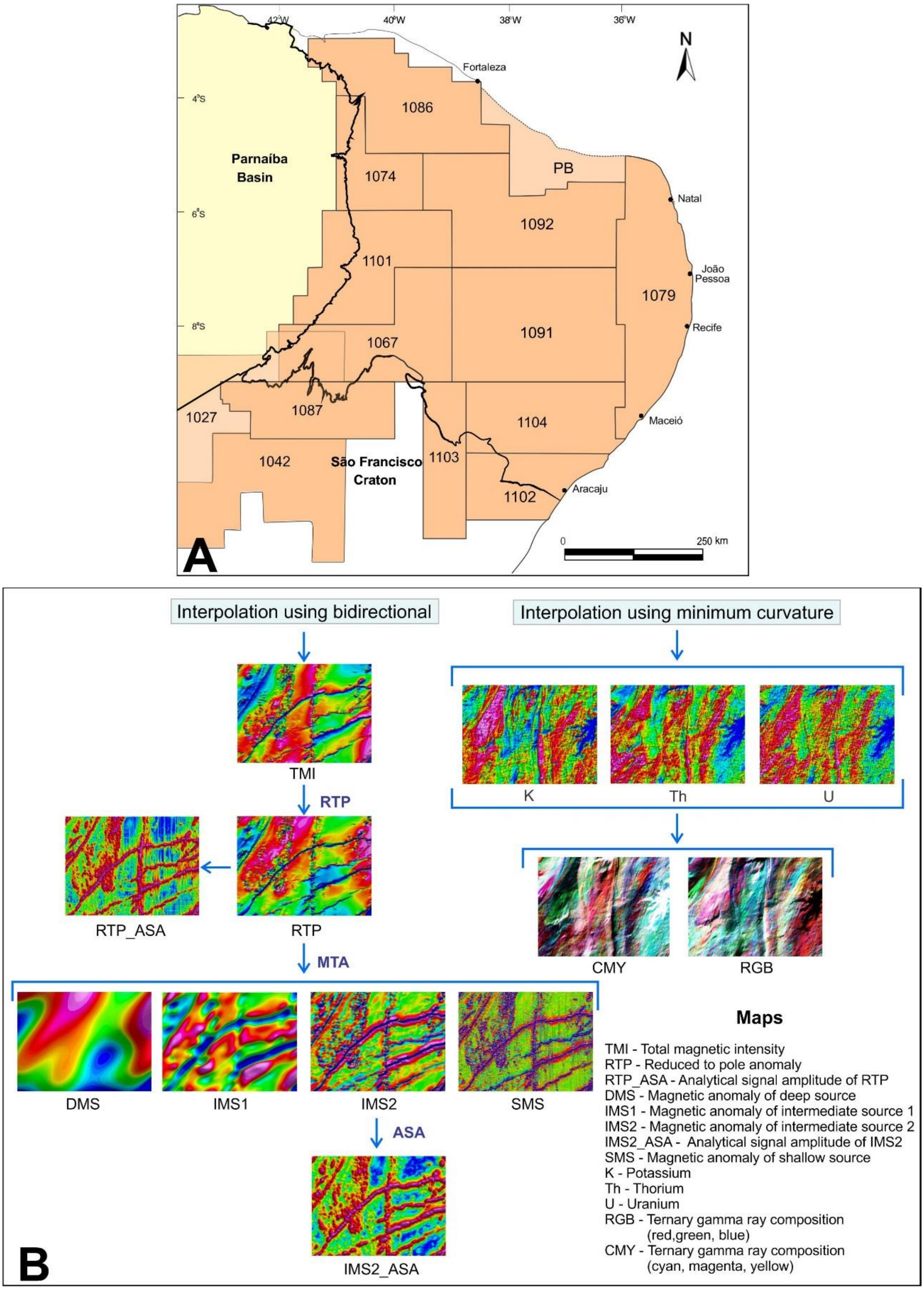

Figure 5.2. Airborne geophysical surveys covering the Borborema Province and its southern boundary with the São Francisco Craton and Parnaíba Basin (A); Data processing workflow applied for each survey (location in Fig. 5.2A) (B). See Table 5.1 for specifications about airborne geophysical surveys.

Table 5.1. Airborne geophysical survey specifications. CS – Company Survey; NFH - nominal flight height; FLD - flight-line direction; FLS - flight-line spacing; TLD - tie-line direction; TLS - tie-line spacing; MFI - magnetic field inclination; MFD - magnetic field declination. Additional information about the surveys are available in the electronic site of the Geophysical Surveys and Associated Products of the Geological Survey of Brazil at http://geosgb.cprm.gov.br/geosgb/downloads_en.html.

Code	**Year**	**CS**	**NFH (m)**	**FLD**	**FLS (m)**	**TDL**	**TLS (m)**	**MFI**	**MFD**
1027	1976	CPRM	100	N-S	500	E-W	10,000	-5.85	-8.78
1042	1979	CPRM	100	N-S	500	E-W	10,000	-10.56	-20.91
1067	2006	CPRM	100	N-S	500	E-W	10,000	-19.05	-22.14
1074	2007	CPRM	100	N-S	500	E-W	10,000	-14.24	-21.63
1079	2008	CPRM	100	N-S	500	E-W	10,000	-30.43	-21.33
1086	2009	CPRM	100	N-S	500	E-W	10,000	-14.16	-21.38
1087	2009	CPRM	100	N-S	500	E-W	10,000	-27.84	-22.59
1091	2010	CPRM	100	N-S	500	E-W	10,000	-21.74	-22.05
1092	2010	CPRM	100	N-S	500	E-W	10,000	-19.8	-21.83
1101	2010	CPRM	100	N-S	500	E-W	10,000	-19.17	-22.11
1102	2011	CPRM	100	N-S	500	E-W	10,000	-28.76	-23.04
1103	2011	CPRM	100	N-S	500	E-W	10,000	-26.26	-22.85
1104	2011	CPRM	100	N-S	500	E-W	10,000	-26.89	-22.78
BP	1981	ANP	500	N70W	400	N60E	20,000	-11.89	-21.80

5.4.1. Gamma-spectrometric Data Processing and Analyzing

The gamma-spectrometric data were interpolated with a 250-m cell size using the method of minimum curvature (Briggs, 1974) (Fig. 5.3A to C). Negative values, eventually generated by interpolation, were removed from the grids. The potassium (K) measurement is expressed in percentage (Fig. 5.3A), while the uranium (eU) (Fig. 5.3B) and thorium (eTh) (Fig. 5.3C) values are described in ppm. The grids of the three radioelements were integrated to compose RGB (Red, Green and Blue) (Fig. 5.3D) and

CMY (Cyan, Magenta and Yellow) (Fig. 5.3E) ternary images to facilitate mapping the contacts between the main outcropping geological units of the Borborema Province (BP). Due to generally low relief and scarce vegetal cover typical of a semi-arid climate, all radioelement maps are very similar and clearly reflect the surface geology, providing good information on the lithological units of the BP, as well as structural lineaments of the crystalline basement.

In general, the RGB ternary map exhibits high K contents (light red areas in Fig. 5.3D) related to granitic intrusions that occurred during Pan-African-Brazilian Orogeny. It is possible to see the reddish tones of the K-calcic bodies and the whitish tones of bodies with alkaline petrochemical, enriched equally in K, Th and U. The blue and green areas are indicating high contents of uranium and thorium, respectively. The white color areas represent high concentrations of the three radionuclides, whereas the black one reflects the low contents of these variables. White zones are represented by Cenozoic sediments and sedimentary basins which are delimited by irregular shapes with black color (Fig. 5.3E). In contrast, darker zones are associated to recent sediments, metasedimentary units and mafic bodies which suggest the presence of magnetite-rich ultramafic rocks.

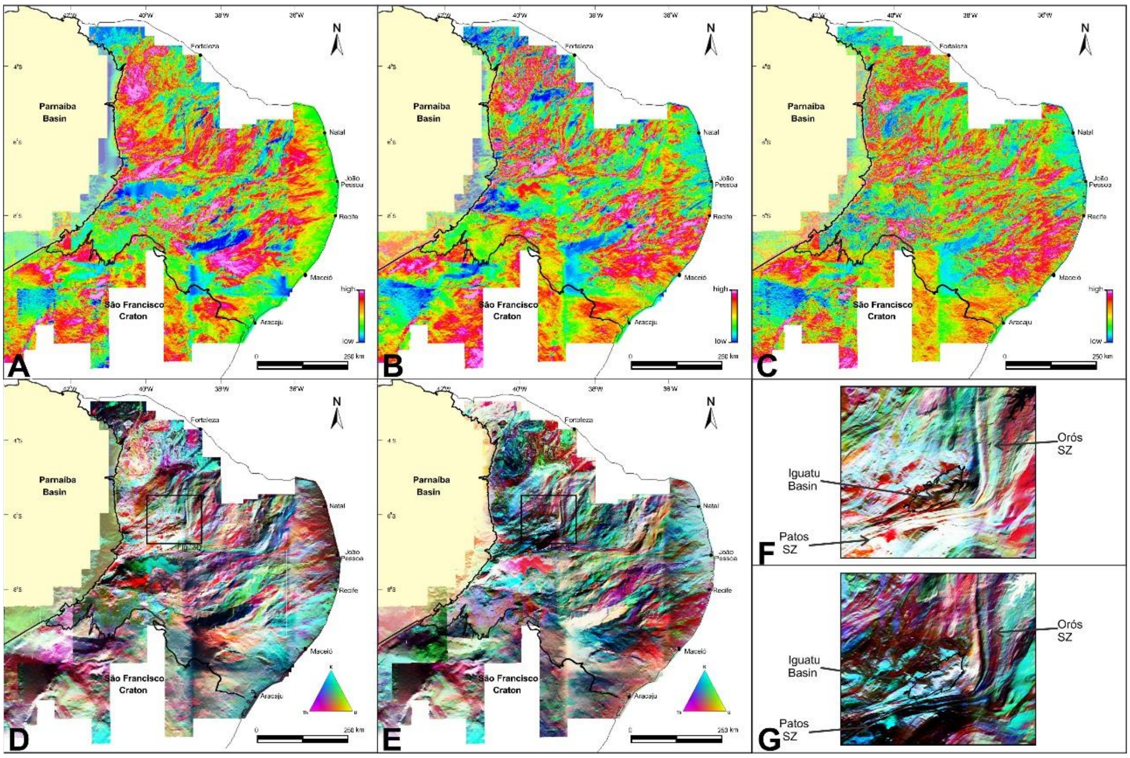

Figure 5.3. Gamma-spectrometric maps: K (A), eTh (b), eU (C), RGB (D), and CMY (E) ternary composition. Shear zones and sedimentary basins are well marked on ternary maps; Iguatu basin in black and Orós shear zone in white color (F); Iguatu basin in white color and Orós shear zone in black color (G).

The analysis of the ternary images also allowed to recognize patterns and trends that define discontinuities of the radiometric responses, which represent contacts between geological units, and some are represented as shear zones with a strong link with the structures observed in the field. The Patos and Pernambuco shear zones are well marked on ternary maps. In RGB there is a predominance of light colors (Fig. 5.3F), while in CMY they are represented by dark colors (Fig. 5.3G).

5.4.2. Magnetic Data Processing and Analyzing

In order to obtain the total magnetic intensity (TMI) map of the BP (Fig. 5.4A), each airborne survey was interpolated applying the bidirectional method, using half of the distance between flight lines as cell size. In some older surveys, it was necessary to apply a directional cosine filter to eliminate high frequency noises along the flight direction, remnants from inappropriate leveling.

The interpretation of magnetic field data at low magnetic latitudes is difficult because the dipolar nature of the magnetic field increases the complexity of the anomalies caused by magnetic sources. Thus, we applied a Reduction to the Pole transformation (RTP), aiming to centralize the magnetic anomaly on its source (Blakely, 1996). The RTP assumes that the remanent magnetism, which eventually occurs in the rocks of the area, has the same orientation of the present magnetic field, which is a valid premise in most cases of the regional-scale magnetic mapping. The magnetic declination and inclination of each surveyed area were used as parameters of the RTP transformation (Tab. 5.1). Figure 5.4B shows the integrated RTP map of the study area.

For the interpretation of the RTP anomalies and their correlation with the surface geology, we applied anomaly enhancement techniques that highlight specific characteristics of the magnetic sources. In this study, we used the matched-filter method (MTF), which separates the wavelength content of the magnetic anomalies in four different spectral bands (Figs. 5.4D to G), using multiple equivalent layers {Formatting Citation}. The RTP map (Fig. 5.4B) shows a magnetic intensity variation between -1454.38 to 1177.09 nT. The MTF was applied to the RTP magnetic anomalies, which allowed an individualization of the spectral content of the magnetic anomalies in four different wavelength bands that provided estimates of source depth for equivalent source layers (Tab. 5.2): (1) zone of deep magnetic sources (DMS) ~ 10.99 km depth, related to structures deep in the upper crust; (2) zone of intermediate magnetic sources 1 (IMS1) between ~2.22 km depth, related to upper crust features; (3) zone of intermediate magnetic sources 2 (IMS2) between ~ 0.48, related to dykes within the Borborema Province and; (4) zone of shallow magnetic sources (SMS) between ~ 0.11 km depth, related to near-surface magnetic sources and residual data noise. The intermediate 2 and shallow RTP anomalies display more clearly the structural lineaments and the magnetic response of the mafic dykes.

The MTF applies the concept of multi-layered equivalent source models, which iteratively fits multiple straight lines to radially averaged power spectral of the magnetic or gravity anomalies (Phillips, 2001). This technique provides estimates of causative source depth for an equivalent source layer. The depth estimates, amplitude and Wiener filters can be designed to emphasize anomalies originating from various layers (de Castro et al., 2018). Each depth layer corresponds to the maximum average depth of a statistical population of true magnetic/gravity sources (Curto et al., 2014).

In addition, we calculated the Analytical Signal Amplitude (ASA) of the RTP (Fig. 5.4C), IMS2 (Fig. 5.4F) and SMS (Fig. 5.4G) anomalies. This mathematical operator produces maxima on the geological contacts and structural features, highlighting the edges of the magmatic bodies. The analytic signal is symmetrical, and it occurs directly over the entire length of the edges of the causative bodies and the center of the boundary (Nabighian, 1972). The IM2-ASA map (Fig. 5.4H) was the most useful in the detection of the mafic dykes.

The DMS (Fig. 5.4D) corresponds to the deepest equivalent layer associated with the longest wavelength anomalies, varying from −1,184 to 2,247 nT. DMS anomalies were characterized by an alternation of positive and negative bands associated to causative sources within the upper crust, representing Precambrian structures such as the E-W shear zones (Patos and Pernambuco) that appear in the interior of the Borborema Province (Fig. 5.1). Free from longer wavelengths, the IMS1 map shows more clearly the main magnetic lineaments, such as the Orós, Jaguaribe, Patos and Pernambuco shear zones (Fig. 5.4E). This magnetic pattern displays more clearly the tectonic compartmentalization of the BP within the large crustal blocks. The IMS2 and SMS maps concentrate the smaller wavelength magnetic signal and reveal the more superficial causative sources (Figs. 5.4F and 5.4G). These spectral components are the most suitable for mapping the outcropping structures of the BP, such as dykes, other magmatic features, and secondary faults. In general, the magnetic highs frequently occur in gneissic-migmatitic complexes, shear zones, mafic rock complex and mafic dykes.

Metavolcanosedimentary sequences and inland aborted rift zones, as Tucano/Jatobá and Potiguar rifts are associated with magnetic lows (Figs. 5.1 and 5 4). The SMS map also exhibits high-frequency noise, which makes it difficult to differentiate structures in regional scale.

The analytical signal calculation was used to improve the geophysical interpretations of the aeromagnetic data. It enhanced the magnetic signal from shallow magnetic sources with high amplitude anomalies. The IM2-ASA map (Fig. 5.4H) allows to characterize magnetic signatures of the dykes, since these bodies, due to their high concentration of magnetic minerals, typically manifest themselves as elongated and straight magnetic ridges with high amplitude of the analytical signal. These maps, making possible to delineate the direction of the dykes, provide good indications about the geometry of the magnetic sources. The contacts of the bodies are in the edges of the anomaly, being possible to infer body size.

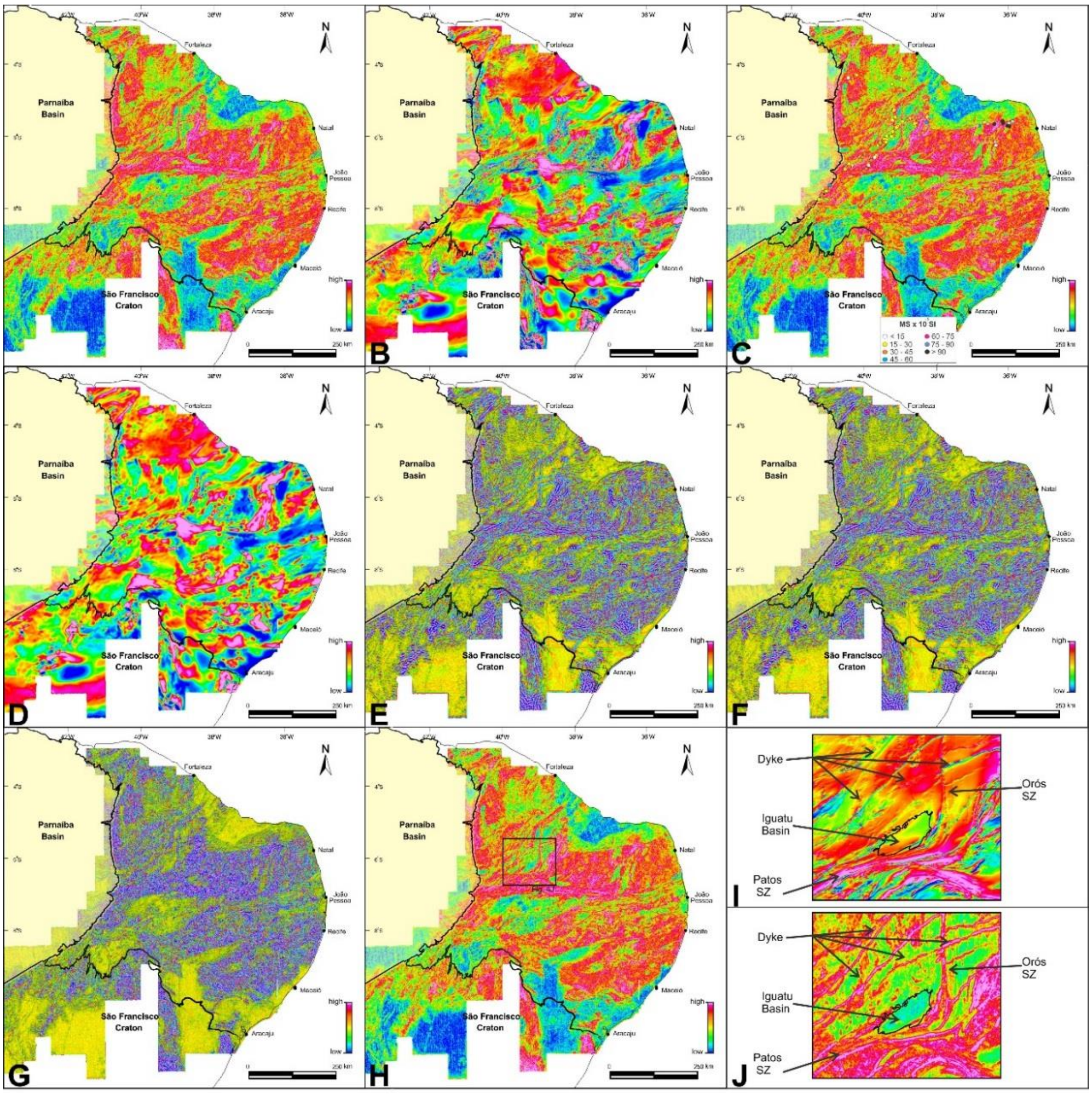

Figure 5.4. Magnetic anomaly maps of the Borborema Province: total magnetic intensity (A); total magnetic intensity reduced to magnetic pole (RTP) (B); analytical signal amplitude of the RTP anomalies (RTP_ASA), with the location of the samples collected and the magnetic susceptibility measurements (colored dots) (C). Matched Filter maps for equivalent source layers: DMS - magnetic anomaly of deep sources, related to structures in the deep upper crust (D); IMS1 - magnetic anomaly of intermediate sources 1, related to upper crust features (E); IMS2 - magnetic anomaly of intermediate sources 2, related to dykes within the province (F); SMS magnetic anomaly of shallow sources, related to near-surface magnetic sources and residual data noise (G); and analytical signal amplitude of intermediate 2 magnetic anomaly (IMS2_ASA) (H). Zoomed IMS2 (I) and IMS2_ASA (J) maps of the Iguatu Basin illustrate details of the magnetic patterns of sedimentary basins, shear zones and dykes.

Table 5.2. Summary of Magnetic Susceptibility (MS in × 10^{-3} SI) of dyke rocks collected in the Borborema Province (NE Brazil).

Lat	Long	MS	Lat	Long	MS
-4.2881	-40.3515	21.62	-5.7991	-39.2838	31.55
-4.3748	-40.5589	13.40	-5.8732	-39.3511	24.13
-4.3637	-39.2523	36.30	-6.8180	-40.4723	28.50
-4.3966	-39.1441	26.66	-6.8293	-40.4985	37.50
-4.3834	-39.1838	31.95	-5.6304	-38.7522	20.00
-4.5570	-39.3524	18.85	-5.6329	-38.7685	24.20
-5.2828	-39.3220	24.60	-5.9878	-39.3685	24.60
-5.5498	-39.3538	20.70	-5.9578	-39.3220	40.10
-5.4668	-39.2904	26.00	-6.1496	-39.5395	21.86
-6.8812	-40.6535	25.40	-5.6218	-38.4392	49.03
-6.8600	-40.6248	30.60	-6.5741	-39.8311	15.10
-6.8190	-40.5890	30.50	-6.5782	-39.8390	8.45
-6.7923	-40.5640	25.00	-6.6650	-39.9352	31.45
-5.9998	-39.5000	25.20	-7.3558	-41.0648	52.00
-5.8761	-39.3514	22.55	-7.4392	-41.1422	42.00
-6.1409	-39.5861	33.45	-7.4597	-41.1540	32.00
-6.1583	-39.6125	33.83	-7.4760	-41.1606	26.00
-6.1693	-39.6414	37.40	-7.6218	-41.2928	36.00

-6.1840	-39.6649	27.03	-7.5326	-41.2113	36.00
-6.2064	-39.6874	35.65	-7.5381	-41.1863	36.00
-6.2376	-39.7241	25.30	-7.8830	-41.5897	38.00
-6.1114	-39.5801	25.95	-7.8724	-41.5517	34.60
-6.0878	-39.5230	29.30	-7.8635	-41.5591	41.40
-6.5791	-40.1761	43.60	-7.8441	-41.5413	33.20
-6.4948	-40.1189	33.00	-7.8241	-41.5193	30.30
-5.4631	-38.4175	23.96	-7.9784	-41.6818	32.30
-5.6792	-39.1846	21.15	-7.9600	-41.6613	36.40
-5.6492	-39.1398	24.20	-7.9473	-41.6457	22.40
-5.5994	-39.0682	22.05	-7.9044	-41.6073	34.00
-5.5367	-38.9523	38.13	-7.7464	-41.3567	21.55
-5.5150	-38.9045	21.16	-5.9702	-38.6292	35.96
-5.4949	-38.7138	39.23	-6.9453	-40.1231	30.00
-5.4777	-38.6614	30.66	-6.8933	-40.0769	30.00
-5.7149	-39.2124	21.73	-6.8030	-40.0083	12.90
-5.7805	-39.2674	24.52	-8.2382	-41.6501	29.00
-8.4828	-41.8692	35.44	-8.5412	-41.9433	36.26
-8.4946	-41.8925	25.43	-8.5569	-41.9512	33.07
-8.5226	-41.9276	34.30	-8.5981	-41.9848	34.97
-37.04305	-5.70593	61.9	-36.35858	-5.58161	91.9
-36.86563	-5.60205	24.1	-36.10604	-5.58275	77.6
-36.77376	-5.65334	62.8	-36.19759	-5.62707	57.0
-36.59636	-5.65235	93.8	-36.55462	-6.23233	9.2
-36.57361	-6.14439	61.2	-37.01302	-5.70707	46.0

-36.19514	-5.71236	104.3	-36.35878	-5.63155	105.0
-36.24102	-5.70607	101.3	-36.35878	-5.58131	42.2

5.4.3. Airborne Geophysical Interpretation

The gamma-spectrometric and magnetic data used in this study were key tools in the identification and cartography of the dykes in the BP. From the geological and geophysical point of view, mafic dykes are presented as linear structures with distinguished compositional, structural, and magnetic contrasts in relation to their host rocks. Indeed, magnetic anomalies associated to mafic dykes exhibit high values, varying between -134 and 198 nT (Fig. 5.4I, and analytical signal amplitudes around 28 x 10^{-2} nT/m (Fig. 5.4J). Those anomalies are dozens to hundreds kilometer long and display short wavelength (1.5-4.0 km) since they are yielded by shallow to intermediate causative sources (0 to 1,900 m deep). However, this typical magnetic pattern could be misinterpreted as the magnetic contribution of shallower basement sources emplaced within the uppermost crust. In fact, it was observed that the analytical signal emphasizes other structures that show magnetic signature very similar to the mafic dykes, as the N-S and E-W trending shear zones. In the BP, these Precambrian structural features are easily distinguished from the dykes, once the mafic dyke swarms were emplaced orthogonally to the shear zones (Fig. 5.4J).

Most of the magnetic anomalies were clearly interpretable as dykes, some of which correspond to the continuation of dykes already mapped. However, in certain cases, an unequivocal differentiation between dykes and host rocks or basement structures is not possible only based on magnetic anomalies. For that, we analyzed the gamma-spectrometric signatures of the dykes, which contrasts with the host rocks, as they have low content of K, Th, and U, thus showing dark colors (black) on the RGB ternary map (Fig. 5.3D and 5.3E). In this way, we assume as dykes the continuations of the magnetic lineaments superimposed on dykes already mapped in previous studies and checked possible ambiguities *in loco* during field work.

Also striking is the observation that the positive magnetic anomaly polarity produced by dykes sometimes reverses along the dyke swarms due to the strong remanent magnetization, whose magnetism direction is presumably opposite to the present-day geomagnetic field in such dykes. Dykes emplaced during periods of inverse polarized Earth's field will have opposite polarity to that expected owing the current magnetism direction. This magnetic pattern can indicate the dykes along the swarms in the BP were originated by different magmatic pulses at different times.

5.5. Field Relationships

The field work was carried out in five excursions, between 2016 and 2020, to the occurrence areas of the RCM and CD (Figure 5.5A). The aim of this activity was to validate the mapping of the dyke swarms based on airborne geophysical maps and visual analysis of Google Earth™ images, as well to describe the morphological features of the magmatic exposures and structural relationships with the host rocks. Measurements of the magnetic susceptibility (MS) of both dykes and surrounding geological units were also conducted to establish the magnetic contrasts between intrusive and host rocks.

In Google Earth™ satellite images, the dykes look like very dark and elongated bodies, showing relatively well-defined contacts and, in general, cutting the structural directions of the embedding rock. We systematically map the dykes across the entire BP, paying greater attention to the occurrence of dykes previously identified on geophysical and geological maps.

The MS is the physical property that allows rocks to magnetize, a process called magnetic induction, being also the main parameter in the magnetic method (Telford et al., 1990). Materials such as rocks and minerals, which have great MS when exposed to an external magnetic field, tend to magnetize more strongly than materials with low MS. Mafic dykes have high content of magnetic minerals (e.g., magnetite), which causes significant MS contrasts between the magmatic bodies and the hosting rocks and, consequently, high amplitude magnetic anomalies. The magnetic mineral content of mafic dykes normally comprises the titanomagnetite series ($Fe_{3-x}Ti_xO_4$; $0 < x < 1$), also known as the spinel group (Dentith and Mudge, 2014).

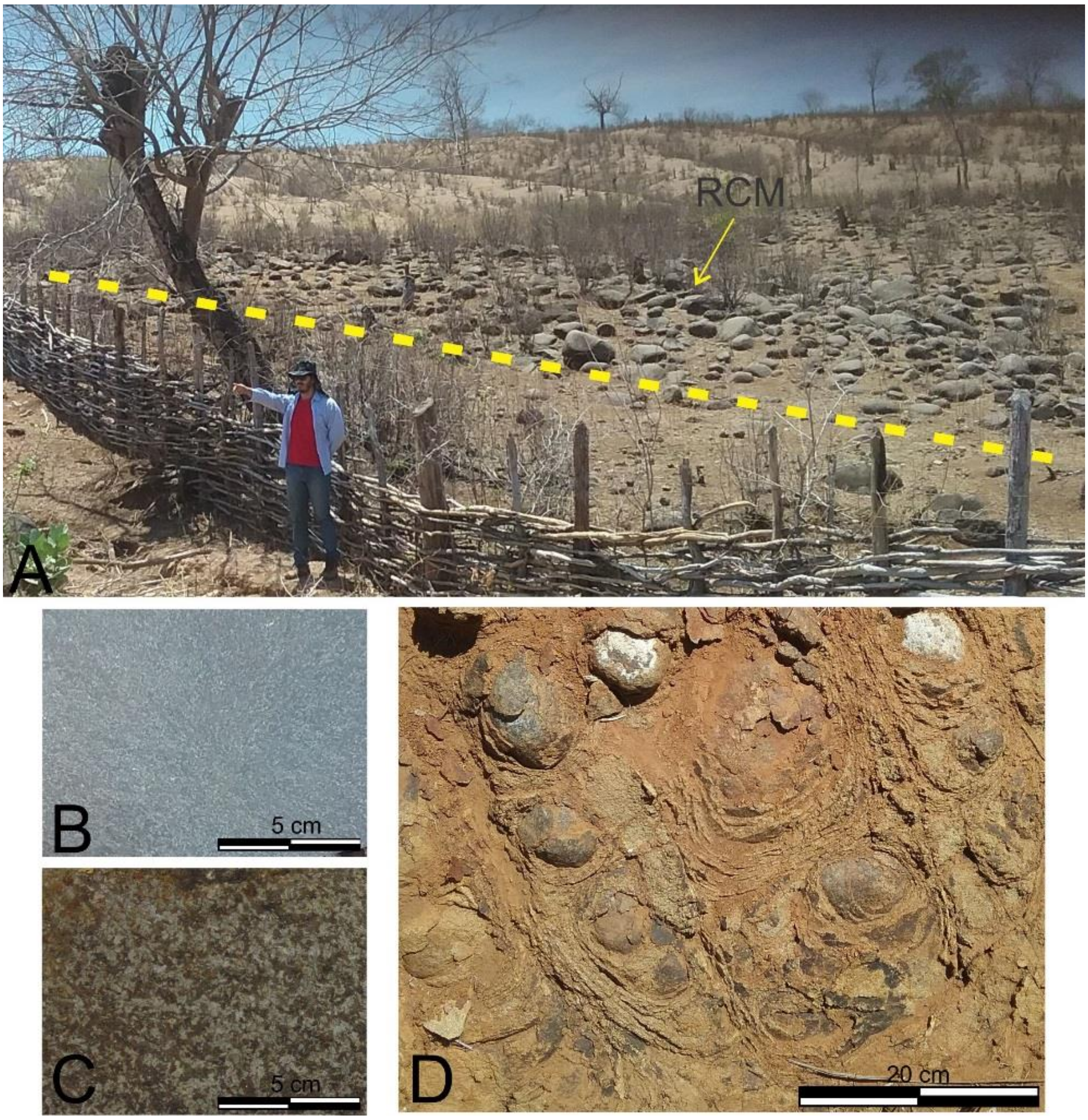

Figure 5.5. Typical exposure of the Rio Ceará-Mirim Dyke Swarm (RCM). Outcrop showing RCM alignment (A); phaneritic texture (basaltic) in a rock sample (B); aphanitic texture in a rock sample (C); Outcrop displaying dyke with spheroidal weathering (D).

During the field work, we collected 90 rock samples of dykes and host rocks (e.g., sandstones and granites) along the most expressive magnetic anomalies (Fig. 5.4C) and measured their MS (Tab. 5.2). We used a portable magnetic susceptibility meter KT-10 v2 (*Terraplus Inc*.), which can provide the MS with a high sensitivity of 1.0×10^{-6} SI units. The MS measurements were carried out in each rock sample, touching the circular sensor of 6.5 cm in diameter to a clean and regular surface of the sample. We repeated three times the measurement process in each sample for validation of the obtained MS values.

The measured MS of the dolerite dykes varies from 8.4 to 105 × 10^{-3} SI units (Tab. 5.2), suggesting different magmatic phases. The average MS values are: mafic dykes 25.8 × 10^{-3} SI, sedimentary rocks 0.4 × 10^{-3} SI, and basement rocks 3.2 × 10^{-3} SI. These strong MS values contrast between dykes and their host rocks are responsible for the high-amplitude magnetic anomalies. Also striking is the observation that no clear correlation between MS and magnetic anomaly sets was recognized. For example, the highest MS was measured in the E-W branch of the RCM dyke swarm south of the Potiguar Basin. While the lowest MS values are concentrated along the NE-SW segment of this swarm. Meanwhile, the dykes of the NE-SW branch display the lowest values of MS north of the Patos SZ, and higher values are concentrated south of this shear zone.

From the petrological point of view, the mafic dykes are light gray to very dark gray, with dolerite textures, varying from aphanitic (basaltic) to phaneritic (equivalent to a gabbroic texture) (Figs. 5.5B and C). In some cases, it is possible to observe the coexistence of two colors (melano- to mesocratic) on a hand-sample scale. In addition, we noticed that fine-grained dolerites are more resistant to erosion, forming smooth hills. On the other hand, coarse-grained dolerites have shown resistance to erosion similar to the host rocks, appearing topographically devastated. In these cases, the dyke exposures can only be mapped by their characteristic spheroidal weathering (Fig. 5.5D).

5.6 Structural Characterization of Dykes

The dyke distribution has been interpreted from several geophysical maps (Figs. 5.3 and 5.4), mainly analytic signal maps (Fig. 5.4G), geological maps, Google Earth™ imagery and field work. We recognized 1388 dykes, including the dykes already knew in the literature, grouped in three sets of mafic dyke swarms (Tab. 5.3): 1389 from RCM, 168 from CD and 85 from RC (Fig. 5.6).

Table 5.3. Dyke swarm length (in km) mapped in the Borborema Province (NE Brazil). RCM – Rio Ceará-Mirim, CD – Canindé, RC – Riacho do Cordeiro.

Dyke swarm	Number of dyke	Min. length	Mean length	Max. length	Total length	Standard deviation
RCM	1389	0.183	4.736	29.967	5375.791	0.126
CD	168	0.846	5.019	5.236	843.244	5.006
RC	86	1.212	6.694	32.814	575.706	5.938

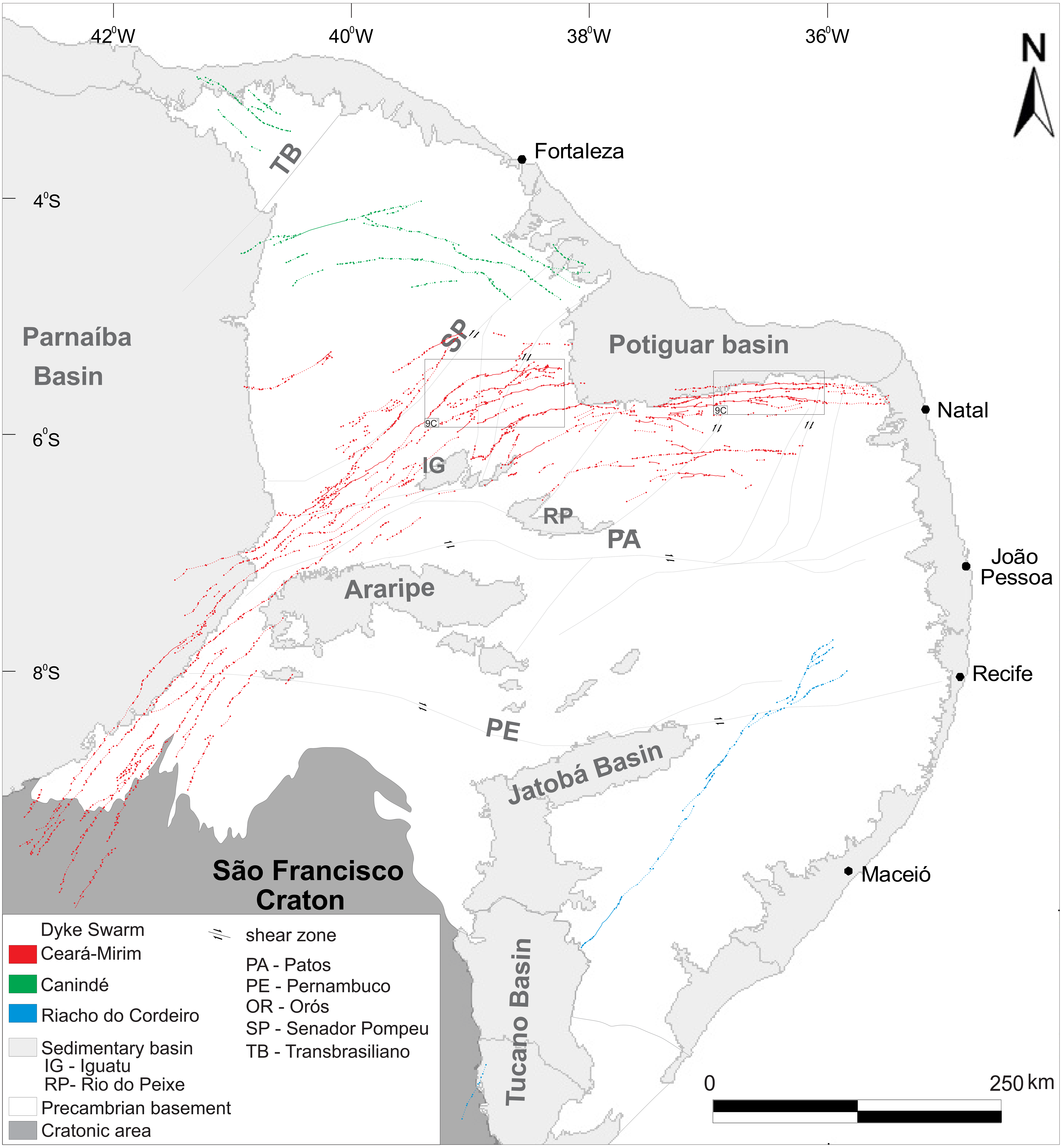

Figure 5.6. Spatial distribution of dyke swarms in the Borborema Province and surrounding areas (NE Brazil), based in our qualitative interpretation. Dotted lines show dykes interpreted from the aeromagnetic maps by Melo et al. (2021). Solid lines denote dykes mapped based on magnetic anomalies, but also visible in Google Earth™ satellite images data and validated by field work

The geophysical maps were the most efficient tool for mapping dykes. We correlated magnetic anomalies as dyke swarms according to some criteria: field work, previous studies, and similarity between magnetic signatures of dykes which were recognized in Google Earth™ imagery. Usually, high-amplitude magnetic anomalies with uniform linear pattern over a substantial length of dozens to hundreds of kilometers, which cross-cut structural features of the crystalline basement, are recognized as dyke. Considering that dykes having similar direction were emplaced at the same time and would, therefore, encompass a same swarm or swarm set.

The dyke orientations were plotted in rose diagrams (Fig. 5.7) to reveal the main structural trends controlling the intrusion emplacement. The NE-SW to NNE-SSW trend constitutes the major and dominant frequency of dykes. Then, two orientation were trending, respectively, E-W to ENE-WSW and NWSE to WNW-ESE with a medium and low frequency (Fig. 5.7). In the western portion of the swarms, the dykes have a direction NE-SW to NNE-SSW. This direction concentrates the largest amount of number of dykes. These intrusive bodies are longer, continuous and extends beyond the limits of the BP, intrude the western edge of the PB and the northwest part of the SFC. The NW-SE to WNW-ESE dykes are scarcer and are concentrated in the northwestern part of the area. These dikes are a few centimeters wider, continuous, and spaced. In the eastern portion of the swarms, the mapped dykes have a preferential E-W to ENE-WSW direction. In this area, it was observed three main alignments of dykes. These dykes are smaller, discontinuous, straight, and more concentrated in the area.

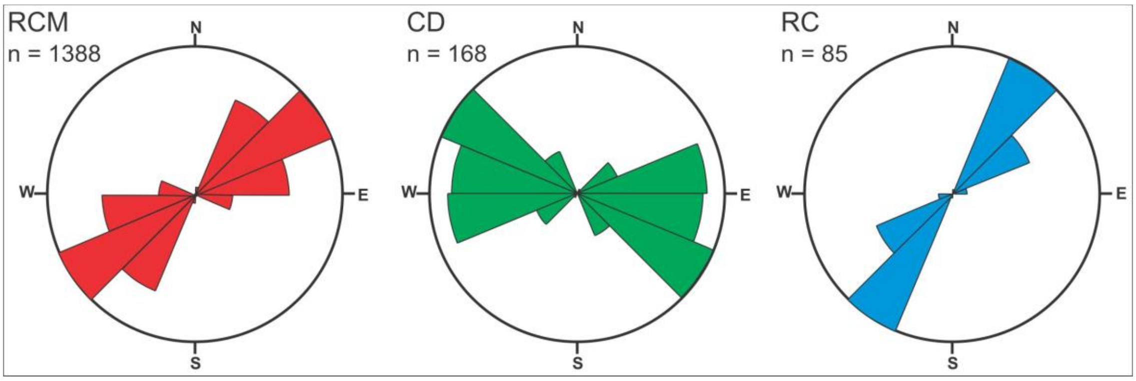

Figure 5.7. Rose frequency diagrams of dyke directions mapped in the Borborema Province (NE Brazil). Red – Rio Ceará-Mirim (RCM), Green – Canindé (CD) and blue – Riacho do Cordeiro (RC).

The dyke swarms mapped in the study area extended for more than 1,000 km, crossing the SW limit of the Borborema Province with the north of SF Craton, bordering its western boundary with the Parnaíba basin NE-SW direction, and inflecting in the E-W direction at the southern limit of the Potiguar basin (Fig. 5.6). The total extension length of dykes is over more than 5.7 $x10^3$ km. In addition, we describe the main characteristics of the dykes, namely thickness, structure, strike, length, and direction, besides geometrical aspects associated to the stress fields of the dykes.

The length analysis of the dykes shows that the NE-SW oriented dyke sets represent over 78.99 % of the total lengths, followed by the E-W oriented dykes set, which assembles 10.56 % of the total lengths. The NW-SE to WNW-ESE set of dykes, with 8.85 % of the lengths, whereas the N-S trending dykes display the lowest percentage, 1.57 % of the total length. The E-W trending dykes are shorter in length than those with NW-SE orientation.

The length of the dyke segments ranges from 0.18 km to 32.81 km, with an average length of 4.7 km (Tab. 5.4). The longest dyke segment is oriented in the NE-SW direction (~72^o Az), which is the dominate structural trend of the main dyke set. The thickness of the dyke swarms varies between 7.5 m and 193.3 m, with an average thickness of 69.4 m. Because of the limited spatial resolution of the Google Earth™ images, dykes thinner than7.5 m are difficult to measure accurately. In contrast, few dykes reach thickness greater than 100 m.

Table 5.4. Dyke width (in meters) mapped in the Borborema Province (NE Brazil). RCM: Rio Ceará-Mirim, CD: Canindé, RC: Riacho do Cordeiro.

Dyke swarm	Number of dyke	Min. width	Mean width	Max. width	Standard deviation
RCM	255	7,50	70,01	193,50	37,74
CD	8	65,30	68,38	73,20	1,40
RC	18	42,10	79,88	105,30	4,59

5.6.1. Rio Ceará-Mirim dyke swarm (RCM)

The RCM is the main dyke swarm in the BP and it was the first that was reported in the literature (Gomes et al., 1981). However, actual dimensions and occurrence of the dykes are not yet fully known, mainly due to the complex geological setting and to the lack of outcrops. Despite recent studies revealing a range several times greater than that described in the pioneer works, the present study provides a detailed description of this dyke swarm (Fig. 5.6). The RCM are divided in two major branches of dykes, one with NE-SW direction on the western edge of the BP and the other oriented in the E-W direction on the eastern portion of the BP. The change in the swarm trend occurs at the 39º W meridian across the Orós-Jaguaribe SZ (OR in Fig. 5.6).

The whole linear extension of the RCM is more than 1,000 km, comprising an area of 6.8 x10^6 km^2, from the northern border of the São Francisco Craton to the NE Brazilian shoreline. In this swarm, the length of the dykes ranges from a few meters (0.18 km) to more than dozens of kilometers (29 km). Around 80% of the dykes has less than 2 km of length.

The RCM is consisted of dykes with 20 to 125 m in width. Typically, the dykes identified in aeromagnetic maps have a thickness above 20 m. Nevertheless, those intrusive bodies with thicknesses less than 20 m are better recognize in satellite imagery (Google Earth^{TM}) and/or in field work. However, it is observed that few dykes, although very well marked in satellite images, are not detected on aeromagnetic maps (Fig. 5.8). Probably, these dykes are likely to have an internal magnetic field, whose magnetic effect reduces its effective magnetism through a phenomenon known as self-demagnetization (Dentith and Mudge, 2014). Massive magnetite rocks and banded iron formations are typical geological materials, which are sufficiently magnetic for self-demagnetization.

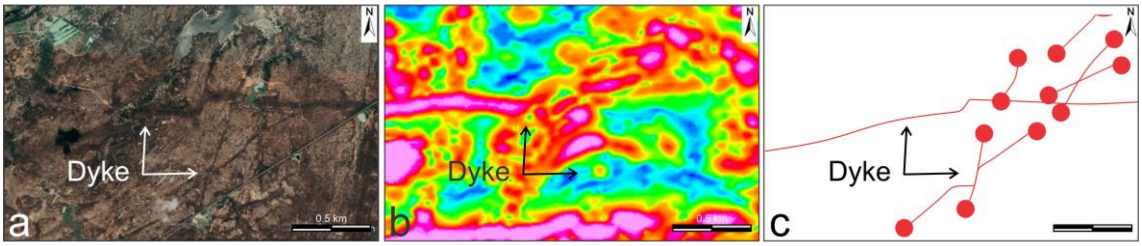

Figure 5.8. Thin dykes well marked on Google Earth^{TM} satellite images (a), which are not detected on aeromagnetic maps (analytical signal of the IMS2 magnetic anomaly - b), probably due to self-demagnetization. Dykes interpreted from Google Earth^{TM} satellite images, geophysical maps and field work (c).

The NE-SW branch of the RCM occurs west of the Orós-Jaguaribe SZ, bending southwest (Fig. 5.6). This swarm segment extends for more than 400 km and it is composed of several series of sub-linear dykes with lengths of 0.2 to 30 km, defining a ~100 km wide arched zone for the entire RCM. In the southwest, the dykes intruding the Parnaíba basin are correlated to the Sardinha Suite, comprising the Equatorial Atlantic Magmatic Province (EQUAMP), proposed by Hollanda et al. (2019).

The NE-SW branch displays dykes scattered and apart from each other, however larger and more discontinuous in comparison to the dykes of the E-W segment. The NE-SW dykes are the most expressive in the magnetic maps, with width varying from 12 to 193.5 m (Figs. 5.4 and 5.6). It is the dominant directional dyke set mapped in this study. This direction of dykes agrees with the NW-SE extension model and present a regional connotation throughout BP in a context of the NW-SE opening during the Latter Jurassic (Matos, 1992; Melo et al., 2016).

The E-W RCM branch occurs in the NE portion of the Borborema Province (Fig. 5.6), where the dyke swarm assumes a main E-W trend. The 0.5 to 25 km wide dykes are emplaced parallel to the southern boundary of the Potiguar basin, from Natal near the current coastline to the 39º W meridian. This RCM segment is composed by three main parallel stripes of simple isolate bodies or an array of two or more dyke segments, separated from each other by dozens of meters gaps and steps (Fig. 5.9A). The dyke strips are mostly linear, sometimes curved and spreading for several kilometers. This type of arrangement occurs due to the paleo-stress of N-S direction, acting on the Precambrian foundation with structuring of E-W direction. Generally, dykes cut foliations and shear zones of the basement, except for a few cases, when they take advantage of plans of weakness of the host rock. To the south, two more isolated stripes are parallel to the main E-W dyke branch (Fig. 5.9B).

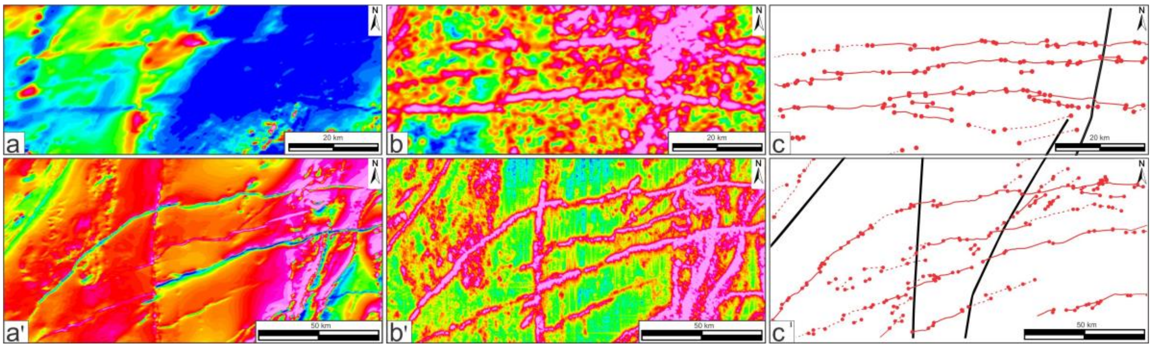

Figure 5.9. Total magnetic intensity (a, a'); Analytical signal of the IMS2 magnetic anomaly (b, b'); and Dykes interpreted from Google Earth™ satellite images, geophysical maps, and field work (c, c') of two areas across the Rio Ceará-Mirim dyke swarm (RCM), whose locations are shown in Figure 5.6.

The E-W RCM dykes crosscut in high angle the NE-SW oriented Precambrian basement grain. The E-W trend of the RCM is related to N-S extensional movements according to Szatmari et al. (1987) in their model of opening the Brazilian Equatorial Margin, in which the Brazilian Eastern Northeast suffered an E-W compression, accompanied by an N-S extension due to the clockwise rotation suffered by the South American Plate in relation to Africa (Françolin and Szatmari, 1987).

The E-W RCM dykes are undulated to straight, sometimes very curved, showing rounded or tipped ends. Dyke terminations on steps or jumps are common in all dyke segments and throughout the E-W swarm, segmentations between dykes per level up to hundreds of meters are observed (Fig. 5.6). Generally, these gaps between dykes are uniform (5 to 10 km) and are aligned in relation to the main direction of the dyke. In some places, a rotation between dyke segments has been identified, featuring an echelon arrangement. In these cases, the rotation of the bodies reaches a maximum of 20º, usually dextral (Fig. 5.9B).

Magnetic maps clearly show the dykes crosscutting shear zones in high angle (Fig. 5.9), indicating that these features were not preferentially filled by the RCM dykes. In fact, the RCM systematically traverses the main Precambrian basement grain, mainly shear zones (e.g., Orós-Jaguaribe, Patos and Pernambuco SZ – Figure 5.6), which was confirmed by the field work. Furthermore, the dykes bordering the limits of the rift basins (e.g., Potiguar, Iguatu, Araripe). Besides, the RCM also spreads out over surrounding geological domains, namely the Parnaíba basin and São Francisco Craton (Figs 5.4 and 5.6).

5.6.2. Canindé Dyke Sub-swarm (CD)

The magnetic anomalies interpreted as CD are located in the NW portion of the Borborema Province, north of the RCM (Figs. 5.4 and 5.6). This dyke set mainly trends to NW-SE direction and secondarily to NE-SW, forming a curved en-echelon dyke system. The CD can be divided in 2 subgroups: a) an arched E-W dyke segment, linking the Parnaíba basin to Potiguar basin; b) a NW-SE segment at the NW-most edge of the BP. The length of the dykes is 0.80 km to 5.00 km. The width of the dykes ranges 68.38 to 73.20 m. In general, this swarm is thinner if compared to the other set of dyke swarms.

5.6.3. Riacho do Cordeiro Dyke Sub-swarm (RC)

The magnetic anomalies attributed to the RC reveals a ~700 km long set of dykes, spreading from the São Francisco Craton until across the Pernambuco SZ to the north (Fig. 5.6). They represent an isolated dyke series with NE-SW direction in the SE portion of the BP, which split in some short NE-SW trending dykes north to the Pernambuco SZ. The RC dykes exhibit length, varying from 1.2 to 57.6 km, and width, ranging between 42.1 to 105.3 m.

5.6.4. Spatial Distribution of Dykes

The density of dykes varies significantly from one area to the next across the BP and neighboring regions (Fig. 5.10). This spatial distribution may be in part due to the vast diversity of the host rocks, complex geological setting of several crustal domains amalgamated in the BP and the different tectonic regimes, acting during the dyke emplacement. The dyke swarms in the study area mainly intruded into Archean to Proterozoic metamorphic units, Precambrian igneous rocks, and Mesozoic sedimentary basins. In addition, the density curves statistically indicate possible occurrences of small dykes that were not detected in aeromagnetic maps and Google Earth™ satellite images, but they were cited in local unpublished studies. It is evident that more systematic field data acquisition is required to check this interpretation, but it is already a quite precise picture of the dyke distribution in the BP.

The spatial density of dyke occurrence was calculated through the number of dykes divided by the host rock area grided in 50-km wide cells. The spatial density of dykes is represented by the number of dykes in each cell. The density map displays high concentration of dykes along the main swarm axes, varying from 5 to 45 dykes per cell (Fig. 5.10). The major concentration of dykes is coincident with the central portion of the swarms in the intersection zone between NE-SW and E-W branches of the RCM. The dyke densities decrease towards the tips of the respective branches. Higher dyke densities also occur along the major axes of the CD and RC swarms, with NW-SE and NE-SW trends, respectively.

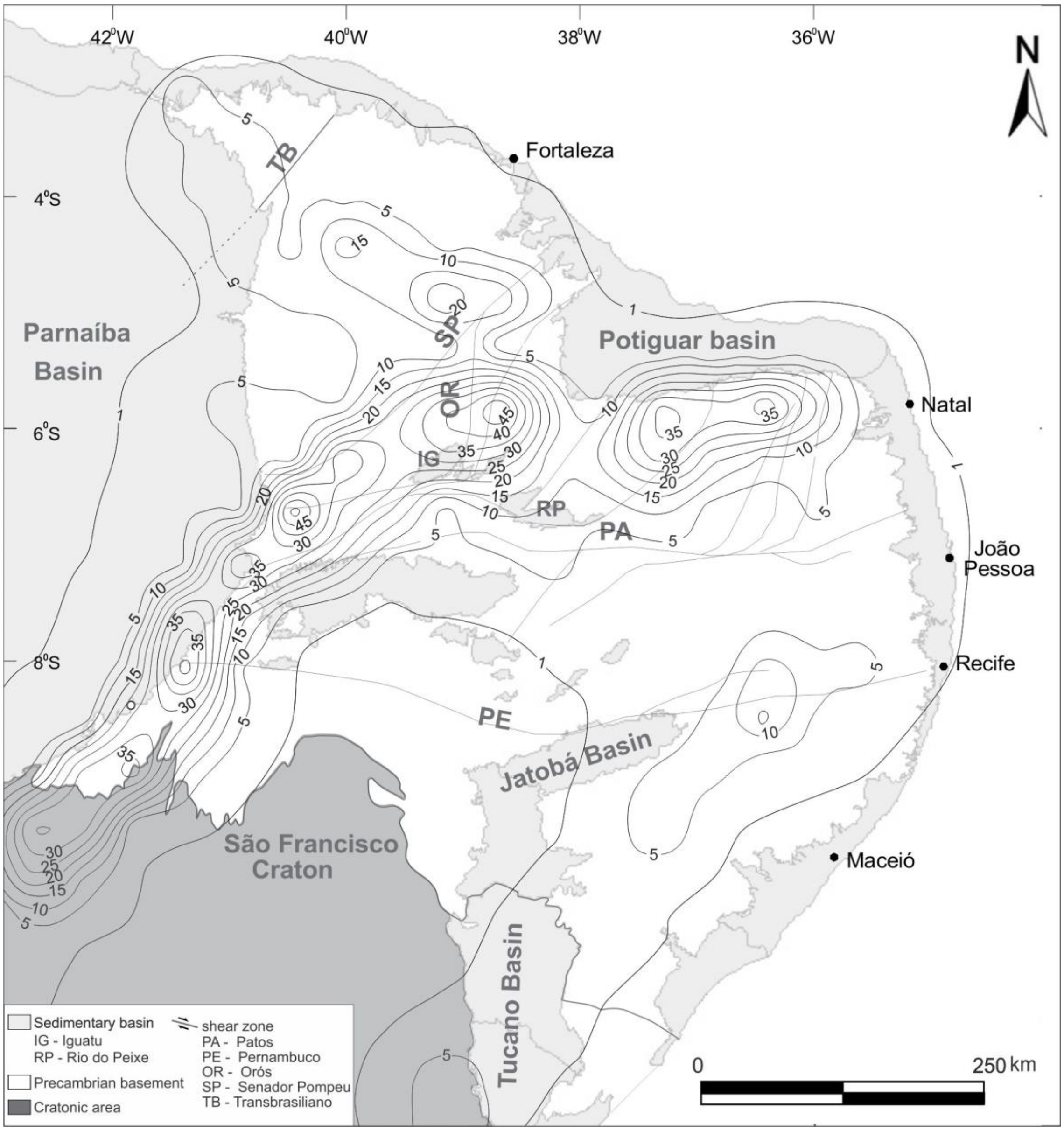

Figure 5.10. Spatial density of mapped dykes in the Borborema Province (NE Brazil). Contour lines represent number of dykes for 50 km cells.

In the RCM it was observed four main zones with high dyke density (Fig. 5.10). The first area is the E-W branch of this swarm, where the dykes are oriented E-W and border the Potiguar basin, reaching more than 35 dykes per cell. The NE-SW branch of the RCM displays three zones with 30 to 45 dykes per cell along its main axis. Higher density (> 45 dykes per cell) occurs where the RCM crosses the Orós-Jaguaribe, Patos and Pernambuco SZ (Fig. 5.6). It suggests that the emplacement mechanism of the dyke swarm should have taken advantage of ancient crustal weakness zones.

In the CD and RC swarms, the concentration of dykes is not so striking as seen in the RCM. In the CD, the main density of dykes (10 to 20 dykes per cell) occurs north of the NE-SW branch of the RCM near to the Senador Pompeu and Óros-Jaguaribe SZ (SP and OR in Figure 5.10). To the NW and W, the density decreases to <5 dykes per cell. In RC, the most dyke density (~10 dykes per cell) is located close to the intersection of an expressive basement structure, the Pernambuco shear zone (Fig. 5.10), as it occurs in the other dyke swarms, namely the RCM.

5.7. Discussions

5.7.1. Chronological relationship analysis of dyke sets

To the best of our knowledge, there are few available geochronological data of the dyke swarms in the BP (e.g. Bellieni et al., 1992; Oliveira, 1992; Mizusaki et al., 2002; Souza et al., 2003; Ngonge et al., 2016; Oliveira et al., 2021) and the most of them is concentrated on the E-W branch of the RCM. The dykes of the RC are not yet properly dated. Moreover, many dykes recognized in the present study area are poorly studied in terms of accurate dating or had not even been previously mapped. Thus, it is a very difficult task to establish a chronological model of these dyke swarms based on sparse radiometric ages. Considering mainly field relations between geological units and structures that host the dykes, the current hypothesis is that the emplacement of mafic dyke swarms in BP is considered contemporaneous to the West Gondwana breakup, during the Late Jurassic to Early Cretaceous.

To contribute solving this problem, our magnetic maps and the Google Earth™ satellite images with a high spatial resolution were used to understand the chronological relationships between the different mafic dyke swarms in the BP. The cross-cutting relationship between dykes is a key geometric data, which reflects their relative ages. Actually, we did not recognize significant points of intersection to establishing a detailed chronological relationship between the different dyke trending sets. Instead, thinner dykes were identified, which show thickness between 7.7 m and 8.9 m and the length is around 1 to 2 km. They are oriented in the NW-SE and NE-SW directions, crossing each other, and cut the mainly expressive dykes with E-W orientation (Figs. 5.8 and 5.9), indicating that there are multiple intrusive events. It is also observed for these dyke swarms with positive magnetic anomaly crosscut dykes with inverted magnetic polarity (Fig. 5.9).

No dykes were observed cross-cutting Mesozoic sedimentary rift basins (Potiguar, Iguatu, Rio do Peixe and Araripe basin). Indeed, the RCM shows bordering on the sedimentary basins, working as a rheological wall, which made it difficult to continue the rifting process. In this case, the magmatism preceded the rifting process or limiting the growth of the Potiguar rift southward. Therefore, the RMC mafic dykes are preterit or coeval to the oldest sedimentary units of these basins dated from Neocomian (Françolin and Szatmari, 1987; Matos, 1992). However, it is possible to observe dyke intrusion in the east of PB, which is a Paleozoic basin, and in the northwest of the SFC. This indicates that the placement of the RMC is latter to the PB and SFC.

5.7.2. Geodynamic Analysis

The geodynamic analysis of the geometrical pattern of the dykes and the structures genetically linked to them made it able to establish the ancient stress field acting during the time of the intrusion of the dyke swarms in the studied area. In our research, the paleostress trajectories for the mafic dykes are valid due to the fact that these swarms do not intrude pre-existing structures (e.g., faults, shear zones, etc.) of the basement (Figs. 5.1, 5.6 and 5.9). This configuration was based on the spatial distribution of the mapped dykes (Fig. 5.6). In such cases, the paleostress orientations were preserved with the same geometric relationship throughout the magmatic event as demonstrated by Moore and Shanti (1973), Halls (1982), Fahrig (1987) and Demarco et al. (2020).

The paleostress trajectories are defined by the position of stress tensors (Anderson, 1951), maximum main vector axis (σ_1) and minimum main vector axis (σ_3), across systems of faults, veins and dykes. In general, the tensors are approximately horizontal or subhorizontal and their directions are orthogonally mapped, according to Moore and Shanti (1973), Moore (1975) and Torkaski (1992). Paleostress map represents all local combinations of stress tensors, showing the behavior of paleostress tensors at a shallow crustal level. According to what was established by Roberts (1970), from the analysis of the spatial distribution homogeneity, it was also possible to establish the paleostress directions at the lithospheric level, since this reflects the same extension of the trajectories at an uppermost crustal level.

For the RCM, the paleostress trajectories denote an extension approximately N-S, rotating to NW-SE in the western part of the swarm, extending in the same direction throughout the whole swarm. In general, the stress field for the RCM, as a whole, is represented by the paleostress trajectories. It is possible to notice that the RCM has two extensional opening directions: a NW-SE direction for the NE-SW swarm branch westwards, and a N-S direction for the E-W swarm branch, in the NE portion of the BP.

The N-S extension is against the model proposed by the Matos (1992) to the opening of the Atlantic Equatorial Margin, which NW-SE extension that rotated to E-W. In this case, Oliveira (1992) argues that the E-W dykes reflects an extension (N-S) located at the extreme northeastern of BP, since its western portion tends to show a NW-SE opening.

It is observed in Figure 5.6, throughout the RCM, that these trajectories are homogeneous (Fig. 5.11), which suggests a response, with the same direction of extension, in deep crustal or lithospheric levels. Locally, the effects of a sudden change in the elastic properties of the crust are verified at the shallow crustal level. This is clearly noticed when there is the development of the en echelon geometry. This is interpreted as a variation of the stress field, due to rheological changes within the host rocks that did not contribute to the regional paleostress trajectories. From the 39° meridian to the east, the RCM dykes change their orientation (rotating from NE-SW to E-W). On this position, it is possible to perceive a superposition of different stress fields, which demonstrate a change in the stress field at a deep crustal or lithospheric level. The change of orientation of the dykes configures a semi-arch geometry to the dykes of the RCM.

Oliveira (1992) analyzed several criteria and scenarios inherent to the strict relationship of the RCM swarm with the occurrence of a mantle plume on the E-W branch of the RCM, concluding that the plausibility of the relationship between the two tectonic entities. Such a swarm geometry and the regional scale extension, more than 1,000 km, indicate a magmatic origin related to a mantle plume according to Ernst and Buchan (1997, 2001). In fact, Heine et al. (2013) proposed an active mantle plume beneath the BP during the rifting and first motions of the South American plate after breakup. This plume would be Saint Helena that originated the EQUAMP, as mentioned recently by Pessano et al. (2020) and Matos et al. (2021).

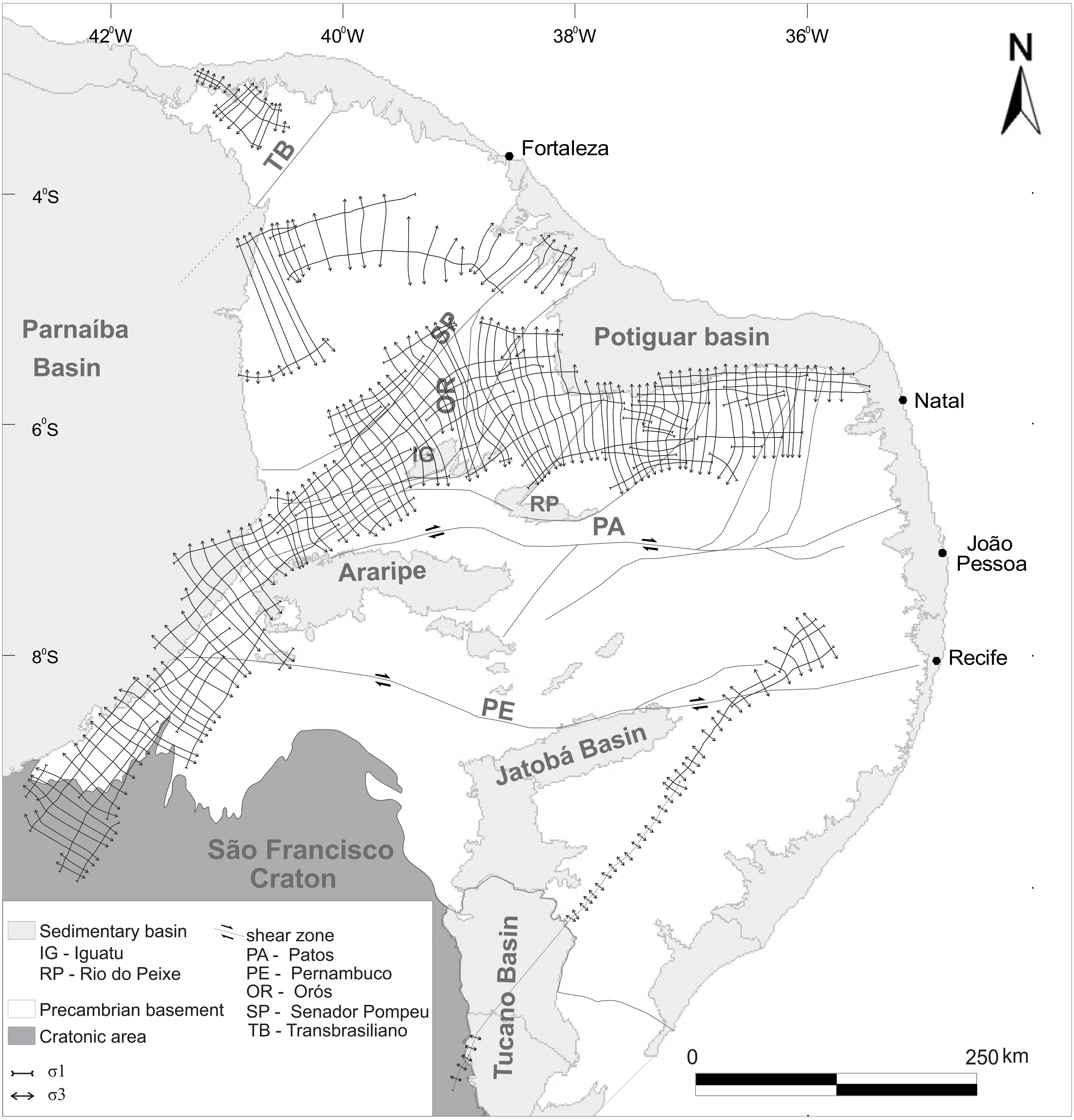

Figure 5.11. Paleostress trajectories of dykes in the Borborema Province (NE Brazil) derived from dyke spatial distribution.

5.8. Conclusions

Airborne geophysical (gamma-spectrometric and magnetic) data, Google Earth™ satellite images, magnetic susceptibility measurements and field work were applied to map Mesozoic dyke swarms in the Borborema Province (BP), NE Brazil. The results were compilated in a new map the distribution of the mafic dykes across the studied area. They allowed us to examine length, width, geometry, orientation, and relationship of the mafic dyke swarms, shedding light on the role of pre-rift magmatic events in the formation of a Large Igneous Province and continental breakup of the South American and African tectonic plates.

Several new dykes are identified in the Precambrian basement and adjacent Paleozoic Parnaíba Basin using geophysical and structural criteria. The magnetic maps reveal more than 6.8 x10^6 km^2 in the areal extension of 1388 mafic dykes that compose three distinct swarms in the BP: Rio Ceará-Mirim (RCM), Canindé (CD), and Riacho do Cordeiro (RC).

The dyke swarms show three preferential orientations to NW-SE, E-W, and NE-SW, which constitutes the major and dominant trend. In some cases, the dykes are crossing each other, demonstrating that different intrusive events occurred in the period before or at the beginning of the rifting in Early Cretaceous. In addition, inversions of magnetic anomaly polarity also indicates diachronic emplacement of dyke sets within the swarms. Indeed, we observed that the dyke sets with positive anomalies are younger than dykes with negative anomalies. Based on this premise, the NW-SE dyke swarm (CD) is the oldest across the entire province.

The new spatial distribution of the dykes shows that the dyke swarms crosscut the regional-scale basement fabric, including the main shear zones and even lithological contacts. On the other hand, we identified no dyke intrusion in the sedimentary rift basins, only bordering them. So, we understand that this magmatism that preceded the Early Cretaceous rift phase and emplaced a considerable volume of intrusive rock have increased the crustal resistance of the BP, preventing crustal rupture and leaving behind a series of aborted rift basins. Therefore, the dykes acted as a barrier that interrupted the development of the sedimentary basins, precluding them from extending.

The geodynamic analysis of the geometric pattern of the dykes allowed to establish the stress field active at the time of the intrusion. To the RCM, the paleostress trajectories represent a N-S extension, rotating to NW-SE in the western portion of the swarm. While for CD, paleostress orientation shows a NW-SE extensional movement, rotating to NE-SW. As for the RC, the trajectories were similar to those traced for the RCM, showing a predominant NW-SE extension. Due to the homogeneity showed by these trajectories, we assumed that it represents the pattern of stress at the lithospheric level. Finally, considering that this paper is a descriptive study, it intends to assist further geoscience studies focused on petrological, geochemical, analogue modelling, and geochronological aspects of the Mesozoic dyke swarm in the South American Platform.

Acknowledgments

ACCM thanks Programa de Formação de Recursos Humanos PRH-PB 229 (FUNPEC/UFRN/PETROBRAS) (project 672013) and the Coordenação de Aperfeiçoamento de Pessoal de Nível Superior (Capes) scholarships (Process N. 88882.461729/2019-01) for her PhD and for supporting a sandwich PhD scholarship at the Australian Commonwealth Scientific and Industrial Research Organization (CSIRO) and University of Queensland (UQ) (Process N. 88881.188664/2018-01). DLC thanks Conselho Nacional de Desenvolvimento Científico e Tecnológico (CNPq) for his PQ grants. We also thank the Geological Survey of Brazil (SGB) for providing the geophysical data; Carlos Archanjo from USP for all the support during the field work and general discussions. This work is part of the ACCM PhD dissertation, the Instituto Nacional de Ciência e Tecnologia em Estudos Tectônicos (INCT-ET) and corresponds to the contribution no. 5 of the EQUAMP LIP Project (grant 2017/08423-9).

References

Almeida, F.F.M., Carneiro, C.D.R., Machado Jr., D.., Dehira, L.., 1988. Magmatismo Pós- Paleozóico no Nordeste Oriental do Brasil. Revista Brasileira de Geociências 18, 451–462. https://doi.org/10.25249/0375-7536.1988441450

Almeida, F.F.M., Hasui, Y., de Brito Neves, B.B., Fuck, R.A., 1981. Brazilian structural provinces: An introduction. Earth Science Reviews 17, 1–29. https://doi.org/10.1016/0012-8252(81)90003-9ui, Y., de Brito Neves, B.B., Fuck, R.A., 1981. Brazilian structural provinces: An introduction. Earth Science Reviews 17, 1–29. https://doi.org/10.1016/0012-8252(81)90003-9

Anderson, E.M., 1951. The Dynamics of Faulting and Dyke Formation with Applications to Britain, 2nd ed. Oliver and Boyd, Edinburgh. https://doi.org/10.1038/149651b0

Angelim, L.A.A., Medeiros, V.C., Nesi, J.R., 2006. Mapa geológico do Estado do Rio Grande do Norte. Programa Geologia do Brasil – PGB. Projeto Geologia e Recursos Minerais do Estado do Rio Grande do Norte.

Archanjo, C.J., Arau, M.G.S., Launeau, P., 2002. Fabric of the Rio Ceará- Mirim mafic dike swarm (northeastern Brazil) determined by anisotropy of magnetic susceptibility and image analysis 107. . https://doi.org/10.1016/0012-8252(81)90003-9

Archanjo, C.J., Launeau, P., 2004. Magma flow inferred from preferred orientations of plagioclase of the Rio Ceară-Mirim dyke swarm (NE Brazil) and its AMS significance. Geological Society Special Publication 238, 285–298. https://doi.org/10.1144/GSL.SP.2004.238.01.17

Bellieni, G., Comin-Chiaramonti, P., Marques, L.S., Melfi, A.J., Nardy, A.J.R., Papatrechas, C., Piccirillo, E.M., Roisenberg, A., Stolfa, D., 1986. Petrogenetic Aspects of Acid and Basaltic Lavas from the Paraná Plateau (Brazil): Geological, Mineralogical and Petrochemical Relationships. Journal of Petrology 27, 915–944. https://doi.org/10.1093/petrology/27.4.915

Bellieni, G., Macedo, M.H.F., Petrini, R., Piccirillo, E.M., Cavazzini, G., Comin-Chiaramonti, P., Ernesto, M., Macedo, J.W.P., Martins, G., Melfi, A.J., Pacca, I.G., De Min, A., 1992. Evidence of magmatic activity related to Middle Jurassic and Lower Cretaceous rifting from northeastern Brazil (Ceará-Mirim): K/Ar age, palaeomagnetism, petrology and Sr/1bNd isotope characteristics. Chemical Geology 97, 9–32. https://doi.org/10.1016/0009-2541(92)90133-P

Blakely, R.J., 1996. Potential Theory in Gravity and Magnetic Applications, Program. https://doi.org/10.1017/CBO9780511549816

Briggs, I. C., 1973. Machine Contouring Using Minimum Curvature. BMR Record 1973/16. http://doi.org/10.1190/1.1440410

Brito Neves, B. B., 1999. America Do Sul: Quatro Fusões, Quatro Fissões E O Processo Acrescionário Andino. Revista Brasileira de Geociências, 29(3), 379–392. https://doi.org/10.25249/0375-7536.199929379392

Bückerl, C., Schultl, A., Guerreiro, S.D.C., 1986. Geophysics Rockmagnetism and palaeomagnetism of an Early Cretaceous / Late Jurassic dike swarm in Rio Grande do Norte. Journal of Geophysics 60, 29–135. https://journal.geophysicsjournal.com/JofG/article/view/126.

Cavalcante, J.C. , Vasconcelos, A.M., Mederios, M.F., Gomes, I., 2003. MAPA GEOLÓGICO DO ESTADO DO CEARÁ. Escala 1:500.000.

Cavalcante, J.C., Ferreira, C.A., Armesto, R.C.G.; Medeiros, M.F.., Ramalho, R., Braun, O.P.G., Baptista, M.B., Cunha, H.C.S., 1983. Mapa geológico do Estado do Ceará, escala 1:500.000.

Cordani, U.G., Brito Neves, B.B., Fuck, R.A., Porto, R., Thomaz Filho, A., Cunha, F.M.B., 1984. Estudo preliminar de integração do Pré-Cambriano com os eventos tectônicos das bacias sedimentares brasileiras. Ciência Técnica Petróleo, Seção Exploração de Petróleo.

Curto, J. B., Vidotti, R. M., Fuck, R. A., Blakely, R. J., Alvarenga, C. J. S., Dantas, E. L., 2014. The tectonic evolution of the Transbrasiliano Lineament in northern Paraná Basin, Brazil, as inferred from aeromagnetic data. Journal of Geophysical Reseach: Solid Earth, 119, 1544–1562, doi:10.1002/2013JB010593.

de Brito Neves, B.B., Cordani, U.G., 1991. Tectonic evolution of South America during the Late Proterozoic. Precambrian Research 53, 23–40. https://doi.org/10.1016/0301-9268(91)90004-T

de Castro, D.L., Bezerra, F.H., Fuck, R.A., Vidotti, R.M., 2016. Geophysical evidence of pre-sag rifting and post-rifting fault reactivation in the Parnaíba basin, Brazil. Solid Earth 7, 529–548. https://doi.org/10.5194/se-7-529-2016

de Castro, D.L., Fuck, R.A., Phillips, J.D., Vidotti, R.M., Bezerra, F.H.R., Dantas, E.L., 2014. Crustal structure beneath the Paleozoic Parna??ba Basin revealed by airborne gravity and magnetic data, Brazil. Tectonophysics 614. https://doi.org/10.1016/j.tecto.2013.12.009

de Castro, D.L., Oliveira, D.C., Hollanda, M.H.B.M., 2018. Geostatistical Interplay Between Geophysical and Geochemical Data: Mapping Litho-Structural Assemblages of

Mesozoic Igneous Activities in the Parnaíba Basin (NE Brazil). Surveys in Geophysics 1–31. https://doi.org/10.1007/s10712-018-9463-5

Delaney, P.T., Pollard, D.D., Ziony, J.I., McKee, E.H., 1986. Field relations between dikes and joints: emplacement processes and paleostress analysis. Journal of Georphvsical Research 91, 4920–4938. https://doi.org/10.1029/JB091iB05p04920

Delgado, I.M., Souza, J.D., Silva, L.C., Silveira Filho, N.C., Santos, R.A., P., A.J., Guimarães, J.T., Angelim, L.A., Vasconcelos, A.M., Gomes, I.P., Lacerda Filho, J.V., Valente, C.R., Perrota, M.M., Heinick, C.A., 2003. Geotectônica do Escudo Atlântico Geotectonics of the Atlantic Shield, in: Bizzi, L.A., Schobbenhaus, C., Vidotti, R.M., Gonçalves, J.H. (Eds.), Geologia, Tectônica e Recursos Minerais Do Brasil: Texto, Mapas e SIG. CPRM, Rio de Janeiro, pp. 281–292.

Demarco, P.N., Masquelin, H., Prezzi, C., Aïfa, T., Muzio, R., Loureiro, J., Peel, E., Campal, N., Sánchez Bettucci, L., 2020. Aeromagnetic patterns in Southern Uruguay: Precambrian-Mesozoic dyke swarms and Mesozoic rifting structural and tectonic evolution. Tectonophysics 789, 228373. https://doi.org/10.1016/j.tecto.2020.228373

Dentith, M., Mudge, S.T., 2014. Geophysics for the Mineral Exploration Geoscientist. Cambridge University Press, Cambridge. https://doi.org/DOI: 10.1017/CBO9781139024358

Ernesto, M., Furtado, M.H., Macedo, J.W.P., Martins, G., 1991. Paleomagnetism of the ceará-mirim dyke swarm, northeastern Brazil. Boletim de Geociências da USP, Publicação Especial 10, 73–76. https://doi: http://dx.doi.org/10.11606/issn.2317-8078.v0i10p73-76

Ernst, R E; Buchan, K L; West, T D; Palmer, H.C., 1996. Diabase (dolerite) dyke swarms of the world: first edition, Geological Survey of Canada.

Ernst, R.E., Buchan, K.L., 1997. In: Giant radiating dyke swarms: Their use in identifying pre-Mesozoic large igneous provinces and mantle plumes. American Geophysical Union, Washington D.C. 100: 3. https://doi: 10.1029/GM100p0297.

Ernst, R., Bleeker, W., 2010. Large igneous provinces (LIPs), giant dyke swarms, and mantle plumes: significance for breakup events within Canada and adjacent regions from 2.5 Ga to the PresentThis article is one of a selection of papers published in this Special

Issue on the the them. Canadian Journal of Earth Sciences 47, 695–739. https://doi.org/10.1139/E10-025

Ernst, R.E., 2014. Large Igneous Provinces. Cambridge University Press, Cambridge. https://doi.org/10.1017/CBO9781139025300

Ernst, R.E., Buchan, K.L., 2013. Giant Radiating Dyke Swarms: Their Use in Identifying Pre-Mesozoic Large Igneous Provinces and Mantle Plumes, in: Geophysical Monograph Series. pp. 297–333. https://doi.org/10.1029/GM100p0297

Ernst, R.E., Buchan, K.L., 2001. The use of mafic dike swarms in identifying and locating mantle plumes, in: Ernst, Richard E. ; Buchan, K.L. (Ed.), Mantle Plumes: Their Identification through Time. Geological Society of America, pp. 247–265. https://doi.org/10.1130/0-8137-2352-3.247

Fahrig, W.F., 1987. The tectonics settings of continental rnafic dyke swans: failed arm and early passive margin, in: Halls, H.C. & Fahrig, W.F. (Ed.), Mafic Dyke Swarms. Geological Association of Canada Special Paper, pp. 331–348.

Françolin, B. D. E. L., Szatmari, P., 1987. Mecanismo de rifteamento da porção oriental da margem norte brasileira. Revista Brasileira de Geociências, 17, 196–207.

Góes, A. D. O., Feijó, F.J., 1994. Bacia do Parnaíba. Boletim de Geociências da Petrobras 8, 57–67.

Goldberg, A.S., 2010. Dyke swarms as indicators of major extensional events in the 1.9-1.2Ga Columbia supercontinent. Journal of Geodynamics 50, 176–190. https://doi.org/10.1016/j.jog.2010.01.017

Gomes, J.R.C., Gatto, C.M.P.P., Souza, G.M.C. de, Luz, D.S. da, Pires, J.L., Teixeira, W., Franca, F.A.B. de, Cabral, E.M.A., Menor, E.A., M., M., Barros, M.J.G., Ribeiro, E.G., Lima, E.A. Fonseca, R.A. da, 1981. Geologia das Folhas SB-24/25, Jaguaribe e Natal. Proj. Radambrasil Rio de MME/Secr. Geral, Lev. Rec. Nat., 23: 27-300.

Guerreiro, S.D.C., Schult, A., 1983. Paleomagnetismo de um enxame de diques tholeíticos de idade meso-cenozóica, localizados no Rio Grande do Norte. Revista Brasileira de Geofisica 1, 89–98.

Halls, H.C., 1982. The importance and potential of mafic dyke swarms in studies of geodynamic processes. Geoscience Canada 9, 145–154.

Hasui, Y., 2012. Cráton do São Francisco, in: Hasui, Y., Carneiro, C.D.R., Almeida, F.F.M., Bartorelli, A. (Eds.), Geologia Do Brasil. Beca Editora, São Paulo, pp. 200–228.

Heine, C., Zoethout, J., Müller, R.D., 2013. Kinematics of the South Atlantic rift. Solid Earth 4, 215–253. https://doi.org/10.5194/se-4-215-2013

Hollanda, M.H.B.M., Archanjo, C.J., Filho, A.A.M., Fossen, H., Ernst, R.E., Castro, D.L. De, Melo, A.C., Oliveira, A.L., 2019. Dyke Swarms of the World: A Modern Perspective, Dyke Swarms of the World: A Modern Perspective, Springer Geology. Springer Singapore. https://doi.org/10.1007/978-981-13-1666-1

Jardim de Sá, E.F., Macedo, M.H.F., Fuck, R.A., Kawashita, K., 1992. Terrenos Proterozicos na Província Borborema e a Margem Norte do Craton São Francisco. Revista Brasileira de Geociências 22, 472–480.

Jessell, M., Santoul, J., Baratoux, L., Youbi, N., Ernst, R.E., Metelka, V., Miller, J., Perrouty, S., 2015. An updated map of West African mafic dykes. Journal of African Earth Sciences 112, 440–450. https://doi.org/10.1016/j.jafrearsci.2015.01.007

Kiselev, A.I., Ernst, R.E., Yarmolyuk, V. V., Egorov, K.N., 2012. Radiating rifts and dyke swarms of the middle Paleozoic Yakutsk plume of eastern Siberian craton. Journal of Asian Earth Sciences 45, 1–16. https://doi.org/10.1016/j.jseaes.2011.09.004

Macêdo Filho, A.A., Archanjo, C.J., Hollanda, M.H.B.M., Negri, F.A., 2019. Mineral chemistry and crystal size distributions of mafic dikes and sills on the eastern border of the Parnaíba Basin, NE Brazil. Journal of Volcanology and Geothermal Research 377, 69–80. https://doi.org/10.1016/j.jvolgeores.2019.03.021

Maluski, H., Baudin, P., 1995. $^{40}Ar/^{39}Ar$ chronology, petrology and geodynamic setting of Mesozoic to early Cenozoic magmatism from the Benue Trough, Nigeria. *Journal of the Geological Society* 152 (2): 311–326. doi: https://doi.org/10.1144/gsjgs.152.2.0311

Marzoli, A., Renne, P.R., Piccirillo, E.M., Ernesto, M., Bellieni, G., De Min, A., 1999. Extensive 200-million-year-old continental flood basalts of the Central Atlantic

Magmatic Province. Science 284, 616–618. https://doi.org/10.1126/science.284.5414.616

Matos, R.M.D. de, Krueger, A., Norton, I., Casey, K., 2021. The fundamental role of the Borborema and Benin–Nigeria provinces of NE Brazil and NW Africa during the development of the South Atlantic Cretaceous Rift system. Marine and Petroleum Geology 127, 104872. https://doi.org/https://doi.org/10.1016/j.marpetgeo.2020.104872

Matos, R.M.D., 1992. The Northeast Brazilian Rift System. Tectonics 11, 766–791. https://doi.org/10.1029/91TC03092

Melo, A. C. C. de, de Castro, D. L., Bezerra, F. H. R., Bertotti, G. 2016. Rift fault geometry and evolution in the Cretaceous Potiguar Basin (NE Brazil) based on fault growth models. Journal of South American Earth Sciences, 71, 96–107. https://doi.org/10.1016/j.jsames.2016.07.006

Melo, A.C.C., de Castro, D.L., Fraser, S.J., Macêdo Filho, A.A., 2021. Using self-organizing maps in airborne geophysical data for mapping mafic dyke swarms in NE Brazil. Journal of Applied Geophysics 192, 104377. https://doi.org/10.1016/j.jappgeo.2021.104377

Merle, R., Marzoli, A., Bertrand, H., Reisberg, L., Verati, C., Zimmermann, C., Chiaradia, M., Bellieni, G., Ernesto, M., 2011. 40Ar/39Ar ages and Sr–Nd–Pb–Os geochemistry of CAMP tholeiites from Western Maranhão basin (NE Brazil). Lithos 122, 137–151. https://doi.org/https://doi.org/10.1016/j.lithos.2010.12.010

Mizusaki, A.M.P., Thomaz Filho, A., Milani, E.J., Césero, P., 2002. Mesozoic and Cenozoic igneous activity and its tectonics control in northeastern Brazil. Journal of South American Earth Sciences 15, 183–198.

Moore, J.M., 1975. A mechanical interpretation of the vein and dyke system of the S. W. England Orefield. Mineral Deposita, 10, 374-388.

Moore, J.M., Shanti, A.M., 1973. The use of stress trajectory analysis in the elucidation of part of the Najd Fault System, Saudi Arabia. Procedding Geological Association of London, 84(4), 383-403

Moraes, L.J., 1924. Serras e montanhas do Nordeste, 58th ed, Serras e montanhas do Nordeste. Brazil. Inspectoria Federal de Obras contra as Seccas, Rio de Janeiro.

Nabighian, M.N., 1972. The analytic signal of two dimensional magnetic bodies with polygonal cross-section: It's properties and use for automated anomaly interpretation. Geophysics, 37, 507-517. https://doi: 10.1190/1.1440276.

Nasuti, A., Roberts, D., Gernigon, L., 2015. Multiphase mafic dykes in the Caledonides of northern Finnmark revealed by a new high-resolution aeromagnetic dataset. Norwegian Journal of Geology 95, 285–297. https://doi.org/10.17850/njg95-3-02

Neves, S.P., Vauchez, A., Feraud, G., 2000. Tectono-thermal evolution, magma emplacement, and shear zone development in the Caruaru area (Borborema Province, NE Brazil). Precambrian Research 99, 1–32. https://doi.org/10.1016/S0301-9268(99)00026-1

Ngonge, E.D., de Hollanda, M.H.B.M., Archanjo, C.J., de Oliveira, D.C., Vasconcelos, P.M.P., Mu??oz, P.R.M., 2016. Petrology of continental tholeiitic magmas forming a 350-km-long Mesozoic dyke swarm in NE Brazil: Constraints of geochemical and isotopic data. Lithos 258–259, 228–252. https://doi.org/10.1016/j.lithos.2016.04.008

Oliveira, D. C., 1992. O papel do Enxame de Diques Rio Ceará Mirim na evolução tectônica do nordeste oriental (Brasil): implicações na formação do Rifte Potiguar. Ms. C. thesis, Universidade Federal de Ouro Preto, Ouro Preto, Brazil.

Oliveira, D.C., Mohriak, W.U., 2003. Jaibaras trough: an important element in the early tectonic evolution of the Parnaíba interior sag basin, Northern Brazil. Marine and Petroleum Geology 20, 351–383. https://doi.org/https://doi.org/10.1016/S0264-8172(03)00044-8

Oliveira, A.L., Hollanda, M.H.B.M., Siqueira, R., Macêdo Filho, A.A., 2021. Using a ‘speedy’ unspiked K–Ar methodology to investigate age patterns in giant mafic dyke swarms. Geological Society, London, Special Publications 518, SP518-2020–250. https://doi.org/10.1144/SP518-2020-250

Oliveira, D.C., Gomes, C.J.S., 1996. A Expressão de reativações pós-intrusão do Enxame de Diques Rio Ceará-Mirim (Mesozóico): Implicações na evolução tectônica da Bacia Potiguar. Boletim de Geociências da Petrobrás, 10, 121–145.

Oliveira, R.G., Medeiros, W.E., 2012. Evidences of buried loads in the base of the crust of Borborema Plateau (NE Brazil) from Bouguer admittance estimates. Journal of South American Earth Sciences 37, 60–76. https://doi.org/10.1016/j.jsames.2012.02.004

Pessano, P.C., Ganade, C.E., Tupinambá, M., Teixeira, W., 2020. UPDATED map of the mafic dike swarms of Brazil based on airborne geophysical data. Journal of South American Earth Sciences 103076. https://doi.org/10.1016/j.jsames.2020.103076

Phillips, J.D., 2001. Designing matched bandpass and azimuthal filters for the separation of potential-field anomalies by source region and source type. ASEG 15th Geophysical Conference and Exhibition, August 2001, Brisbane.

Reeves, C., 2000. The geophysical mapping of Mesozoic dyke swarms in southern Africa and their origin in the disruption of Gondwana. Journal of African Earth Sciences 30, 499–513. https://doi.org/10.1016/S0899-5362(00)00035-X

Renne, P.R., Ernesto, M., Pacca, I.G., Coe, R.S., Glen, J.M., Prevot, M., Perrin, M., 1992. The age of Paraná fl ood volcanism, rifting of Gondwanaland, and the Jurassic-Cretaceous boundary. Science 258, 975–979. https://doi.org/doi:10.1126/science.258.5084.975

Roberts, J.L. ,1970. The intrusion of magma into brittle rocks. In: Newall, G. & Rast, N. (eds.). Mechanism of igneous intrusion. Liverpool. Gallery Press. p. 287-338.

Santos, E.J., 1968. Contribuição ao estudo da geologia da quadrícula de Açú. Série Geologia Regional, 6. SUDENE/Divisáo de Geologia, Recife.

Sial, A.N., Oliveira, E.P., Choudhuri, A., 1987. Mafic dyke swarms of Brazil. In: Halls, H. C., Fahrig, W.F. (Eds.), Mafic Dyke Swarms, vol. 34. Geological Association of Canada Special Papers, pp. 467–481.

Silva Filho, M.A., Bomfim, L.F.C.,Santos, R.A., Leal, R.A., Braz Filho, P. de A., Santana, A.C., Rodrigues, T.L., Santos, J.C., 1981. Projeto Complexo Canindé do São Francisco. DNPM, Série Geologia. DNPM, Série Geologia No. 19, Seção Geologia Básica No. 14, Brasília.

Souza, Z.S., Vasconcelos, P.M.P., Nascimento, M.A.L., Silveira, F.V., Paiva, H.S., Dias, L.G.S., Thiede, D., Carmo, I.O., 2003. 40Ar/39Ar geochronology of Mesozoic and Cenozoic magmatism in NE Brazil. (No. 2). Salvador.

Szatmari, P., Françolin, J.B.L., Zanotto, O., Wolff, S., 1987. Evolução tectônica da Margem Equatorial Brasileira. Revista Brasileira de Geociências, 17(2), 180-1 88. https://doi: 10.25249/0375-7536.1987180188

Telford, W. M., Geldart, L. P., Sheriff, R. E., 1990. Applied Geophysics. 2. ed. Cambridge: Cambridge University Press. 1608 p.

Thiede, D.S., Vasconcelos, P.M., 2010. Paraná flood basalts: Rapid extrusion hypothesis confirmed by new 40Ar/39Ar results. Geology, 38(8), 747–750. https://https://doi.org/10.1130/G30919.1

Tokarski, A.K., 1990. Dyke swarms as stress indicators: two constraints. In: Parker et a/. (eds.). Mafic dykes and emplacement mechanisms. Rotterdam. Balkema. p.101-104.

Trompette, R., Uhlein, A., da Silva, M.E., Karmann, I., 1992. The Brasiliano Sao Francisco craton revisited (central Brazil). Journal of South American Earth Science 6, 49–57. https://doi.org/10.1016/0895-9811(92)90016-R

Trumbull, R.B., Vietor, T., Hahne, K., Wackerle, R., Ledru, P., 2004. Aeromagnetic mapping and reconnaissance geochemistry of the Early Cretaceous Henties Bay-Outjo dike swarm, Etendeka Igneous Province, Namibia. Journal of African Earth Sciences 40, 17–29. https://doi.org/10.1016/j.jafrearsci.2004.07.006

Tucker, D.H. and Boyd, D.M., 1987. Dykes of Australia Detected by Airbone magnetic Surveys, in: Halls, H.., Fahring, W.F. (Eds.), Mafic Dyk Swarms. Geological Association of canada Special Paper 34, pp. 163–1972.

Van Schmus, W.R., De Brito Neves, B.B., Williams, I.S., Hackspacher, P.C., Fetter, A.H., Dantas, E.L., Babinski, M., 2003. The Seridó Group of NE Brazil, a late Neoproterozoic pre- to syn-collisional basin in West Gondwana: Insights from SHRIMP U-Pb detrital zircon ages and Sm-Nd crustal residence (TDM) ages. Precambrian Research 127, 287–327. https://doi.org/10.1016/S0301-9268(03)00197-9

Xiong, S., Yang, H., Ding, Y., Li, Z., Li, W., 2016. Distribution of igneous rocks in China revealed by aeromagnetic data. Journal of Asian Earth Sciences 129, 231–242. https://doi.org/10.1016/j.jseaes.2016.08.016

Zaineldeen, U.F., 2012. Mapping the Dyke Swarms of the Neoproterozoic Basement in Southwestern Jordan Using Remote Sensing and GIS Techniques. Earth Science Research 2, 156–164. https://doi.org/10.5539/esr.v2n1p156

Zembruscki, S.G., Campos, J.N.P., 1988. Comportamento geotérmico regional e provável movimentação de fluidos na Bacia do Parnaíba, Maranhão. Boletim de Geociência da Petrobras 2, 133–145.

CONSIDERAÇÕES FINAIS

O método Self-Organizing Maps (SOM) foi aplicado a 14 levantamentos aerogeofísicos para o mapeamento dos enxames de diques máficos mesozoicos – cenozoicos da Província Borborema e regiões adjacentes, Cráton São Francisco e Bacia do Parnaíba. Três variáveis gama-espectrométricas e duas magnéticas foram selecionadas como parâmetros de entrada no SOM, que forneceu dois grupos de soluções associadas as ocorrências dos diques. Os resultados foram validados por meio da análise de imagens de satélite do Google Earth™, levantamento de campo e medidas de susceptibilidade magnética de amostras de rocha.

Uma área teste foi utilizada para treinar e otimicar o procedimento de classificação multivariada do método SOM na detecção dos diques a partir dos dados geofísicos. O mapa resultante providenciou um aumento substancial de ~80% da área afetada por enxames na Província Borborema em comparação com o que era conhecido anteriormente. Os levantamentos de campo aferiram que o SOM teve mais de 90% de precisão na detecção de diques máficos de forma semiautomática. Os enxames de diques formam uma estrutura arqueada de mais 1000 km de extensão e 150 km de largura, estendendo-se desde o norte do Cráton São Francisco, afetando a borda sudeste da Bacia do Parnaíba, atingindo até a extremidade nordeste da Província Borborema. Dois outros enxames menores, Canindé (CD) e Riacho do Cordeiro (RC), ocorrem tanto a NW quanto a SE do enxame central, denominado de Enxame de Diques Rio Ceará-Mirim (RCM). A integração do mapeamento SOM com imagens de satélite do Google Earth™ e estudos de campo revelou a presença de diques até então desconhecidos no embasamento pré-cambriano da área estudada. Como resultado, foram identificados 1388 diques em uma área de 6,8 x 10^6 km^2, ocorrendo em três orientações preferenciais NW-SE, E-W e NE-SW, sendo esta última a tendência principal e dominante.

No mapeamento detalhado dos diques, foi verificado que estes corpos cortam as estruturas do embasamento cristalino em alto ângulo e que não intrudem as bacias rifte da área, mas bordejam seus limites tectônicos, em especial a borda sul da Bacia Potiguar. Sendo assim, entende-se que o magmatismo que precedeu a fase rifte do Cretáceo Inferior, acrescentando um volume considerável de rocha intrusiva. Pode-se pressupor que a acresção magmática possa ter aumentado a resistência crustal da Provincia Borborema, que atuou como uma barreira para o desenvolvimento das bacias sedimentares, impedindo uma ruptura crustal e deriva continental.

Este trabalho permitiu não só analisar as relações dos diques com as anisotropias crutais, como também as relações entre os diferentes segmentos de diques. Em alguns locais foram identicados intrecruzamentos de diques, demostrando a ocorrência de diferentes pulsos magmáticos diacrônicos na intrusão dos diques. Além disso, foram observadas alternância de polaridade nas anomalias magnéticas exibidas pelos diques. As anomalias positivas cruzam as anomalias negativas, sendo consideradas mais novas. Com base nessa premissa, o enxame de diques CD de direção NW-SE pode ser considerado como o mais antigo em toda a província.

A partir do mapeamento detalhado, foi também realizada uma análise geodinâmica do padrão geométrico dos diques para estabelecer o campo de tensões ativo no momento da intrusão. Para o RCM, as trajetórias de paleotensões representam uma extensão N-S, rotacionando para NW-SE na porção oeste do enxame. Já para CD, a orientação da paleotensão mostra um movimento distensional NW-SE, com rotação para NE-SW. Já para o RC, as trajetórias foram semelhantes às traçadas para o RCM, apresentando uma extensão NW-SE predominante. Devido à homogeneidade mostrada por essas trajetórias, presumimos que ela representa o padrão de tensão no nível litosférico.

Por fim, os resultados desta tese pretendem auxiliar futuros estudos de geociências com foco em petrologia, geoquímica, modelagem analógica e aspectos geocronológicos do enxame de diques mesozoicos na plataforma sul-americana. Para uma melhor caracterização dos enxames de diques, recomenda-se a continuidade das pesquisas de modo a contemplar um maior adensamento dos diques mapeados, a fim de propor um modelo que explique a origem desses enxames de diques.

REFERÊNCIAS

Almeida, F.F.M., Brito Neves, B.B., Dal Ré Carneiro, C., 2000. The origin and evolution of the South American Platform. Earth-Science Reviews 50, 77–111. https://doi.org/10.1016/S0012-8252(99)00072-0

Almeida, F.F.M., Hasui, Y., Brito Neves, B.B., Fuck, R.A. ,1981. Brazilian structural Provinces: An introduction, Earth-Science Reviews, 17(1–2),1-29. https://doi.org/10.1016/0012-8252(81)90003-9

Anderson, E.M., 1951. The Dynamics of Faulting and Dyke Formation with Applications to Britain, 2nd ed. Oliver and Boyd, Edinburgh.

Angelim, L.A.A., Medeiros, V.C., Nesi, J.R., 2006. Programa Geologia do Brasil – PGB. Projeto Geologia e Recursos Minerais do Estado do Rio Grande do Norte. Mapa geológico do Estado do Rio Grande do Norte. Escala. 1:500.000. Recife: CPRM/FAPERN, 2006. 1 mapa color.

Bação, F., Lobo, V., and Painho, M., 2005, The self-organizing map, the Geo-SOM, and relevant variants for geosciences: Computers and Geosciences, v. 31, p. 155–163, doi: 10.1016/j.cageo.2004.06.013.

Baranov V., Naudy H. 1964. Numerical Calculation of the Formula of Reduction to the Magnetic Pole, Geophysics, v. 29, 67-79. https://doi.org/10.1190/1.1439334

Bierlein, F.P., Fraser, S.J., Brown, W.M., and Lees, T., 2008, Bierlein, F.P., Fraser, S.J., Brown, W.M., and Lees, T., 2008, Advanced methodologies for the analysis of databases of mineral deposits and major faults.: Australian Journal of Earth Sciences, v. 55, p. 79–99, doi: 10.1080/08120090701581406.Advanced metho: Australian Journal of Earth Sciences, v. 55, p. 79–99, doi: 10.1080/08120090701581406.

Blakely, R.J., 1996. Potential Theory in Gravity and Magnetic Applications, Program. https://doi.org/10.1017/CBO9780511549816

Brito Neves, B.B., Cordani, U.G., 1991. Tectonic evolution of South America during the Late Proterozoic. Precambrian Research 5, 23–40. https://doi:10.1016/0301-9268(91)90004-T

Bryan, S., Ernst, R.E., 2008. Revised definition of Large Igneous Provinces (LIPs). Earth-Science Reviews, 86: 175–202. https://doi.org/10.1016/j.earscirev.2007.08.008

Carneiro, C. C., 2010. Modelagem espacial de dados aerogeofísicos e interpretação de imagens SAR aplicados ao mapeamento geológico e metalogenético da região central do Domínio Bacajá, Estado do Pará. PhD. thesis, Univ. Estadual de Campinas, Campinas, Brasil.

Carneiro, C.D.C., Fraser, S.J., Crósta, A.P., Silva, M., Eduardo, C., Barros, D.M., 2012. Semiautomated geologic mapping using self-organizing maps and airborne geophysics in the Brazilian Amazon. Geophysics 77, 17-24. https://doi.org/10.1190/GEO2011-0302.1

Cavalcante, J.C. , Vasconcelos, A.M., Mederios, M.F., Gomes, I., 2003. Mapa geológico do estado do Cear. Escala 1:500.000. Fortaleza: CPRM, 2003.

Cinzia, F., Hofmann, A., 2011. Mantle Plumes. Encyclopedia of Earth Sciences Series. 1-9. https://doi.org/857-869.10.1007/978-90-481-8702-7_132

Coffin, M. F., Eldholm, O., 1994. Large igneous proinces: crustal structure, dimensions, and external consequences. Reviews of Geophysics, 32(1), 1-36. https://doi.org/10.1029/93RG02508

de Castro, D.L., Oliveira, D.C., Hollanda, M.H.B.M., 2018. Geostatistical Interplay Between Geophysical and Geochemical Data: Mapping Litho-Structural Assemblages of Mesozoic Igneous Activities in the Parnaíba Basin (NE Brazil). Surv. Geophys. 1–31. https://doi.org/10.1007/s10712-018-9463-5

Delaney, P.T., Pollard, D.D., Ziony, J.I., McKee, E.H., 1986. Field relations between dikes and joints: emplacement processes and paleostress analysis. J. Georphysical Res. 91, 4920–4938. https://doi.org/10.1029/JB091iB05p04920

Delgado, I.M., Souza, J.D., Silva, L.C., Silveira Filho, N.C., Santos, R.A., Pedreira, A.J., Guimarães, J.T., Angelim, L.A.A, Vasconcelos, A.M., Gomes, I.P., Lacerda Filho, J.V., Valente, C.R., Perrotta M.M. and Heineck, C.A., 2003. Geotectônica do Escudo Atlântico, in: Bizzi, L.A., Schobbenhaus, C., Vidotti, R.M. and Gonçalves, J.H. (Eds.), Geologia, Tectônica e Recursos Minerais do Brasil. CPRM, Brasília, pp. 227-334.

Demarco, P.N., Masquelin, H., Prezzi, C., Aïfa, T., Muzio, R., Loureiro, J., Peel, E., Campal, N., Sánchez Bettucci, L., 2020. Aeromagnetic patterns in Southern Uruguay: Precambrian-Mesozoic dyke swarms and Mesozoic rifting structural and tectonic evolution. Tectonophysics 789, 228373. https://doi.org/10.1016/j.tecto.2020.228373

Dickson, B.L. and Scott, K.M., 1997. Interpretation of Aerial Gamma-Ray Surveys-Adding the Geochemical Factors. Journal of Australian Geology and Geophysics, 17, 187-200. http://hdl.handle.net/102.100.100/224930?index=1

D'Urso, P., De Giovanni, L., and Massari, R., 2014, Self-Organizing Maps for imprecise data: Fuzzy Sets and Systems, v. 237, p. 63–89. https://doi: 10.1016/j.fss.2013.09.011.

Ernst, R.E., 2014. Large Igneous Provinces. Cambridge University Press, Cambridge. https://doi.org/10.1017/CBO9781139025300

Ernst, R.E., Buchan, K.L., 1997. In: Giant radiating dyke swarms: Their use in identifying pre-Mesozoic large igneous provinces and mantle plumes. American Geophysical Union, Washington D.C. 100: 3. https://doi: 10.1029/GM100p0297.

Ernst, R.E., Buchan, K.L., 2001. The use of mafic dike swarms in identifying and locating mantle plumes, in: Ernst, Richard E. ; Buchan, K.L. (Ed.), Mantle Plumes: Their Identification through Time. Geological Society of America, pp. 247–265. https://doi.org/10.1130/0-8137-2352-3.247

Ernst, R E; Buchan, K L; West, T D; Palmer, H.C., 1996. Diabase (dolerite) dyke swarms of the world: first edition, Geological Survey of Canada.

Folger, G.R., 2007. The plate model for genesis of melting anomalies. Geological Society of America Special Paper, 430, 1-28. https://doi.org/10.1130/2007.2430(01)

Fraser, S. H., Dickson, B.L., 2007. A new method of data integration and integrated data interpretation: Self-organizing maps, in B. Milkereit, ed., Proceedings of Exploration 07: Fifth Decennial International Conference on Mineral Exploration, 907–910. http://dmec.ca/ex07-dvd/E07/pdfs/67.pdf

Gudmundsson, A., 1990. Emplacement of dikes, sills and crustal magma chambers at divergent plate boundaries. Tectonophysics,176 (3–4), 257-275. http://doi.org/10.1016/0040-1951(90)90073-H

Halls, H.C., 1982. The importance and potential of mafic dyke swarms in studies of geodynamic processes. Geoscience Canada 9, 145–154.

Halls, H.C.; Fahrig, W.F.,1987. Mafic Dike Swarms. Geological Association of Canada., Specical Paper, 34, 503p.

Holmes, A., 1944. Principles of Physical Geology (1 ed.); Edimburgh, Thomas & Sons, 580 p.

Jessell, M., Santoul, J., Baratoux, L., Youbi, N., Ernst, R.E., Metelka, V., Miller, J., Perrouty, S., 2015. An updated map of West African mafic dykes. J. African Earth Sci. 112, 440–450. https://doi.org/10.1016/j.jafrearsci.2015.01.007

Kearey, P., Brooks, M., and Hill, I., 2009, Geofísica de exploração: São Paulo, Oficina de Textos, 437 p.

Kohonen, T., 1982. Analysis of a simple self-organizing process. Biological Cybernetics 44, 135-140, https://doi:10.1007/BF00317973

Kohonen, T., and Somervuo, P., 1998, Self-organizing maps of symbol strings: Neurocomputing, v. 21, p. 19–30, doi: 10.1016/S0925-2312(98)00031-9.

Kohonen, T., 2001. Self-Organizing Maps, Third edit. ed. Berlin, Heidelberg: Springer Berlin Heidelberg, Berlin, Heidelberg. https://doi: 10.1007/978-3-642-56927-2

Mckenzie, D.P. 1984. A possible mechanism for epeirogenic uplift. Nature, 307(16); 616-618. https://doi.org/10.1038/307616a0

Minty, B.R.S., 1997. Fundamentals of airborne gamma-ray spectrometry. AGSO Journal of Australian Geology and Geophysics, 17(2), 39-50.

Nabighian, M.N., 1972. The analitic signal of two dimensional magnetic bodies with poligonal cross-section: It's properties and use for automated anomaly interpretation. Geophysics, v. 37, 507-517. https://doi.org/10.1190/1.1440276

Neves, S.P., Vauchez, A., Feraud, G., 2000. Tectono-thermal evolution, magma emplacement, and shear zone development in the Caruaru area (Borborema Province, NE Brazil). Precambrian Res. 99, 1–32. https://doi.org/10.1016/S0301-9268(99)00026-1

Ni, N., Chena, N., Ernstb, R.E., Yanga, S., Chend, J., 2018. Semi-automatic extraction and mapping of dyke swarms based on multiresolution remote sensing images: Applied to the dykes in the Kuluketage region in the northeastern Tarim Block Precambrian Research. 329, 262-272, https://doi: 10.1016/j.precamres.2018.05.020

Oliveira, D. C., 1992. O papel do Enxame de Diques Rio Ceará Mirim na evolução tectônica do nordeste oriental (Brasil): implicações na formação do Rifte Potiguar. Ms. C. thesis, Univ. Fed. de Ouro Preto, Ouro Preto, Brazil.

Oliveira, R.G., Medeiros, W.E., 2012. Evidences of buried loads in the base of the crust of Borborema Plateau (NE Brazil) from Bouguer admittance estimates: Journal of South American Earth Sciences, 37, 60–76, https://doi: 10.1016/j.jsames.2012.02.004

Penn, B.S., 2005, Using self-organizing maps to visualize high-dimensional data: Computers and Geosciences, v. 31, p. 531–544, doi: 10.1016/j.cageo.2004.10.009.

Phillips, J. D. (2001), Designing matched bandpass and azimuthal filters for the separation of potential-field anomalies by source region and source type, Australian Society of Exploration Geophysicists, 15th Geophysical Conference and Exhibition, Expanded Abstracts CD-ROM, 4 pp., doi:10.1071/ASEG2001ab110.

Pollard, D.D., 1987. Elementary fracture mechanics applied to the structural interpretation of dykes, in: Halls, H.C. and Fahrig, W.H. (Ed.), Mafic Dyke Swarms. Geological Association of Canada Special Paper, Canada, pp. 112–128.

Reeves, C., 2000. The geophysical mapping of Mesozoic dyke swarms in southern Africa and their origin in the disruption of Gondwana. J. African Earth Sci. 30, 499–513. https://doi.org/10.1016/S0899-5362(00)00035-X

Ribeiro, V.B., Mantovani, M.S.M., Louro, V.H.A., 2013. Aerogamaespectrometria e suas aplicações no mapeamento geológico. Terra e Didática. 10, 29–51. https://doi.org/10.20396/td.v10i1.8637386

Rickwood, P.C. 1990. The anatomy of a dyke and the determination of propagation and magrna flow directions. In: Parker et al. (eds.). Mafic dykes and emplacement mechanisms. Rotterdam. Bakema. p. 81-100.

Spector, A. Grant, F.S., 1970. Statistical Models for interpreting aeromagnetic data. Geophysics, Vol. 35, N.2, p. 293-302. https://doi.org/10.1190/1.1440092

Trumbull, R.B., Vietor, T., Hahne, K., Wackerle R., Ledru, P., 2004. Aeromagnetic mapping and reconnaissance geochemistry of the Early Cretaceous Henties Bay-Outjo dike swarm, Etendeka Igneous Province. Namibia. Journal of African Earth Sciences, 40,17–29. https://doi:10.1016/j.jafrearsci.2004.07.006

Van Schmus, W.R., Oliveira, E.P., Silva Filho, A.F, Toteu, F.S., Penaye, J., Guimarães, I.P., 2008. Proterozoic links between the Borborema Province, NE Brazil, and the Central African Fold Belt. In: Pankhurst, R.J., Trouw, R.A., Brito Neves, B. B., De Wit, M.J. (eds) West Gondwana: pre-cenozoic correlations across the South Atlantic, 294, 669-99. https://doi.:10.1144/SP294.5

Xiong, S., Yang, H., Ding, Y., Li, Z., Li, W., 2016. Distribution of igneous rocks in China revealed by aeromagnetic data. J. Asian Earth Sci. 129, 231–242. https://doi.org/10.1016/j.jseaes.2016.08.016

Zaineldeen, U.F., 2012. Mapping the Dyke Swarms of the Neoproterozoic Basement in Southwestern Jordan Using Remote Sensing and GIS Techniques. Earth Sci. Res. 2, 156–164. https://doi.org/10.5539/esr.v2n1p156